ANALYSIS OF RADIATIVE AND PHASE-CHANGE PHENOMENA WITH APPLICATION TO SPACE-BASED THERMAL ENERGY STORAGE*

Final Report

by

Kurt O. Lund

Center for Energy and Combustion Research 0310
University of California
La Jolla, CA 92093-0310

December 6, 1991

---

* Parts 2 and 3 of this report were completed under NASA contract NAG3-1106. Part 1 was subsequently completed at the above affiliation.

Executive Summary

This report covers the results of activities of NASA Grant NAG3-1106, and extensions: "Analysis of Radiative and Phase-Change Phenomena with Application to Space Based Thermal Energy Storage". The simplified geometry for this analysis is an infinite, axis symmetric annulus with a specified solar flux at the outer radius. The inner radius is either adiabatic (modeling Flight Experiment conditions), or convective (modeling Solar Dynamic conditions). Liquid LiF either contacts the outer wall (modeling ground-based testing), or faces a void gap at the outer wall (modeling possible Space-based conditions).

The analysis is presented in three parts representing sequential stages of development: Part III, the initial interim report, considers an adiabatic inner wall and linearized radiation equations; Part II adds effects of convection at the inner wall; and Part I includes the effect of the void gap, as well as the previous effects, and develops the radiation model further. Although the results of Parts II and III are preliminary, and constitute background material for Part I, they are nevertheless included here for reference, and because they contain details not found in Part I, which concurrently with this report is submitted as a journal publication.

The original scope of the grant was to investigate analytically the effects of internal radiation upon the phase change processes in monocrystalline LiF, with extension to effects of polycrystalline structure. However, consultations with D. Namkoong during the summer of 1990, indicated that the presence of a void gap could have a much stronger radiative effect than the change in properties represented by a polycrystalline structure. This, indeed, turns out to be the case as examination of the results in Part I will show.

The question of the structure of LiF solidifying in vacuum under microgravity conditions is moot. Visual observation at room temperature of the eutectic, LiF-CaF_2, solidified in canisters under 1-g conditions, show a partially transparent (translucent) optical property for the visible spectrum. However, recent experiments and analyses of radiation in clear and cloudy ice, indicate a relatively small effect of the crystal structure on the overall phase change effect. For LiF "cloudy" properties are not available and it is felt that using the thin film data of Palik and Hunter is the most accurate approach at present.

The main result from the analysis is the considerable differences in melting behavior which can occur between ground based 1-g experiments and the microgravity Flight Experiments. In the ground based tests, under axial 1-g conditions, melted PCM will always contact the outer wall having the heat flux source, thus providing conductance from this source to the phase change front; for this case, melting was found to occur primarily from the outer wall, with radiative effects causing a small amount of melting from the inner wall. In Space based tests and applications under microgravity conditions, where a void gap may likely form during solidification, the situation is reversed: radiation is now the only mode of heat transfer (under the axis symmetric conditions of this analysis) and the majority of melting takes place from the inner wall. Concurrently there is a large temperature excursion in the outer wall facing the void gap. However, in both cases, complete melting occurs in about the same time, for the adiabatic inner wall condition (which is well approximated in the Flight Experiments).

Another major result is the difference between adiabatic and non-adiabatic boundary conditions. When there is convection at the inner wall, it was found that non-melted, partially melted, and fully melted conditions exist depending upon the level of the source flux at the outer wall. Indeed, the flux level for the planned Flight tests would produce no melting at all if the Space Station "Freedom" convective conditions were applied. Therefore, results from the Flight Experiments can not be extended directly to applications with convection, nor can ground based test results be directly extended to the microgravity environment.

Overall, the results of this analysis support the requirement for interpretive analytical/numerical models in conjunction with flight experiments, and it is hoped that they provide useful fundamental information and insight. However, difficulties associated with void formation and its prediction are (perhaps) better addressed with redesign, rather than too extensive numerical modeling. For example, incorporation of ribbed surfaces on the canister interior walls (similar to heat-pipe groves) would provide conductance to the PCM, even in the presence of voids; such surfaces are currently being investigated under ESA programs in Germany. Even more promising is the concept of introducing a capillary mesh, or matrix, within the canister volume; not only does this provide void control, but it enhances the effective PCM conductivity, as well; preliminary analyses at UC-San Diego, and experiments at local industry, indicate potential for vastly improved operation and weight reduction. For future and ongoing Solar Dynamic receiver development, it is recommended that such redesign efforts receive a high priority.

PART I

Radiation and Phase Change of Lithium Fluoride in an Annulus

by

Kurt O. Lund*
Member, AIAA

---

* Asst. Research Engineer
Center for Energy and Combustion Research
University of California
La Jolla, CA 92093-0310

ABSTRACT

A one-dimensional thermal model is developed to evaluate the effect of radiation on the phase change of LiF in an annular canister under gravitational and microgravitational conditions. Specified heat flux at the outer wall of the canister models focussed solar flux, or electrically simulated flux; adiabatic and convective conditions are considered for the inner wall.

A two-band radiation model is used for the combined-mode heat transfer within the canister, and LiF optical properties relate metal surface properties in vacuum to those in LiF. For axial gravitational conditions the liquid LiF remains in contact with the two bounding walls, whereas a void gap is used at the outer wall to model possible micro-gravitational conditions. With outer-wall initial conditions at the melting temperature, and with the specified flux condition, it is shown that the phase-change process is quasi-steady, leading to a simplified, but nonlinear system of equations.

For the adiabatic cases exact integrals are obtained for the time required for complete melting of the LiF. Melting was found to occur primarily from the outer wall in the 1-g model, whereas it occurred primarily from the inner wall in the μ-g model. For the convective cases partially melted steady-state conditions, and fully melted conditions, are determined to depend on the source flux level, with radiation extending the melting times. It is concluded from this study that radiation is an important effect to include, and that fundamentally different behaviors may occur for different gravitational and boundary conditions.

NOMENCLATURE

A	designates adiabatic wall-2, area [m^2]
B	designates Biot-type (convective) wall-2
C	designates liquid contact at wall-1
c	specific heat [J/kg K]
f	radiation function (from Appendix A)
G	designates void gap at wall-1
g_s	scaled heat flux source ($=g_{sm}/\epsilon_{0m}$)
g_{sm}	scaled heat flux source ($=q_s/\sigma T_m^4$)
h	heat transfer coefficient [W/m^2K]
H	heat of fusion [J/kg]
I	radiation integral (from Appendix A)
K	scaled linearized radiation conductance
k	conductivity [W/m K]
N	radiation/conduction number ($=\epsilon_{0m}N_m$)
N_m	radiation/conduction number ($=\sigma T_m^3 \Delta r/k_{e\ell}$)
N'	radiation/conduction number ($=NK_a$)
P	radiation exchange function (from Appendix A)
Q	rate of heat transfer [W]
q_s	heat flux source [W/m^2]
R	thermal resistance [K/W, K^4/W]
r	radius [m]
Δr	PCM overall thickness ($=r_j-r_2$)
T	absolute temperature [K]
t	time [s]
t_c	time constant [s] ($=\rho_\ell H_{s\ell} \Delta r^2/k_{e\ell} T_m$)
u,v	logarithmic functions
w	width (thickness) of wall [m]

Greek:

α	wall energy storage ratio ($=w_1\rho_w c_w T_m \Delta() \rho_\ell H_{s\ell}$)
β	Biot number ($=h_2 \Delta r / k_{e\ell}$)
δ_j	outer scaled liquid thickness ($=(r_j - r_{jm})/\Delta r$)
δ_2	inner scaled liquid thickness ($=(r_{2m} - r_2)/\Delta r$)
ϵ	emissivity
ϕ	flux index
Γ	radius ratio ($=r_2/r_j$)
κ	conductivity ratio ($k_{es}/k_{e\ell}$)
Λ	$1 - \Gamma = \Delta r / r_1$
μ	radiation parameter (≈ 0.163)
ρ	density [kg/m^3]
σ	Stefan-Boltzmann constant ($=5.67 \times 10^{-8}$ W/m^2K^4)
τ	scaled time ($=t/t_c$)
τ'	scaled time for adiabatic wall-2 ($=Ng_s\tau = tq_s/\rho_\ell H_{s\ell} \Delta r$)
τ''	scaled time for conv. wall-2 ($=(1-\psi_f)\tau = tk_\ell (T_m - T_f)/\rho_\ell H_{s\ell} \Delta r^2$)
θ	scaled temperature defect ($=(\psi - 1)/Ng_s$)
ψ	temperature ratio, ($=T/Tm$)

Subscripts:

0	vacuum, initial conditions
1	wall-1 (outer wall)
2	wall-2 (inner wall)
3	surface-3 (at gap facing outer wall)
a	a-band (transparent band) of spectrum
b	b-band (optically thick band)
e	effective
f	fluid boundary
fm	fully melted
h	convective

i	surface index (= j or 2)
j	surface index (= 1 or 3)
k	conduction
ℓ	liquid
m	melting condition or temperature
r	radiative
s	solid, source
st	storage
w	wall

1. INTRODUCTION

The behavior of phase transition is central to the understanding of phase-change thermal energy storage for development of Solar Dynamic Space Power [e.g., Labus et al. 1989]. Therefore, ground tests have been conducted [Strumpf and Coombs 1990], Space Shuttle flight experiments have been planned [Namkoong 1989a, 1989b], and numerical analyses have been performed to determine two and three dimensional effects of the phase transition process [Kerslake and Ibrahim 1990, Wichner et al. 1988]. These analyses and experiments utilize an annular canister containing the phase change material (PCM), where a solar heat flux (or electrically simulated flux) is impressed on the outer wall of the canister (radius r_1 in Figure 1); the inner wall (radius r_2) either is convective, or is nearly adiabatic during the heat addition.

In application to heat receivers the PCM's are high-temperature salts, such as lithium-fluoride (LiF) with a melting temperature of 1120 K (1556 F) [or the eutectic LiF-CaF2 which melts at 1040 K (1412 F)]. At these temperatures radiative transport can be a significant part of the overall heat transfer processes within the canisters. In the previous two-dimensional model [Kerslake and Ibrahim 1990] radiation was not included, and in the three-dimensional model [Wichner et al. 1988] the effect of radiation is obscured by the complexity of the numerical computations; in the flight experiments [Namkoong 1989] radiation will occur naturally, but the radiative effect cannot be determined directly and must be deduced from canister surface temperatures. There is, thus, a need for basic models and solutions for the high-temperature enclosure with PCM and radiation; to this end a one-dimensional analysis is here presented.

The high-temperature salts exhibit considerable contraction upon solidification, which can lead to void formation at the outer wall under microgravity conditions in Space. Hence, in this case, radiation is the dominant mode of heat transfer, in contrast to axial 1-g conditions where liquid PCM contacts the wall and conduction is dominant. Four cases are considered here which model behaviors for adiabatic and convective inner wall conditions, and under axial 1-g and μ-g conditions.

Radiation within the canister enclosure follows conventional spectral exchange between surfaces, except that the intervening medium, LiF, has spectral properties which differ from those of vacuum. Therefore, accurate application requires spectral integrations; these are presented in Appendix A where metal surface properties in vacuum are related to those in the presence of the LiF medium. Following Williams [1988], and Song and Viskanta [1990], a two-band approximation is made utilizing recent measurements of LiF optical properties [Palik and Hunter 1985].

A two-surface thermal model is developed in Section 2 for adiabatic and convective boundary conditions at the inner radius,

and imposed heat flux at the outer radius. This differs from the usual Stefan problem where the temperature at a boundary is suddenly changed [e.g., Yao and Prusa 1989, Burmeister 1983, or Solomon 1981], resulting in a boundary layer growing in time as the error function [e.g., Arpaci and Larsen 1984]. However, as shown in Appendix B, with the presently imposed heat flux boundary condition, this layer does not develop, with the result that PCM temperatures change only slowly in a quasi-steady fashion, as was previously observed [Song and Viskanta 1990].

For the liquid PCM it is assumed that the conduction limit applies, such that natural convection boundary layers do not develop significantly and such that the phase-change boundary remains axially uniform. This is valid for Rayleigh numbers below 1700, for rectangular enclosures [Incropera and DeWitt 1985, p. 401], but has also been demonstrated experimentally for much larger Rayleigh numbers with a heat flux boundary and an aspect ratio of 4.5 [Zhang and Bejan 1989]. This is considered an excellent approximation under 1-g axial gravitational acceleration; under microgravity conditions the magnitude of natural convection is suppressed, although some convection effects can be present [Bayazitoglu and Lam 1987, Arnold et al. 1990].

2. PROBLEM FORMULATION

The thermal model is for a solid region surrounded by liquid at either or both radii r_{3m} and r_{2m}, as indicated in Figure 1, and (in some cases) having a narrow void gap near r_1. The gap models microgravity conditions where the PCM could completely solidify, radially outwards, without making contact with the outer wall. Under axial 1-g conditions, there will be contact with the wall by liquid filling the annular gap. In these annular liquid gaps convection will be driven by the gravitational and temperature fields, but without feedback to the thermal process for small Rayleigh numbers and long aspect annuli [Arpaci and Larsen 1984]. In the following, four cases of analysis are considered: A and B referring respectively to adiabatic and convective boundary conditions at wall 2, and C and G referring respectively to contact and gap conditions at wall 1.

The heat transfer processes shown in Figure 1 constitute a combined radiation and conduction network. Radiation occurs between walls 1 and 2 in the transparent spectral band of the PCM (the a-band), and to a lesser extent between surfaces 1 and 3 in the optically thick band of the spectrum (the b-band), as shown in Appendix A. In each case considered, the initial condition is fully solidified PCM at wall 1 (or surface 3), and at the melting temperature, T_m. Under this condition the sensible heat terms do not enter the problem, and the quasi-steady network indicated in Figure 1 provides the whole solution, as shown in Appendix B.

With reference to Figure 1, the conduction heat transfer from surface i to im (i = j or 2 , j = 1 or 3) is given by:

$$Q_{ki} = \frac{T_i - T_{im}}{R_{ki}} \tag{2.1}$$

where resistances are

$$R_{kj} = \frac{\ell n(r_j/r_{jm})}{2\pi k_{e\ell}} \ , \ j=1,3; \ R_{k2} = \frac{\ell n(r_{2m}/r_2)}{2\pi k_{e\ell}} \tag{2.2,3}$$

and the effective liquid conductivity is $k_{e\ell}$. Similarly

$$Q_{ks} = \frac{T_{jm} - T_{2m}}{R_{ks}} \ ; \quad R_{ks} = \frac{\ell n(r_{jm}/r_{2m})}{2\pi k_{es}} \ , \ j=1,3 \tag{2.4,5}$$

$$Q_{h2} = h_2 A_2 (T_2 - T_f) \ ; \quad Q_{st1} = (\rho c)_w A_1 w_1 \ dT_1/dt \tag{2.6,7}$$

Energy balances yield, respectively, on surface 1

$$Q_s = Q_{ra} + \begin{cases} Q_{k1} \ ; \ C - - \text{ contact} \\ Q_{rb} + Q_{st1} \ ; \ G - - \text{ gap} \end{cases} \tag{2.8}$$

on surface 2

$$Q_{ra} = \begin{cases} Q_{k2} \ ; \ A - - \text{ adiabatic} \\ Q_{h2} - Q_{ks} \ ; \ B - - \text{ convection} \end{cases} \tag{2.9}$$

and on surface 3

$$Q_{rb} = Q_{k3} \tag{2.10}$$

The radiative heat rates are related to temperatures as

$$Q_{ra} = 2\pi r_1 \epsilon_{0m} \sigma T_m^4 \ P_a(\psi_1, \psi_2) \tag{2.11}$$

$$Q_{rb} = 2\pi r_1 \epsilon_{0m} \sigma T_m^4 \ \mu P_b(\psi_1, \psi_3) \tag{2.12}$$

where, from Appendix A,

$$P_a = \psi_1^{4.5} \ I_1(\psi_1, \psi_2) - \psi_2^{4.5} \ I_2(\psi_1, \psi_2) \tag{2.13}$$

$$P_b = \psi_1^4 - \psi_3^4 \tag{2.14}$$

and $\mu \approx 0.163$ is a small parameter.

At the phase boundaries the heat added results in the movement of the boundaries through $H_{s\ell}$, the latent heat:

$$Q_{kj} - Q_{ks} = - 2\pi \rho_\ell H_{s\ell} \ r_{jm} \frac{dr_{jm}}{dt} \ , \ j=1,3 \tag{2.15}$$

$$Q_{k2} + Q_{ks} = + 2\pi \rho_\ell H_{s\ell} \ r_{2m} \frac{dr_{2m}}{dt} \tag{2.16}$$

In scaled, nondimensional terms the above relations are combined and summarized as follows,

Wall 1:

$$Ng_s = NP_a + \begin{cases} (\psi_1 - 1)/v_1 \ , \ C \\ \mu NP_b + \alpha d\psi_1/d\tau \ , \ G \end{cases} \tag{2.17}$$

Wall 2:

$$\frac{\psi_2 - 1}{u_j} + \beta\Gamma(\psi_2 - \psi_f) = NP_a \tag{2.18}$$

$$u_j = \begin{cases} \ell n\{1 + \Lambda\delta_2/\Gamma\}/\Lambda \ , \ A \\ \ell n\{(1 - \Lambda\delta_j)/\Gamma\}/\kappa\Lambda \ , \ B \end{cases} \tag{2.19}$$

Surface jm (j = 1 or 3):

$$\{1 - \Lambda\delta_j\}\frac{d\delta_j}{d\tau} = \frac{\psi_j - 1}{v_j} - \begin{cases} 0 \ , \ A \\ (1 - \psi_2)/u_j \ , \ B \end{cases} \tag{2.20}$$

$$v_j = \ell n\{1/(1 - \Lambda\delta_j)\}/\Lambda \tag{2.21}$$

Surface 2m:

$$\{\Gamma + \Lambda\delta_2\}\frac{d\delta_2}{d\tau} = NP_a \ , \ A \tag{2.22}$$

Surface 3:

$$\frac{\psi_3 - 1}{v_3} = \mu NP_b \ , \ G \tag{2.23}$$

Here, the radiation/conduction number is

$$N = \frac{\epsilon_{0m}\sigma T_m^3(r_j - r_2)}{k_{e\ell}} = \epsilon_{0m}N_m \tag{2.24}$$

the Biot number is

$$\beta = \frac{h_2(r_j - r_2)}{k_{e\ell}} \tag{2.25}$$

the liquid thickness ratios are

$$\delta_j = \frac{r_j - r_{jm}}{r_j - r_2} \ , \quad \delta_2 = \frac{r_{2m} - r_2}{r_j - r_2} \tag{2.26,27}$$

where $\tau = t/t_c$,

$$t_c = \frac{\rho_\ell H_{s\ell}(r_j - r_2)^2}{T_m k_{e\ell}} \tag{2.28}$$

$$g_s = \frac{q_s}{\epsilon_{0m}\sigma T_m^4} = \frac{g_{sm}}{\epsilon_{0m}} \tag{2.29}$$

$$\alpha = \frac{\rho_w}{\rho_\ell} \frac{w_1}{r_j - r_2} \frac{c_w T_m}{H_{s\ell}} \tag{2.30}$$

and where $\Gamma = r_2/r_j$, $\Lambda = 1 - \Gamma$, and $\kappa = k_{es}/k_{e\ell}$.

3. RESULTS

3.1 Case C-A:

Under axial 1-g conditions with liquid contacting wall 1 ("C"-cases), the energy storage in the canister walls is negligible and the impressed heat flux effectively acts directly on the PCM. With an adiabatic wall-2, conservation of energy requires all of the energy to go into phase change; this results in a closed form solution of the system, (2.17) to (2.32), obtained from the sum of (2.20) and (2.23):

$$\delta_1 - \Lambda\delta_1^2/2 + \Gamma\delta_2 + \Lambda\delta_2^2/2 = Ng_s\tau \equiv \tau' \qquad (3.1)$$

In particular, for complete melting when $r_{2m} = r_{1m}$ ($\delta_1 + \delta_2 = 1$), the scaled time is obtained from (3.1) as

$$Ng_s\tau_{fm} = \tau'_{fm} = (1 + \Gamma)/2 \qquad (3.2)$$

or, in dimensional variables, the fully melted time is

$$t_{fm} = \frac{\pi(r_1^2 - r_2^2)\rho_\ell H_{s\ell}}{2\pi r_1 q_s} \qquad (3.3)$$

Thus, for case C-A the time to melt the PCM is the Phase-change heat content, divided by the input heat transfer rate.

Because of the liquid contact with the canister walls, the wall temperatures do not depart strongly from T_m; therefore, for the "C" cases, it is adequate to use the linearized radiation exchange, $P_a(\psi_1,\psi_2) \approx K_a(\psi_1 - \psi_2)$, where the constant is $K_a \approx 4.5\, f_{0c}(1)$, and f_{0c} is from Figure A-2 of Appendix A.

For the parallel plate limit (Λ ---> 0, Γ ---> 1) the adiabatic, linearized system has the exact solutions:

$$\theta_1 = \frac{\tau'}{2}\left[\frac{2 + N'\tau'}{1 + N'\tau'}\right] \quad , \quad \theta_2 = \frac{\tau'}{2}\left[\frac{N'\tau'}{1 + N'\tau'}\right] \qquad (3.4,5)$$

$$\delta_1 = \frac{\tau'}{4}\left[\frac{2 + N'\tau'}{1 + N'\tau'}\right]\ \frac{1 + (1+N'\tau')^2}{(1 + N'\tau')^2} \qquad (3.6)$$

$$\delta_2 = \frac{\tau'}{2}\left[\frac{2 + N'\tau'}{1 + N'\tau'}\right]\ \left[\frac{N'\tau'}{1 + N'\tau'}\right]^2 \qquad (3.7)$$

where $N' = NK_a$, $\tau' = Ng_s\tau$ and $\theta = (\psi - 1)/Ng_s$.

These solutions clearly show the double surface phase-change phenomenon (as also indicated in Figure 2-1,A). It is seen in equations (3.6,7) that δ_1 grows linearly with τ' for small $N'\tau'$ (i.e., initially), whereas δ_2 grows quadratically; the initially linear phase boundary growth has been observed previously in the absence of radiation [Evans et al. 1950].

Wall temperatures are determined in this analysis, rather than specified. The gradual increase in the wall temperatures in (3.4,5) shows the absence of thermal boundary layers, as proved in Appendix B. From (3.4) the maximum wall temperature increase at complete melting when $\tau' = 1$ is $\psi_{1,max} - 1 = Ng_s$; in physical terms $T_{1,max} - T_m = q_s(r_1-r_2)/k_{\ell}$, or about 25 K above 1120 K, which validates linearization of the radiation term.

In the case of an annulus with finite radii ($r_2/r_1 = \Gamma \neq 1$), equations (2.17) to (2.22) were solved by numerical integration, with results as shown in Figure 2, for $\Gamma = 0.5$. The initially linear and quadratic growth of the two phase fronts is evident; complete melting occurred at $\tau'_{fm} = 0.75$, as predicted by (3.2).

3.2 Case C-B:

With the convection heat sink at the inner wall, the possibility exists that q_s may not be sufficient to cause any melting at all. This is seen from the combination of (2.17) to (2.20) which yields

$$(1 - \Lambda\delta_1)\frac{d\delta_1}{d\tau} = Ng_s - \beta\Gamma(\psi_2 - \psi_f) \tag{3.8}$$

where the initial slope must be positive for δ_1 to grow; thus, Ng_s must be greater than the minimum

$$Ng_{s0} = \beta\Gamma(\psi_{20} - \psi_f) = \beta\Gamma\,\frac{N' + 1/u_0}{N' + 1/u_0 + \beta\Gamma}(1 - \psi_f) \tag{3.9}$$

where from (2.19) $u_0 = \ell n(1/\Gamma)/K\Lambda$, and $\psi_{20} = \psi_2(0)$ is obtained from (2.18). In dimensional variables with $h_{r1} = \epsilon_{0m}\sigma T_m^3 K_a$, the limiting minimum heat flux for phase change to occur is

$$q_{s0} = \frac{T_m - T_f}{\dfrac{r_1}{h_2 r_2} + \dfrac{r_1}{h_{r1}r_1 + k_s/\ell n(r_1/r_2)}} \tag{3.10}$$

which is the initial overall temperature difference over the total thermal resistance. Similarly, there is a critical heat flux for which the PCM just becomes 100% melted and at steady state with zero slope at $\delta_1 = 1$; this is given by (3.8) as:

$$Ng_{s1} = \beta\Gamma(1 - \psi_f)\ , \text{ or, } \quad q_{s1} = h_2(T_m - T_f)r_2/r_1 \tag{3.11,12}$$

Partially melted, and unmelted, conditions have also been observed experimentally [Strumpf and Coombs 1990]. Finally, there is a limiting flux above which melting occurs from both sides,

$$Ng_{s2} = Ng_{s1}\left[1 + \frac{1}{\frac{N'}{\kappa\Lambda}\,ln\left\{\frac{1}{1-\Lambda}\right\}}\right] \qquad (3.13)$$

however, for small N', this is a high flux which is usually not encountered.

To summarize, $g_s < g_{s0}$ results in no phase change, $g_{s0} \le g_s < g_{s1}$ results in a steady state with only partial melting, $g_{s1} \le g_s < g_{s2}$ results in 100% melting in finite time from wall-1, and $g_s \ge g_{s2}$ results in 100% melting in finite time from both walls.

The numerical integration of the system equations for the partially melted case is shown in Figure 3, where the scaled heat flux was taken as

$$g_s = \phi g_{s1} + (1 - \phi)g_{s0}\ , \quad 0 \le \phi \le 1 \qquad (3.14)$$

For the parallel plate limit the partially melted steady-state condition can be obtained analytically as

$$\delta_{1,ss} = \phi\,\frac{N' + \kappa + \beta}{N' + \kappa + \phi\beta + (1-\phi)(\kappa-1)N'} \qquad (3.15)$$

For $g_s > g_{s1}$, the pase-change front grows rapidly to complete melting, as shown in Figure 4, where the applied flux was taken as $g_s = \phi g_{s1} < g_{s2}$.

3.3 Case G-A:

Under microgravity conditions where a void gap may form between the PCM and the outer wall ("G"-cases), there is only radiative transport between the outer wall and the PCM. This will cause considerable temperature increase in wall-1, and some energy storage in the wall.

There are no further simplifications possible to the system (2.17) to (2.23). Nevertheless, for an adiabatic wall-2, it possesses the exact integral:

$$\alpha(\psi_1 - 1) + \delta_3 - \Lambda\delta_3^2/2 + \Gamma\delta_2 + \Lambda\delta_2^2/2 = Ng_s\tau \equiv \tau' \qquad (3.16)$$

which, for the fully melted condition, $\delta_2 + \delta_3 = 1$, reduces to

$$\tau'_{fm} = (1 + \Gamma)/2 + \alpha(\psi_{1,fm} - 1) \qquad (3.17)$$

By comparison with (3.1) and (3.2), these results represent the sum of the energies stored in the PCM and in wall-1. Exact calculation of the melting time from (3.17) is not immediate because the original system must be solved to determine wall temperature, ψ_1, at any time; however, the ratio of wall

capacitance to phase-change capacitance is a small quantity, $\alpha = 0(0.1)$, so that melting times are only slightly longer than for liquid contacting wall-1.

A numerical integration of system (2.17) to (2.23) for $\Gamma = 0.5$, $g_{sm} = 0.1$, $\alpha = 0.1$, and for radiation functions from Figure A-1, is shown in Figure 5. In contrast to case C-A, most of the melting takes place from the inner wall, and only a slight amount near the outer wall; otherwise the melting is completed in about the same time as previously because of the small value of α.

The corresponding wall temperature variations are shown in Figure 6, where there is a dramatic sudden increase in the outer wall temperature, in contrast to the liquid contact case where this temperature increased only slightly and gradually. Asymptotic analysis shows this initial temperature "jump" to be approximated by

$$\psi_{1,outer}(0) = \left[1 + g_{sm}/\epsilon_{0m} f_{0g}(1)\right]^{1/4.5} \qquad (3.18)$$

The effect of the emissivity on ψ_1 is evident in both (3.18) and Figure 6, whereas there is a smaller effect on ψ_2; the interface temperature, ψ_3, increased only slightly from 1. Clearly from (3.18), an increase in the applied flux, g_{sm}, would cause a further increase in the outer wall temperature.

3.4 Case G-B:

With the gap at the outer wall, and convection at the inner wall, the flux limit definitions for g_{s0}, (3.9), and g_{s1}, (3.11), apply as previously; however, ψ_2 must now be calculated from the nonlinear equations. Because μ is a small quantity it is found for the steady-state limit that $\psi_{20} = 1 - 0(\mu N)$, such that $g_{s0} = g_{s1}(1 - 0(\mu))$; that is, for any phase change to occur at all, g_s must be very near the limit, g_{s1}. Above this limit, $g_{s2} = g_{s1}(1 + 0(\mu))$, so that melting will occur from wall-2 for g_s just slightly above g_{s1}.

An example of this behavior is shown in Figure 7, where $g_s = \phi g_{s1}$: for $\phi = 1$ there is only slight melting from surface 3, and no melting at surface 2; for $\phi = 1.5$ the melting rates are about the same from both surfaces, but a long time is required for complete melting; for $\phi \geq 2$ the melting rate is greater from surface 2, the inner wall, and complete melting was attained for the times, τ'', shown in the figure. Comparison with the adiabatic cases in Figure 4 shows that a longer melting time is needed with convective heat transfer, as expected.

Corresponding temperatures are shown in Figure 8: after the initial jump, these remain essentially constant during the melting process. With the initial condition of $\delta_3(0) = 0$ ($\psi_3(0) = 1$), $\psi_1(0)$ is greater than 1, approximately as given by (3.18), and $\psi_2(0)$ is slightly less than 1, as shown.

CONCLUSION

Four analytical cases have been considered for the melting of Lithium-Fluoride in an annulus with impressed heat flux at one boundary, including the effect of internal radiation heat transfer. It was found that this process is quasi-steady when the solid LiF near the outer wall is initially at the melting temperature. Radiation was found to be an important effect, especially in the presence of void gaps near the outer wall.

For the adiabatic inner wall condition, the time for complete melting is a fixed quantity which depends only slightly on voids. However, the location of the phase boundaries is strongly influenced by the void gap, with melting occurring primarily form the outer wall when there is liquid contact, and primarily from the inner wall when there is a void gap at wall 1. Wall temperatures remained close to the melting temperature with liquid PCM contacting wall 1; but, the wall-1 temperature has a large and sudden increase above the melting temperature when a void gap is present at wall-1.

For the convective inner wall conditions there may, or may not, be complete melting, depending on the level of impressed heat flux, relative to the fluid temperature and other problem parameters. For liquid PCM contacting wall 1, melting occurred only from wall 1 for moderate heat fluxes, and steady-state partially melted conditions were determined; for a void gap at wall -1, conditions for partial melting almost did not exist, and a substantially high heat flux is required in order to cause any melting at all.

In summary, the results show fundamentally different behaviors depending on the boundary conditions employed. Thus, experimental results from the flight experiments, where the inner wall is essentially adiabatic, can not be used directly for convection applications, without interpretive analytical/numerical modeling; nor can ground-based results, under 1-g acceleration, be used directly in microgravity applications.

ACKNOWLEDGEMENTS

This work was carried out under NASA contract NAG3-1106, Lewis Research Center, Cleveland, OH 44135.

REFERENCES

Arnold, W., Gaug, J. R., and Chait, A., 1990, "Convection Phenomena in Low-Gravity Processing: The GTE GaAs Space Experiment," Paper No. AIAA 90-0409, Aerospace Sciences Meeting, Reno, Nevada, Jan. 8-11.

Arpaci, V. S. and Larsen, P. S., 1984, *Convection Heat Transfer*, Prentice-Hall.

Bayazitoglu, Y. and Lam T. T., 1987, "Marangoni Convection in Radiating Fluids," J. Heat Transfer, Vol. 109, pp. 717-721.

Burmeister, L. C., 1983, *Convective Heat Transfer*, Wiley & Sons, p 169.

Edwards, D. K., 1981, *Radiation Heat Transfer Notes*, Hemisphere Publishing.

Evans II, G.W., Isaacson, E., and MacDonald, J.K.L., 1950, "Stefan-Like Problems," Quart. Appl. Math. Vol. VIII, No. 3, pp. 312-319.

Incropera, F. P., and DeWitt, D. P., 1985, *Introduction to Heat Transfer*, Wiley & Sons.

Kerslake, T. W. and Ibrahim, M. B., 1990, "Analysis of Thermal Energy Storage Material with Change-of-Phase Volumetric Effects", Proc. ASME Int'l Solar Energy Conf., Miami, FL, April 1-4, pp. 315-325.

Labus, T.L., Secunde, R.R., and Lovely, R.G., 1989, "Solar Dynamic Power for Space Station Freedom," Space Power, Vol. 8, Nos.1/2, pp. 97-114.

Namkoong, D., 1989a, "Thermal Energy Storage Flight Experiments", Proc. ASME Solar Energy Conference, San Diego, CA., April 2-5, pp. 19-24.

Namkoong, D., 1989b, "Flight Experiment of Thermal Energy Storage", Proc. 24th Intersociety Energy Conversion Engineering Conf., Washington, D.C., August 6-11.

Nayfeh, A.H., 1981, *Introduction to Perturbation Techniques*, Wiley, New York.

Palik, E. D., and Hunter, W. R., 1985, "Lithium Fluoride (LiF)," *Handbook of Optical Constasnts of Solids*, Academic Press, pp. 675-693.

Seban, R.A., 1965, "The Emissivity of Transition Metals in the Infrared," J. Heat Trans., Vol. 87, pp. 173-176.

Siegel, R., and Howell, J. R., 1981, *Thermal Radiation Heat Transfer*, 2nd Ed, Hemisphere Publishing.

Smith, D.R., 1985, *Singular Perturbation Theory*, Cambridge University Press.

Solomon, A., 1981, "A Note on the Stefan Number in Slab Melting and Solidification," Letters Heat Mass Transfer, Vol 8, pp. 229-235.

Song, B., and Viskanta, R., 1990, "Deicing of Solids Using Radiant Heating," J. Thermophysics and Heat Trans., Vol. 4, No. 3, pp 311-317.

Sparrow, E. M., and Cess, R. D., 1978, *Radiation Heat Transfer - Augmented Edition*, McGraw-Hill.

Strumpf, H. J., and Coombs, M. G., 1990, "Solar Receiver Experiment for the Space Station Freedom Brayton Cycle," J. Solar Energy Eng., Vol 112, pp. 12-18.

Touloukian, Y.S. and DeWitt, D.P., 1970, *Thermal Radiative Properties*, Vol. 7, from *Thermophysical Properties of Matter*, TPRC Data Series, Y.S. Touloukian and C.Y. Ho, Eds., IFI Plenum, New York.

Wichner, R.P., et al., 1988, "Thermal Analysis of Heat Storage Canisters for a Solar Dynamic, Space Power System", Proc. ASME Solar Energy Conference, Denver, CO., April 10-14, pp. 319-328.

Williams, P. T., 1988, "Thermal Radiative Transport through Lithium Fluoride for Temperatures near the Melting Point," Report K/CSD/TM-77, Oak Ridge Gaseous Diffusion Plant, Oak Ridge, Tennessee,

Yao, L. S., and Prusa, J., 1989, "Melting and Freezing," *Advances in Heat Transfer*, Vol. 19, Academic Press, pp. 1-95.

Zhang, Z., and Bejan, A., 1989, "Melting in an Enclosure Heated at a Constant Rate," Int. J. Heat Mass Transfer, Vol. 32, No. 6, pp. 1063-1076.

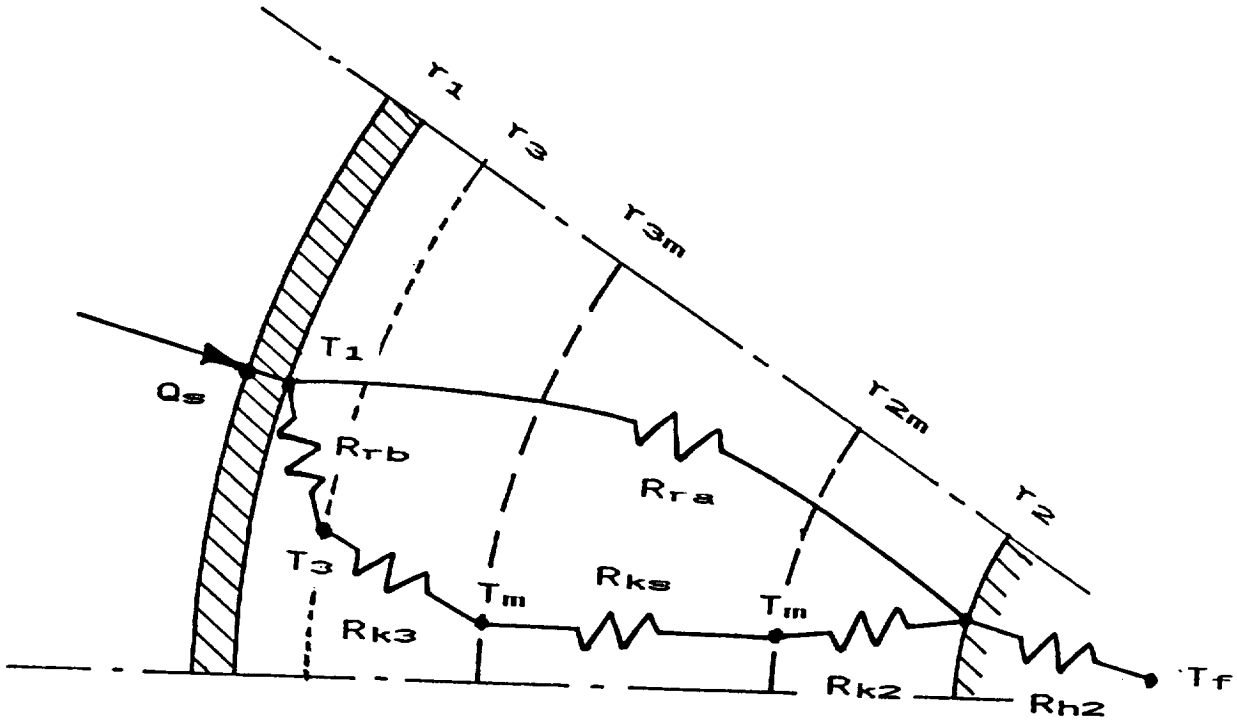

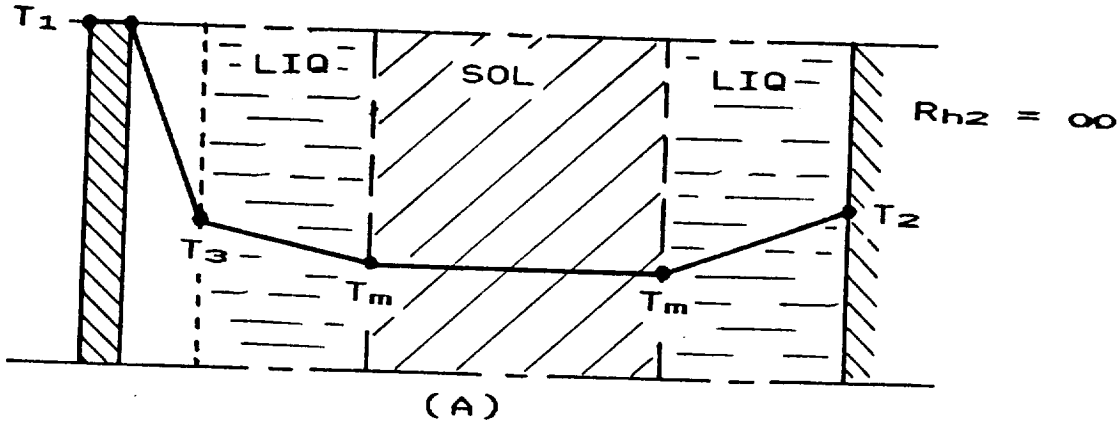

(A)

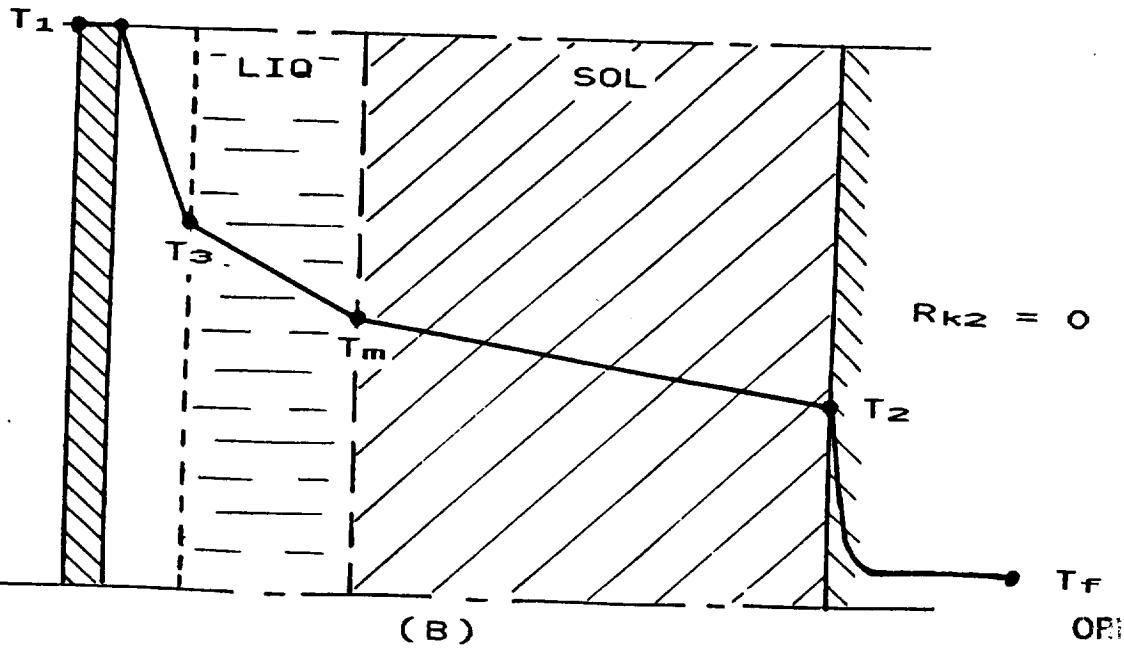

(B)

Fig. 1. Thermal Model for Radiation and Phase-Change in an Annulus [(A): Adiabatic Inner Wall, (B): Convective Inner Wall].

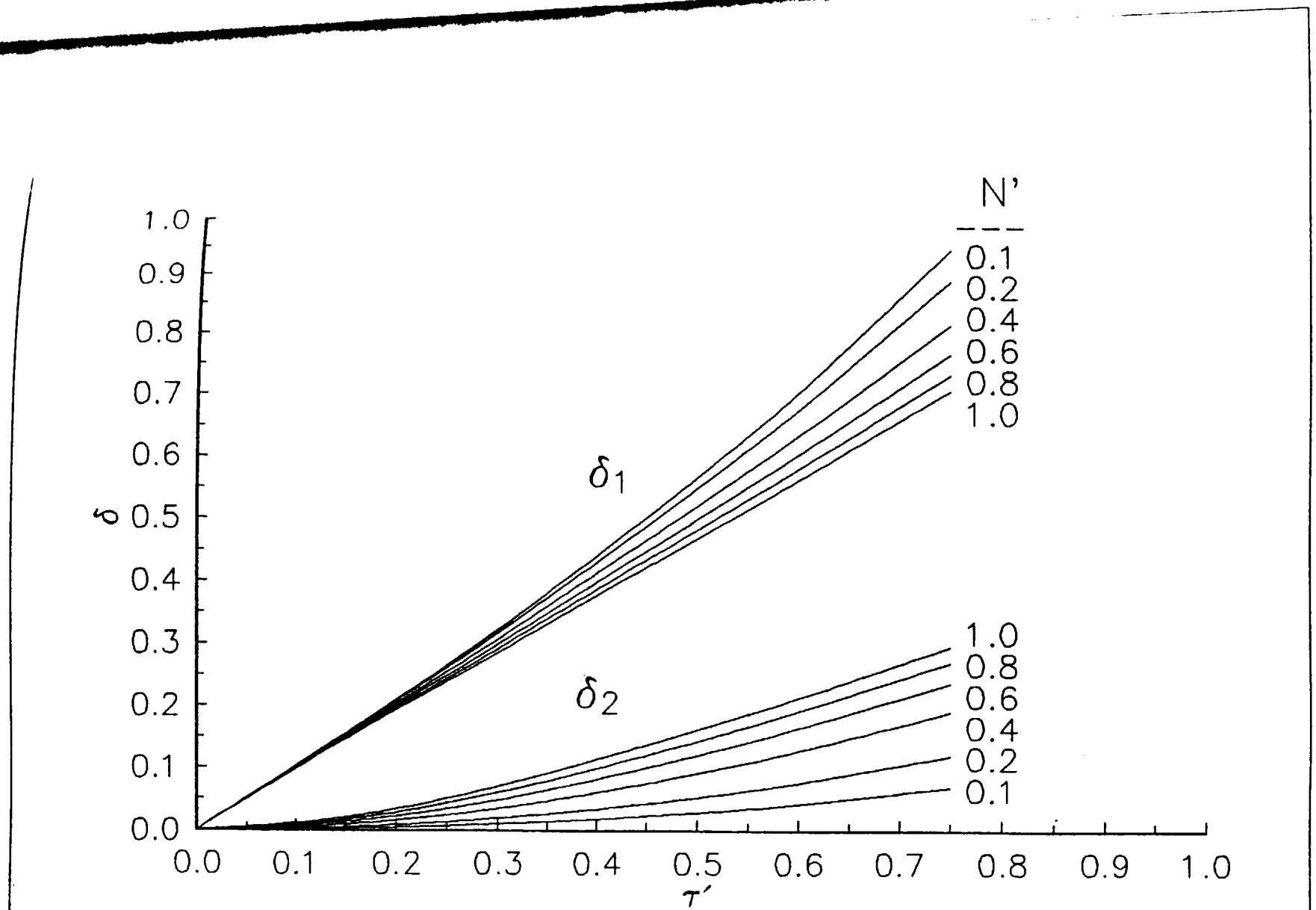

Fig. 2. Growth of Phase-Change Fronts for Annulus with $\Gamma = 0.5$ [Liquid Contacts Outer Wall; Adiabatic Inner Wall].

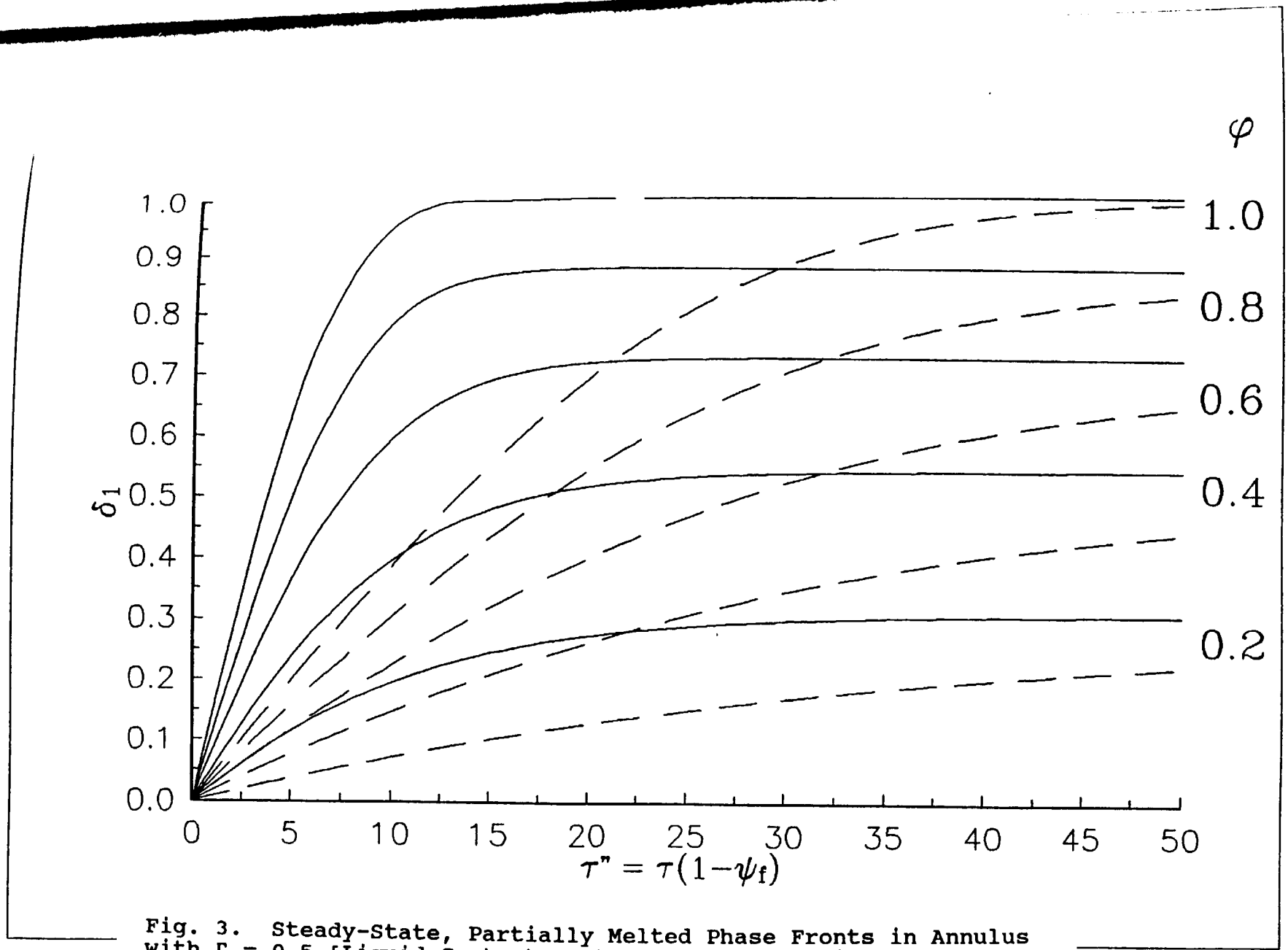

Fig. 3. Steady-State, Partially Melted Phase Fronts in Annulus with $\Gamma = 0.5$ [Liquid Contacts Outer Wall; Convective Inner Wall; $N' = 0.2$; $\kappa = 1.5$; ——, $\beta = 1$; -----, $\beta = 0.5$].

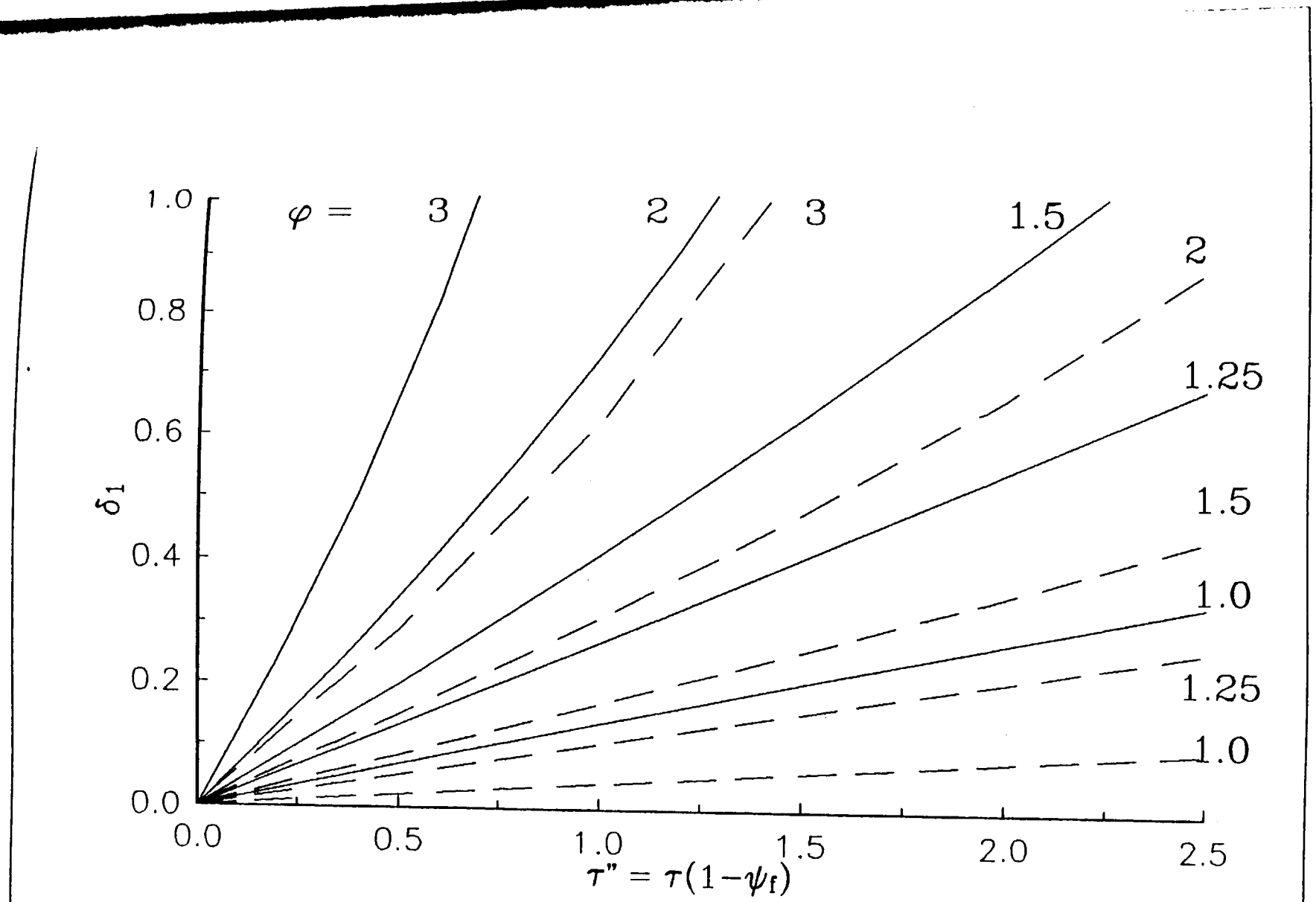

Fig. 4. Fully-Melted Phase Fronts in Annulus with Γ = 0.5 [Liquid Contacts Outer Wall; Convective Inner Wall; N' = 0.2; K = 1.5; ———, β = 1; -----, β = 0.5].

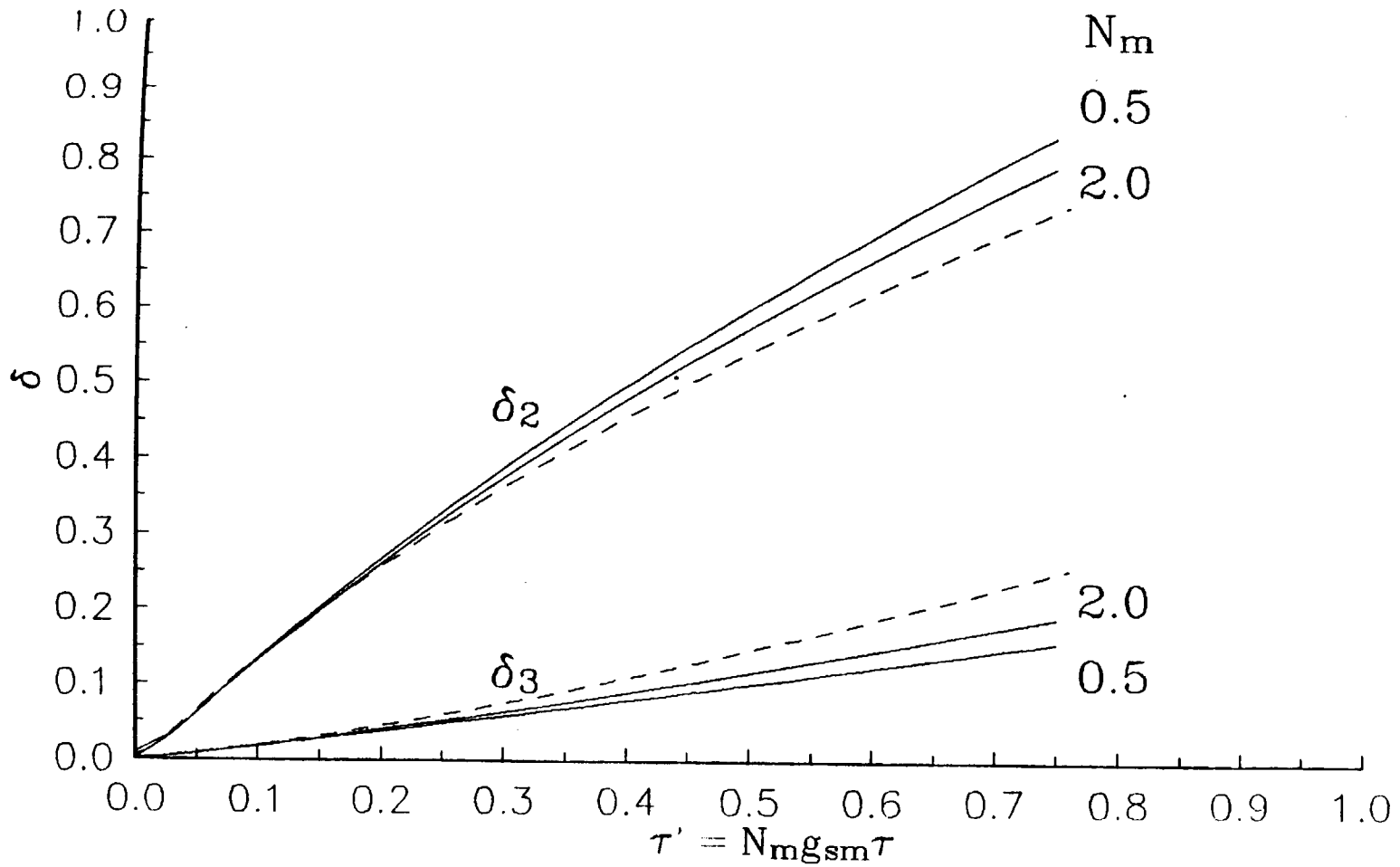

Fig. 5. Growth of Phase-Change Fronts for Annulus with $\Gamma = 0.5$ [Gap at Outer Wall; Adiabatic Inner Wall; $g_{sm} = 0.1$; $\alpha = 0.1$; ———, $\epsilon_{0m} = 0.1$; -----, $\epsilon_{0m} = 0.3$].

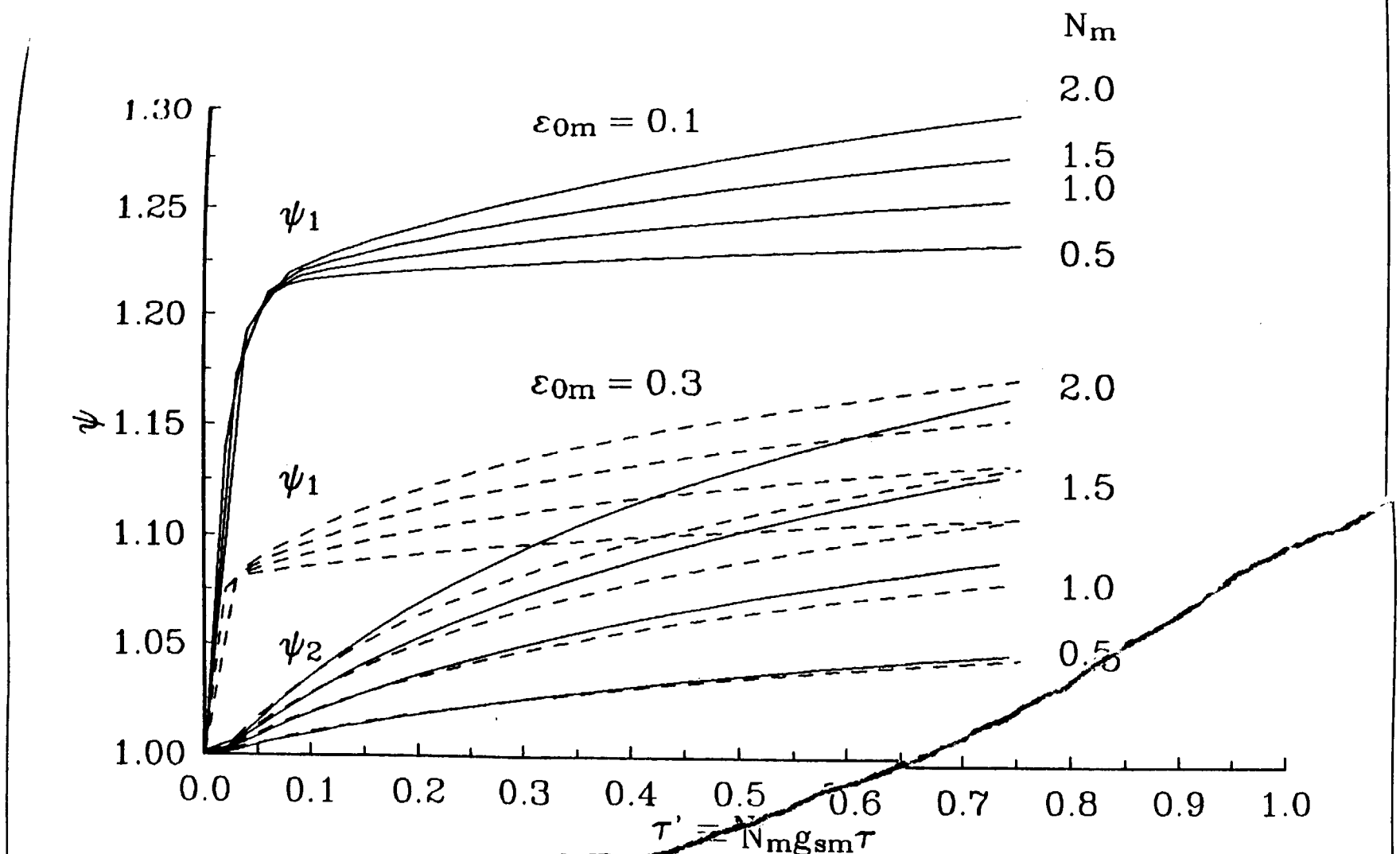

Fig. 6. Wall Temperatures for Annulus with $\Gamma = 0.5$ [Gap at Outer Wall; Adiabatic Inner Wall; $g_{sm} = 0.1$; $\alpha = 0.1$].

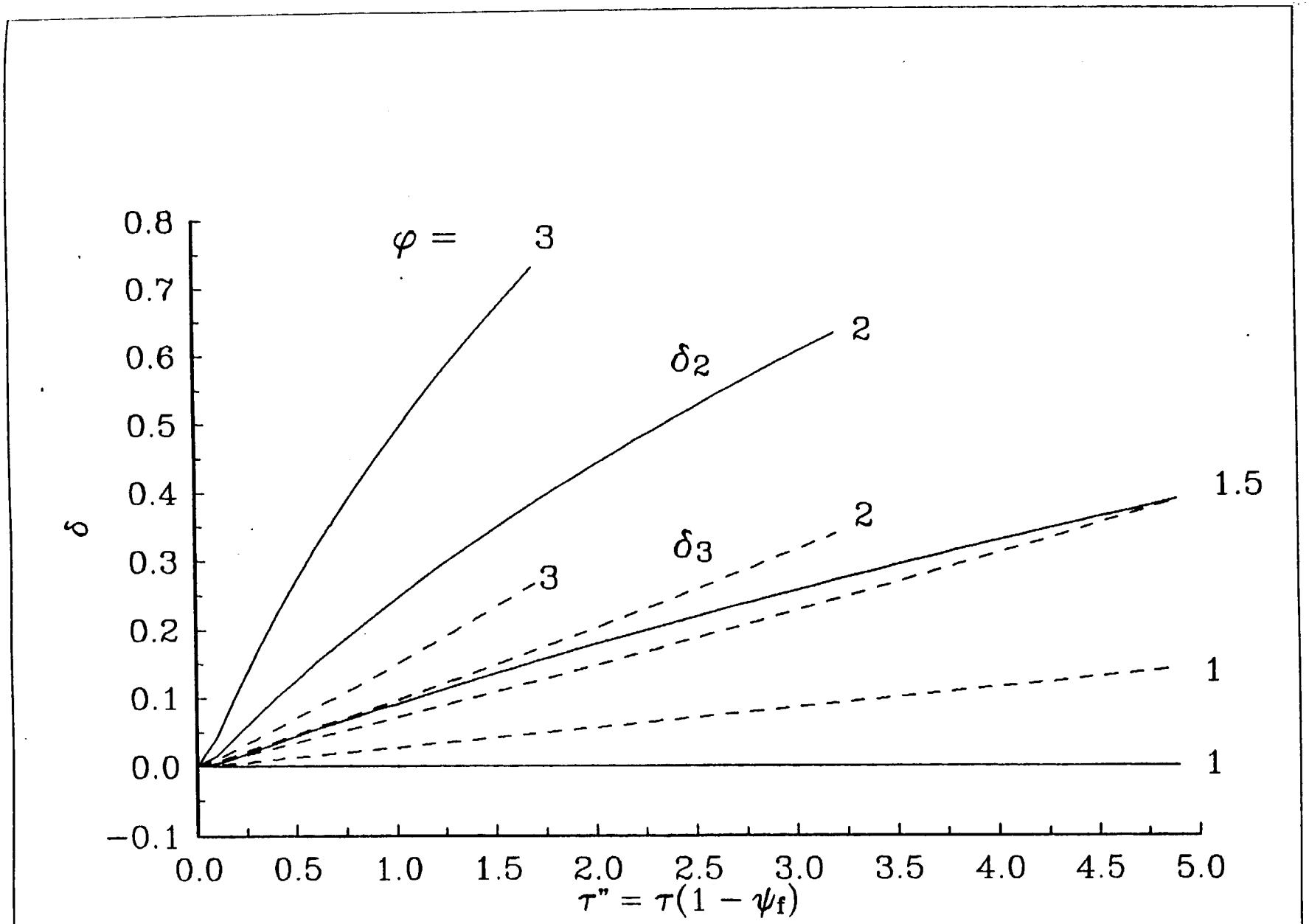

Fig. 7. Growth of Phase-Change Fronts for Annulus with $\Gamma = 0.5$ [Gap at Outer Wall; Convective Inner Wall; $\alpha = 0.1$; $\epsilon_{0m} = 0.1$; $\beta = 0.5$; $N_m = 1$; $\psi_f = 0.8$; $\kappa = 1.5$].

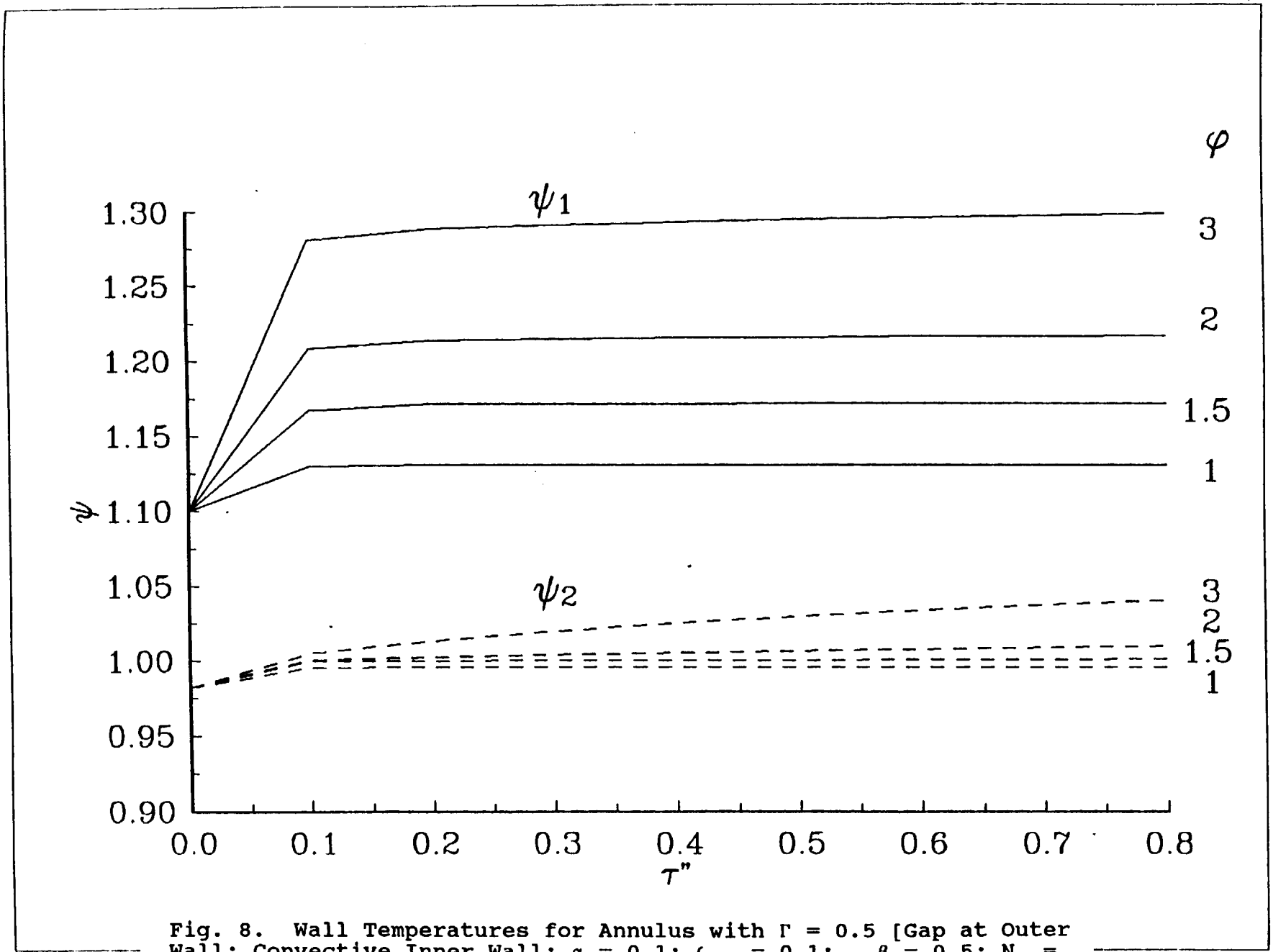

Fig. 8. Wall Temperatures for Annulus with $\Gamma = 0.5$ [Gap at Outer Wall; Convective Inner Wall; $\alpha = 0.1$; $\epsilon_{0m} = 0.1$; $\beta = 0.5$; $N_m = 1$; $\psi_f = 0.8$; $K = 1.5$].

APPENDIX A

RADIATION MODEL

Experimental data for Lithium Fluoride indicate a near perfect transparency for wavelengths below 5.5 μm, and optically thick properties for wavelengths above about 7 μm [Palik and Hunter 1985]. Therefore, a two-band radiation model is considered where the LiF is transparent for wavelengths below 5.5 μm (the a-band), and optically thick for wavelengths above this value (the b-band). (This model obviously neglects processes in a narrow band where the LiF is neither transparent nor optically thick.)

In the a-band there is radiation exchange between the two bounding metal walls, and spectral variations of properties of the walls, and of the LiF with index of refraction n, are included. In the vicinity of T_m = 1120 K most of the emitted radiation is in this transparent band. In the b-band, there is a minor radiative addition to the LiF conductivity and, in the prescence of a void, minor radiation between wall-1 and the LiF surface.

Wall Emissivity:

Spectral emission in to a medium with refractive index n is given by the Planck formula and the spectral emissivity [e.g. Sparrow and Cess 1978]:

$$e_\nu = \epsilon_\nu e_{b\nu} = n^2 \epsilon_\nu e_{b\zeta} \equiv \epsilon_\zeta e_{b\zeta} \qquad (A.1)$$

where $\zeta = c_2/n\lambda T = \nu/\nu_0$, $\nu_0 = c_0 T/c_2$, $c_0 = 3\times10^8$ m/s, $c_2 = 14{,}388$ μm K, and where

$$e_{b\zeta} = \frac{15}{\pi^4} \frac{\sigma T^4}{\nu_0} \frac{\zeta^3}{e^\zeta - 1} \qquad (A.2)$$

Here ϵ_ν represents emission into the medium relative to blackbody emission into the medium, and ϵ_ζ represents emission into the medium relative to blackbody emission into vacuum; the latter can be greater than 1 whenever n is greater than 1.

For a number of metal surfaces at the high temperatures under consideration, experiments have shown that the normal spectral emissivity varies with wavelength to the -1/2 power, even into the visible part of the spectrum [Seban 1965, Touloukian 1970]; therefore, consistent with electromagnetic theory, we take

$$\epsilon_\nu = \epsilon_\lambda = n\, \epsilon_{\lambda c} \sqrt{\frac{\lambda_c}{n\lambda}} = n\, \epsilon_{\lambda c} \sqrt{\frac{\zeta}{\zeta_c}} \qquad (A.3)$$

where $\epsilon_{\lambda c}$ is the best-fit emissivity for n = 1 at wavelength λ_c, and where $\zeta_c = c_2/\lambda_c T$. For emission into vacuum this model

yields the total normal emissivity

$$\epsilon_{0t} = \frac{\epsilon_{\lambda c}}{\sqrt{\zeta_c}} \frac{15}{\pi^4} \int_0^\infty \frac{\zeta^{3.5} d\zeta}{e^\zeta - 1} = \frac{1}{c_4} \frac{\epsilon_{\lambda c}}{\sqrt{\zeta_c}} \tag{A.4}$$

where $c_4 = \pi^4/(15 \times 12.27) = 0.529$. For example, for Nickel at 1390 K with the experimental value $\epsilon_{\lambda c} = 0.25$ at $\lambda_c = 1$ μm [Seban 1965], the model yields $\epsilon_{0t} = 0.147$; for $\epsilon_{\lambda c} = 0.08$ at $\lambda_c = 9$ μm it yields $\epsilon_{0t} = 0.141$, which indicates good agreement with experimental measurements for this material at this temperature.

Now combining (A.1), (A.2) and (A.4), the effective spectral emissivity for emission into medium n is given by

$$\epsilon_\zeta = c_4 n^3 \epsilon_{0t} \sqrt{\zeta} \tag{A.5}$$

Thus, if the total normal (hemispherical) emissivity function $\epsilon_{0t}(T/T_m)$ for emission into vacuum is known in the vicinity of T_m, then (A.5) yields an approximate spectral normal (hemispherical) emissivity for emission into medium n. For example, with $\epsilon_{0t} = 0.147$ from the above calculation, the emissivity at $\lambda = 1$ μm for emission into LiF ($n \approx 1.4$), is 0.58.

A-Band Radiation Exchange:

Application of radiosity microbalance to the phases and surfaces indicated in Figure 1 yields the spectral flux at wall 1 [e.g. Siegel and Howell 1981]:

$$q_{\zeta 1} = \frac{e_{b\zeta 1} - e_{b\zeta 2}}{\frac{1}{\epsilon_{\zeta 1}} + \frac{1/F_{12}}{\epsilon_{\zeta 2}} - \tau_e} \tag{A.6}$$

where the effective interface transmittance is $\tau_e = (1 - 2\rho_3)/(1 - \rho_3) \approx \tau_3 \approx 0.98$. Thus, the a-band total radiative flux is

$$q_{a1} = \int_{\nu_a}^\infty q_{\nu 1} d\nu = \nu_0 \int_{\zeta_a}^\infty q_{\zeta 1} d\zeta \tag{A.7}$$

Combining (A.2) with (A.5) to (A.7) results in

$$\frac{q_{a1}}{\epsilon_{0m} \sigma T_m^4} = \psi_1^{4.5} I_1 - \psi_2^{4.5} I_2 \tag{A.8}$$

where

$$I_i = \frac{1}{12.27} \int_{\zeta_{ai}}^{\infty} \frac{\zeta^{3.5}/(e^{\zeta} - 1)\, d\zeta}{\frac{\epsilon_{0m}\sqrt{\psi_1}}{n_1^3\, \epsilon_{0t}(\psi_1)} + \frac{\epsilon_{0m}\sqrt{\psi_2}}{F_{12}\, n_2^3\, \epsilon_{0t}(\psi_2)} - c_4 \epsilon_{0m} \tau_3 \sqrt{\psi_i \zeta}} \tag{A.9}$$

and $\zeta_{ai} = \zeta_{am}/\psi_i$, $\zeta_{am} = c_2 \nu_a / c_0 T_m$, $\psi_i = T_i/T_m$, $\epsilon_{0m} = \epsilon_{0t}(1)$.

In (A.9), $n_1 = n(\psi_1 \zeta)$ and $n_2 = n(\psi_2 \zeta)$ for LiF contact with both walls, whereas $n_1 = 1$ in the prescence of a void gap at wall-1; for the region considered, the LiF spectral refraction index data of Palik and Hunter [1985] may be represented as a function of wave number, as follows:

$$n(\psi\zeta) = 1.38 + 7.79 \times 10^{-4}\, \psi\zeta - 2.3\, e^{-1.87\, \psi\zeta} \tag{A.10}$$

A closed-form integration of (A.9) is not possible; however, it may be evaluated in the vicinity of T_m by use of Taylor series expansions about this temperature. Since wall temperatures, on an absolute scale, do not depart strongly from T_m, this is a valid procedure, which yields for LiF contact with wall 1 and 2,

$$I_{i,c} = f_{0c}(\psi_i) + \left[\psi_1 - 1 + \frac{\psi_2 - 1}{F_{12}}\right]\left\{\left[\frac{\epsilon'_{0m}}{\epsilon_{0m}} - \frac{1}{2}\right] f_{1c}(\psi_i; n(\zeta)) + f_{2c}(\psi_i)\right\} + \epsilon_{0m}\, (\psi_i - 1) f_{3c}(\psi_i) \tag{A.11}$$

and for a void gap at wall 1,

$$I_{i,g} = f_{0g}(\psi_i) + (\psi_1 - 1)\left[\frac{\epsilon'_{0m}}{\epsilon_{0m}} - \frac{1}{2}\right] f_{1g}(\psi_i; 1) + \frac{\psi_2 - 1}{F_{12}}\left\{\left[\frac{\epsilon'_{0m}}{\epsilon_{0m}} - \frac{1}{2}\right] f_{1g}(\psi_i; n(\zeta)) + f_{2g}(\psi_i)\right\} + \epsilon_{0m} \tau_3\, (\psi_i - 1) f_{3g}(\psi_i) \tag{A.12}$$

where for γ = c or g,

$$f_{0\gamma}(\psi_i) = \frac{1}{12.27} \int_{\zeta_{am}/\psi_i}^{14} \frac{g(\zeta)\, d\zeta}{D_{0\gamma}} \tag{A.13}$$

$$f_{1\gamma}(\psi_i; n) = \frac{1}{12.27} \int_{\zeta_{am}/\psi_i}^{14} \frac{g(\zeta)\, d\zeta}{D_{0\gamma}^2 n^3} \tag{A.14}$$

$$f_{2\gamma}(\psi_i) = \frac{3}{12.27} \int_{\zeta_{am}/\psi_i}^{14} \frac{\zeta\, n'(\zeta)\, g(\zeta)\, d\zeta}{D_{0\gamma}^2 n^4(\zeta)} \tag{A.15}$$

$$f_{3\gamma}(\psi_i) = \frac{c_4/2}{12.27} \int_{\zeta_{am}/\psi_i}^{14} \frac{\sqrt{\zeta}\, g(\zeta)\, d\zeta}{D_{0\gamma}^2} \tag{A.16}$$

Here the denominators are

$$D_{0c} = \frac{1 + 1/F_{12}}{n^3(\zeta)} - c_4 \epsilon_{0m} \sqrt{\zeta} \tag{A.17}$$

$$D_{0g} = 1 + \frac{1}{F_{12} n^3(\zeta)} - c_4 \epsilon_{0m} \tau_3 \sqrt{\zeta} \tag{A.18}$$

and the numerator function is

$$g(\zeta) = \frac{\zeta^{3.5}}{e^{\zeta} - 1} \tag{A.19}$$

which is less than 1% at the computational upper limit of $\zeta = 14$; here the apostrophe (') denotes the derivative with respect to the function argument. A sample evaluation of $f_{0\gamma}$ is shown in Fig. A-2.

B-Band Radiation Effect:

In the optically thick region of the spectrum, there is radiation exchange across the wall-1 void gap according to

$$q_{b1} = \int_0^{\zeta_a} \frac{e_{b\zeta 1} - e_{b\zeta 3}}{\frac{1}{\epsilon_{\zeta 1}} + \frac{1}{\epsilon_{\zeta 3}} - 1} d\zeta \tag{A.20}$$

where $\epsilon_{\zeta 1}$ is obtained as before, but with n = 1, and $\epsilon_{\zeta 2}$ is obtained from electromagnetic theory as

$$\epsilon_{\zeta 2} = \frac{4n}{(n+1)^2 + k^2} \tag{A.21}$$

With the data of Palik and Hunter [1985], evaluation of (A.20) and (A.21) resulted in

$$q_{b1} = \mu \epsilon_{0m} \sigma T_m^4 (\psi_1^4 - \psi_3^4) \tag{A.22}$$

where μ is a slightly decreasing function of increasing temperature, with an average value of $\mu = 0.163$. Thus, radiation exchange across the gap is quite small.

Energy absorption in the medium is modeled as Rosseland conductivity [e.g., Edwards 1981, p. 296; Özisik 1973, p. 318]:

$$k_R = \int_{\lambda_a}^{\infty} \frac{4}{3a_\lambda} \frac{\partial e_{b\lambda}}{\partial T} d\lambda = \frac{5}{\pi^4} \sigma T^3 \int_0^{\zeta_a} \frac{\zeta^4 e^\zeta}{a_\lambda (e^\zeta - 1)^2} d\zeta \qquad (A.23)$$

where $a_\lambda = 4\pi k/\lambda$. Evaluation of this function showed but a weak temperature dependence, and an approximate value of 0.005 W/cm K, which is an order of magnitude less than the medium thermal conductivity. Thus, there is only minor b-band radiative effect on the phase-change heat transfer problem.

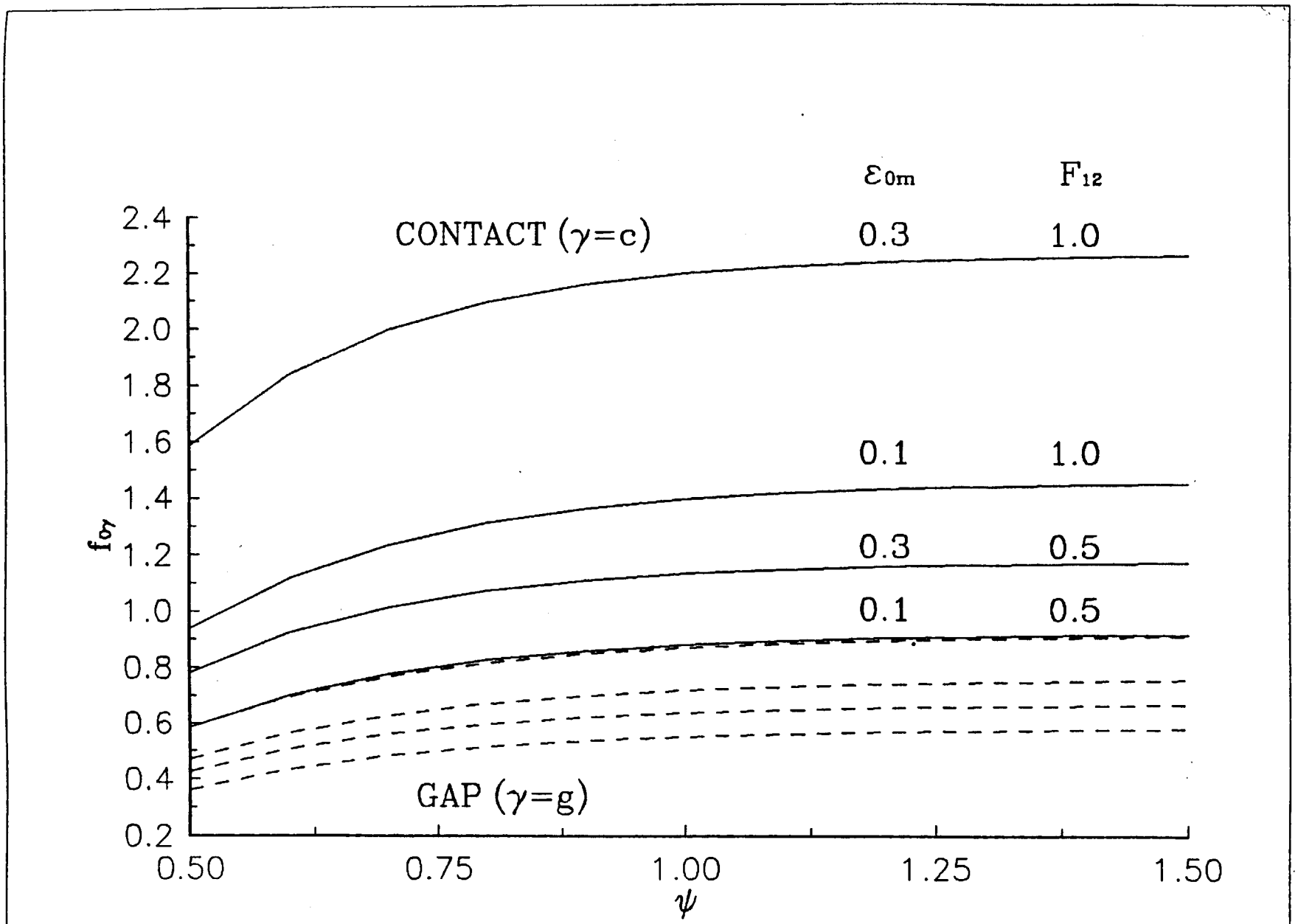

Fig. A-1. Radiation Function Evaluation.

APPENDIX B

ASYMPTOTIC ANALYSIS OF THE FLUX STEFAN PROBLEM

Consider a plane layer of liquid PCM initially in equilibrium at the melting temperature, T_m, and having initial thickness L_0; it is in contact with the canister wall at $X = 0$, and with solid PCM at $X = L_0$. At time $t_0 = 0$, heat flux q is suddenly applied at $X = 0$, yielding the following boundary value problem:

$$\frac{1}{a}\frac{\partial T}{\partial t} = \frac{\partial^2 T}{\partial X^2} \tag{B.1}$$

$$T(X,t_0) = T[L(t),t] = T_m \tag{B.2,3}$$

$$-k\left.\frac{\partial T}{\partial X}\right|_{X=0} = q \tag{B.4}$$

$$-k\left.\frac{\partial T}{\partial X}\right|_{X=L(t)} = \rho H \frac{dL}{dt} \tag{B.5}$$

$$L(0) = L_0 \tag{B.6}$$

Here a = thermal diffusivity, k = conductivity, ρ = density, and H = latent heat of fusion.

This is a penetration-type boundary layer problem in which the "disturbance", q, propagates from $X = 0$ as the boundary layer thickness

$$\delta(t) = \sqrt{6at} \tag{B.7}$$

to reach the phase-change boundary in time t_1, where $\delta(t_1) = L_0$ [Arpachi and Larsen 1984]:

$$t_1 = L_0^2/6a \tag{B.8}$$

During this time interval, $0 \le t \le t_1$, the wall temperature increases as

$$T_w = T_m + q\delta(t)/2k = T_m + q\sqrt{(6at)}/2k$$

with

$$T_{w1} = T_w(t_1) = T_m + qL_0/2k \tag{B.9}$$

(B.10)

No changes occur at the phase-change boundary until $t > t_1$. It is noted, however, that for arbitrarily thin initial liquid layers ($\lim\{L_0\} \rightarrow 0$), both t_1 and $\delta(t)$ approach zero, so that there is no temperature increase in this limit. This is the case when the solid PCM initially contacts the canister wall.

Two time scales are evident in the system, (B.1) to (B.6), the diffusion time, $t_d = L_0^2/a$, and the phase-change time, $t_p = \rho HL_0/q$, with $t_d << t_p$. This makes the system a classical

singular perturbation problem in time, which may be solved by asymptotic expansions or multivariable methods [Nayfeh 1981, Smith 1985]; in combination with the integral approximation [Arpachi and Larsen 1984] this yields to lowest order the composite expansion

$$T_w = T_{w1} + \frac{q^2}{k\rho H}(t-t_1) + \frac{qL_0}{2k}\left[1 - e^{-3a(t-t_1)/L_0^2}\right] \qquad (B.11)$$

It is seen in (B.12) that there is a discontinuity in wall temperature as represented by the "inner-time" exponential. But, again, for $L_0 \dashrightarrow 0$, this singularity is removed and only the outer, "quasi-steady" solution remains:

$$T_{w,outer} = T_m + \frac{q^2}{k\rho H}\, t \qquad (B.12)$$

It is noteworthy that the linear outer-time solution satisfies the initial condition $T_w(0) = T_m$, in contrast to the conventional temperature Stefan problem where the initial wall temperature at t_0^+ is not T_m.

Therefore, for the solid PCM initially contacting the canister wall, or for small initial liquid layers, there is no significant boundary layer effect, or effect of the liquid specific heat, and the outer-time solution provides the whole solution to the problem. This conclusion is also reached when the initial temperature profile is different from constant at T_w.

PART II

RADIATION AND PHASE-CHANGE OF MONOCRYSTALLINE LITHIUM-FLUORIDE IN AN ANNULAR ENCLOSURE WITH SPECIFIED HEAT FLUX

by

Kurt O. Lund
135 Sixth Street
Del Mar, CA 92014

Abstract

A two-band radiation model is utilized for radiation exchange of LiF contained within an annular canister, and its effect on phase change is evaluated. Linearization and the quasi steady approximation leads to simplified one-dimensional heat transfer models, having a specified heat flux at one boundary and either an adiabatic or convective condition at the other, and to several exact solutions.

For the adiabatic case, radiation caused phase-change to occur from both boundaries, and eliminated the influence of solid conductivity; for the convective case, partially melted steady-state conditions, and fully melted conditions were determined to depend on the heat flux level, with radiation extending the melting times.

Radiative exchange between the two walls was found to be about twice as high for the LiF medium as for vacuum, but the overall effect of radiation was limited to about ten percent of the total heat transfer rate for practical heat flux levels and annulus dimensions. Further analysis is required to access the effect of voids within the enclosure, where radiation may have a stronger effect.

NOMENCLATURE

a	bsorption coefficienty 1/(cs)
a,b	fitted constants
C	modified blackbody radiosity (W/cm^2)
c	radiation constant
e	emmissive power (W/cm^2)
f	emissivity fractional function
g	scaled, nondimensional heat flux)
H	latent heat of fusion (J/g)
h	heat transfer coefficient (W/cm^2K)
k	extinction coefficient, thermal conductivity (W/cmK)
N	radiation number
n	refractive index
Q	heat transfer rate per unit length (W/cm)
q	heat flux (W/cm^2)
q+	radiosity (W/cm^2)
R	radiation or thermal network resistance (cm^{-2}), (cm-K/W)
r	electrical resistivity (Ohm-cm), radius (cm)
T	absolute temperature (K)
t	time minutess)
u,v,w	logarithmic conduction terms

Greek

α	absorptivity
β	convection Biot number
δ	scaled liquid thickness
ϵ	emissivity
ϕ	fraction of limiting heat fluxes
Γ	radius ratio
θ	nondimensional surface temperature
κ	ratio of eff. solid to eff. liquid conductivity
λ	wave length
Λ	$1 - \Gamma$
ρ	density (g/cm^3), reflectivity
σ	Stefan-Boltzmann constant (W/cm^2K^4)
τ	nondimensional time
ξ	integration variable

Subscripts

0	pertaining to T_0
a	pertaining to transparent upper limit,
b	blackbody
e	effective

f	fluid of convection boundary
h	convection boundary
i	surface i
k	conduction
ℓ	liquid
m	melting or phase-change temperature
n	normal direction
r	radiation, reference
s	solid, source
v	vacuum
λ	spectral quantity
1,2	surfaces 1 and 2
0,1,2	flux limits

1. INTRODUCTION

The behavior of phase transition is central to the understanding of phase-change thermal energy storage for development of Solar Dynamic Space Power [e.g., Labus et al. 1989]. Therefore, ground tests have been conducted [Strumpf and Coombs 1990], Space Shuttle flight experiments have been planned [Namkoong 1989a, 1989b], and numerical analyses have been performed to determine two and three dimensional effects of the phase transition process [Kerslake and Ibrahim 1990, Wichner et al. 1988]. These analyses and experiments utilize an annular canister containing the phase change material (PCM), where a solar heat flux (or electrically simulated flux) is impressed on the outer wall of the canister (radius r_1), and convection at the inner wall (radius r_2). In the Flight Experiments the convection is simulated by conduction in a rod and subsequent radiation to space [Lund 1991]; the effect is a near adiabatic condition at r_1 during application of the heat flux at r_2.

In application to heat receivers the PCM's are high-temperature salts, such as lithium-fluoride (LiF) with a melting temperature of 1120 K (1556 F), or the eutectic $LiF-CaF_2$ which melts at 1040 K (1412 F). At these temperatures radiative transport may be a significant part of the overall heat transfer processes within the canisters. In the previous two-dimensional model [Kerslake and Ibrahim 1990] radiation was not included, and in the three-dimensional model [Wichner et al. 1988] the effect of radiation is obscured by the complexity of the numerical computations; in the flight experiments [Namkoong 1989] radiation will occur naturally, but the radiative effect cannot be determined directly as only canister surface temperatures will be measured. Combined convection and radiation in vacuum was investigated for a square enclosure [Yucel et al. 1989], radiation with scattering in an annulus was considered [Tsai and Ozisik 1990], and plane one-dimensional combined radiation, conduction and phase change was investigated for low-temperature ablation [Yuen and Khatami 1990] and ice removal [Song and Viskanta 1990]. There is, however, a need for basic models and solutions for the high-temperature enclosure with PCM and radiation; to this end a one-dimensional analysis is here presented. The present analysis is limited to monocrystalline salts in contact with the canister walls; the presence of voids and/or polycrystalline structure will be treated in a separate publication.

Although the canisters invariably are finite in length, and actual heat fluxes may be circumferentially and axially non-uniform, there are a number of reasons why a one-dimensional approximation is useful:

a) closed-form or simplified solutions are possible which illustrate the basic phenomenological interactions;
b) solutions provide bases against which complex numerical models may be compared for identical boundary conditions;
c) solutions provide ready estimation of experimental behaviors, such as surface temperature-time variations;
d) the phase-change process is predominantly one-dimensional in the radial direction for canisters with larger length-to-thickness aspect ratios. This was the case even at a lower ratio [Kerslake and Ibrahim 1990].

Radiation within the canister enclosure follows conventional exchange between diffuse surfaces, except that the intervening medium, LiF, has spectral properties which differ from those of vacuum. Therefore, accurate application requires spectral integration. Following Williams [1988], and Song and Viskanta [1990], a two-band approximation is made utilizing recent measurements of LiF optical properties [Palik and Hunter 1985]. It is shown in Section 2 that at the melting temperature, Tm = 1120 K, the majority of radiation emissive power occurs in the transparent part of spectrum for LiF. For the smaller part at longer wavelengths, a "thick-gas" approximation is used which adds a term to the apparent thermal conductivity.

The emissive properties of the metal canister surfaces is assumed to follow the Hagen-Rubens relation. With the spectral properties of LiF this leads to a spectrally integrated emissivity fractional function which is the ratio of the average emissivity of the surface contacting LiF to the emissivity of the surface in vacuum at the same temperature.

A two-surface thermal model is developed in Section 3 for adiabatic and convective boundary conditions at the inner radius, and imposed heat flux at the outer radius. This differs from the usual Stefan problem where the temperature at a boundary is suddenly changed [e.g., Yao and Prusa 1989, Burmeister 1983, or Solomon 1981], resulting in a boundary layer growing in time as the error function [e.g., Arpaci and Larsen 1984]. However, with the presently imposed heat flux boundary condition, this layer does not develop, with the result that surface temperatures change only slowly in a quasi-steady fashion, as was previously observed [Song and Viskanta 1990]; this phenomenon is utilized presently as the quasi-steady approximation.

Besides the quasi-steady approximation in the liquid, it is further assumed that the conduction limit applies, such that natural convection boundary layers do not develop

significantly and such that the phase-change boundary remains axially uniform. This is valid for Rayleigh numbers below 1700, for rectangular enclosures [Incropera and DeWitt 1985, p. 401], but has also been demonstrated experimentally for much larger Rayleigh numbers with a heat flux boundary and an aspect ratio of 4.5 [Zhang and Bejan 1989]. This is considered an excellent approximation under 1-g axial gravitational acceleration; under microgravity conditions the magnitude of natural convection is suppressed, although some convection effects can be present [Bayazitoglu and Lam 1987, Arnold et al. 1990].

The results of the analysis in Section 4 are that, with an adiabatic inner wall, the rate of melting of the PCM is independent of radiative and conductive effects within the annulus, but depends only on the heat flux at the outer wall, and the volume and heat of fusion of the PCM. The effect of radiation and liquid conduction is to redistribute energy and cause melting of the solid PCM at both its outer and inner surfaces; solid conductivity did not enter into this process. With convection at the inner wall, melting occurred from the outer wall, only, at practical flux levels, and a partially melted steady-state condition was found for moderate fluxes; at a somewhat higher flux, complete melting is shown, with the required time dependent on all problem parameters.

Although the radiative effect in LiF is about twice that in vacuum, the radiation/conduction number is quite small for the annulus geometries considered, and the effect on phase-change remains small compared to conduction. Nevertheless, the effect is significant, and a simplified radiation model should be included in analytical and numerical models.

2. TWO-BAND RADIATION MODEL

The effect of radiation within the enclosure is determined using the optical properties of LiF: refractive index, n, and absorptive index, or extinction coefficient, k. A summary of recent measurements is shown in figures 2-1 and 2-2 for the spectral region of interest [Palik and Hunter 1985]; also shown is the Planck spectral emissive power for the melting temperature, 1120 K, which shows that emissions whithin the canister lie primarily between 1 μm and 6 μm. It is seen that there is a transparent region of the spectrum near 1 μm (where k --> 0); the refraction index appears relatively constant in this region, but decreases somewhat with increasing wave length. In addition to the optical properties of the LiF, the canister surface properties are required, as will be shown.

2.1 Emissivity and Absorptivity

The assumption is made in this analysis that the metal surfaces bounding the LiF are diffuse. For spectral emissivity, ε_λ, the emissive power of the surface is given by [Sparrow and Cess 1978]

$$e_a = \int_0^{\lambda_a} \varepsilon_\lambda e_{b\lambda} d\lambda = \sigma T_s^4 \frac{15}{\pi^4} \int_{\xi_a}^{\infty} \frac{n^3}{n + \lambda n'} \varepsilon_\lambda \frac{\xi^3 d\xi}{e^\xi - 1} \qquad (2.1)$$

where $\xi = c_2/n\lambda T$, $\xi_a = c_2/n_a\lambda_a T = c_3/T = 1995(K)/T$, $n' = dn/d\lambda$, and where c_2 is the radiation constant, $c_2 = 14{,}388$ μmK. Here, the index of refraction for LiF is the spectral quantity shown in figure 2-1, which is approximated as

$$n = 1.39 - 0.00271\lambda^2 = a - b\lambda^2 \qquad (2.2)$$

and the upper limit of integration is taken as $\lambda_a = 5.5$ μm.

For the metal surfaces bounding the LiF the Hagen-Rubens relation is assumed for the spectral normal emissivity [e.g., Sparrow and Cess 1978]

$$\varepsilon_{\lambda n} = 36.5\sqrt{r/\lambda} \qquad (2.3)$$

where r is the electrical resistivity in Ohm-cm, and λ is the wavelength in μm. The result in vacuum of spectrally integrating

(2.3) is the total normal emissivity

$$\varepsilon_{n,v} = 0.576\sqrt{rT_s} \tag{2.4}$$

where T_s is the surface temperature in degrees Kelvin. The form (2.3) applies well to resistive alloys, such as stainless steel [Edwards and Bayard de Volo 1975, as quoted in Edwards 1981], and is assumed here to represent, approximately, other canister materials such as the Haynes alloy [Strumpf and Coombs 1990].

Let r be proportional to the absolute temperature, then $r = r_0 T_s/T_0$, where r_0 is the resistivity at temperature T_0, and where from (2.4) the total normal vacuum emissivity at this temperature is $\varepsilon_{0,v}$. Substitution of these variables into (2.3) results in the normal (or hemispherical) emissivity ratio

$$\frac{\varepsilon_\lambda}{\varepsilon_{0,v}} = \frac{36.5}{0.576T_0}\sqrt{T_s/\lambda} = \frac{T_s}{T_0} c_4 \sqrt{n\xi} \tag{2.5}$$

where c_4 is the nondimensional number, $c_4 = 36.5/0.576\sqrt{c_2} = 0.529$. Now, substitution of (2.5) into (2.1) results in

$$e_a = \sigma T_s^4 \left[T_s/T_0\right] \varepsilon_{0,v} f_{\varepsilon a}(T_s) \tag{2.6}$$

where the emissivity fractional function is defined by

$$f_{\varepsilon a}(T) = c_4 \frac{15}{\pi^4} \int_{\xi_a}^{\infty} \frac{n^3}{n + \lambda n'} \sqrt{n\xi} \frac{\xi^3 d\xi}{e^\xi - 1} \tag{2.7}$$

This function is shown in figure 2-3 for $\lambda_a = 5.5$ μm, where it is seen that the effective total emissivity is roughly twice that of the value in vacuum:

$$\varepsilon_a(T_s) = \varepsilon_{0,v} (T_s/T_0) f_{\varepsilon a}(T_s) \tag{2.8}$$

A completely similar procedure yields the effective absorptivity

$$\alpha_a(T_s,T_e) = \varepsilon_{0,v} \frac{\sqrt{T_s T_e}}{T_0} f_{\varepsilon a}(T_e) \tag{2.9}$$

where T_e is the environment (other surface) temperature.

For subsequent calculations, the emissivity function is approximated as

$$f_{\varepsilon a} = 2.07(T/T_m)^{0.278} = f_{\varepsilon m}(T/T_m)^s \qquad (2.10)$$

Although the preceding model is approximate, it nevertheless incorporates the essential features of emission and absorption of the surfaces bounding the LiF in its transparent region. In any event, results cannot be more accurate than $\varepsilon_{0,v}$ is known. In the subsequent calculations, T_0 is taken as T_m, such that $\varepsilon_{0,v} = \varepsilon_{m,v}$ and the above temperature dependence need only be accurate near the melting temperature, T_m.

2.2 Thick Gas Approximation

It would appear from figure 2-2 that k is sufficiently small for the wavelengths of interest that the medium can be considered perfectly transparent. there is, however, a region at the longer wavelengths where absorption occurs in the medium, as can be shown by evaluating the absorption coefficient [Siegel and Howell 1981, p. 427] from the data of Palik and Hunter [1985]:

$$a_\lambda = \frac{4\pi k}{\lambda} , \qquad (2.11)$$

as shown in figure 2-4. These values may also be read as the optical thickness for a 1 cm layer of LiF (or as half the optical thickness for a 2 cm layer). The results are in general agreement with previous measurements [Amr. Inst. Phys. Handbook 1957]; thus, the assumption of an optically thick gas above λ = 6 or 7 μm is supported by the more recent measurements. The net effect is an additive term to the LiF thermal conductivity [Williams 1988]:

$$k_r = \frac{16\sigma n^2 T^3}{3a_\lambda} \approx 0.02\frac{T(K) - 320}{800} \ [W/cmK] \qquad (2.11a)$$

Since, as seen in figure 2-1, there is but little radiant energy at the higher wavelengths, this two-band radiation model is considered an adequate approximation, especially in view of uncertainties associated with the canister surface properties.

2.3 Radiant Energy Exchange

For each surface, i, in the enclosure the net radiative heat transfer rate can be expressed as follows,

$$Q_i = \frac{C_i - q_i^+}{R_i} \tag{2.12}$$

where q_i^+ is the radiosity, where $C_i = \varepsilon_i \sigma T_i^4 / \alpha_i$ is the modified blackbody radiosity, and where the surface resistance is

$$R_i = \frac{1 - \alpha_i}{\alpha_i A_i} \tag{2.13}$$

These relations may be combined with formulas for radiosity between surfaces [e.g., Edwards 1981, p. 117] so that conventional radiation network solutions may be used with the modified blackbody surface radiation, and with the surface resistance given by (2.13). A closed-form analytical solution is, of course, not possible as α_i depends on the "other-surface" temperatures, as shown in (2.9); however, an adequate iterative solution can be obtained with a weighted average for T_e. For a two-surface enclosure, (2.12) and (2.13) yield

$$Q_1 = -Q_2 = \frac{C_1 - C_2}{\frac{1 - \alpha_1}{A_1 \alpha_1} + \frac{1}{A_1 F_{12}} + \frac{1 - \alpha_2}{A_2 \alpha_2}} \tag{2.14}$$

or, with $F_{21} = 1$, $\Psi = T/T_m$, and (2.8) to (2.10), the radiation exchange is

$$Q_1 = A_1 \sigma T_m^4 P(\Psi_1, \Psi_2) \tag{2.15}$$

where

$$P(\Psi_1,\Psi_2) = \frac{\Psi_1^{5+2s} - \Psi_2^{5+2s}}{\frac{1}{\varepsilon_{m,v} f_{\varepsilon m}}\left[\Psi_1^{s} + \frac{A_1}{A_2}\Psi_2^{s}\right] - 1} \tag{2.16}$$

A linearization of (2.16) about $T = T_m$ ($\Psi = 1$) results in

$$P(\Psi_1,\Psi_2) = K_{r1}(\Psi_1 - \Psi_2) \tag{2.17}$$

where

$$K_{r1} = \frac{5 + 2s}{\frac{1}{\varepsilon_{m,v} f_{\varepsilon m}}\left[1 + A_1/A_2\right] - 1} \tag{2.18}$$

Since, as will be shown, wall temperatures differ only slightly from T_m, the linearization is valid and within the accuracy of other approximations made.

3. HEAT TRANSFER MODEL

The PCM contained by the annular canister in the Flight Experiment [Namkoong 1989], as well as in applications with annular geometry [Strumpf and Coombs 1990], is to cycle between the charging (heat addition) and discharging (heat removal) modes. In the first mode heat is added to (impressed upon) the large-diameter, outer wall to melt the PCM while some heat transfer may or may not occur at the small-diameter, inner wall; in the second mode, heat is transferred from the inner wall to solidify the PCM while the outside wall is, more or less, insulated.

We consided the basic charging mode where at time zero the external heat source is Q_s(W/m) and the PCM is 100% solid and at temperature, T_m, at the outer wall. Furthermore, to obtain a basic (or fundamental) solution, an infinitely long cylinder is assumed together with axis-symmetric heat input. Additionally, axial gravitational acceleration is assumed such that any void is removed to the end region, and such that liquid remains continuously in contact with the two walls and the phase-change boundaries.

The above assumptions result in a radially one-dimensional time-dependent system, as illustrated in figure 3-1. Because of the transparent part of the LiF spectrum there is radiation from the outer wall (surface 1) to the inner wall (surface 2), represented by resistance, R_r. Two boundary conditions are considered on the inner wall: a) adiabatic condition, which is representative of the Flight Experiment [Namkoong 1989], and b) convective condition, which represents the Space Station [Strumpf and Coombs 1990] (although this application uses the eutectic LiF-CaF_2 as PCM, the preceding optical properties of LiF are used in sample calculations, as seen in Table 3-1).

In case *a* the inner wall acts as a refractory or reradiation surface, such that the energy source, Q_s, causes phase change at both melt-surfaces, 1m and 2m, as shown in figure 3-1(a). The result is that the solid PCM remains at the initial uniform temperature, T_m, until complete melting has occured; thus, solid properties do not enter in to this heat transfer problem (i.e., $R_{ks} = \infty$).

In case *b* the inner wall act as a heat sink whenever $T_2 > T_f$;

therefore, T_2 will initially be less than $T_1(0) = T_m$, as shown in figure 3-1(b). Thus, no initial melting occurs at the inner wall (i.e., $R_{k2} = 0$); however, with radiation, a high enough imposed heat flux can exist for which T_2 reaches T_m before complete melting. With the convective boundary and initial conditions there is conduction in the solid, as well as in the liquid.

Finally, the quasi-steady and radiation-linearization approximations are made. The first of these is permissible because no temporal, mathematical boundary layers occur with the heat-flux boundary condition (in contrast to the conventional Stefan problem with specified temperatures), as will be shown, and because diffusion in the solid is exceedingly rapid (on the order of a few seconds) compared to the melting process; the effect in case *a* is to render the inner wall adiabatic, as the "plug" wall material rapidly reaches uniform temperature, T_2, throughout; in case *b* the effect is to quickly establish the initial temperature profile, with $T_1(0) = T_m$, from a uniform condition at fluid temperature, T_f. Linearization of the radiation term simplifies the model equations, reduces by one the number of problem parameters, and results in some closed-form analytical solutions; this approximation resulted in less than 3% error.

Solidification, or discharging, occurs for case *b* in the reverse direction, with $Q_s = 0$ and sink temperature, T_f; minor heat loss from the outer wall is not included. For case *a* the heat removal process has a strong axial component [Lund 1991] and, therefore, is beyond the scope of the present formulation; however, the results of this investigation may assist in future modeling of that two-dimensional problem.

Although the above stated problem is quite restrictive from a practical view, it nevertheless results in simple equations and solutions, to which more general numerical solutions may be compared. Additionally it enhances our basic understanding of the phase-change process when radiation is included.

3.1 Model Equations

The model considered is for a solid region surrounded by liquid at either or both radii r_{1m} and r_{2m}, as indicated in figure 3-1. In these annular liquid gaps convection will be driven by the temperature field, but without feedback to the thermal process for small Rayleigh numbers and an infinitely long annulus with

axial gravitational acceleration [Arpaci and Larsen 1984]. Thus, the conduction heat transfer from surface i to im (i = 1 or 2) is given by:

$$Q_{ki} = \frac{T_i - T_{im}}{R_{ki}} \qquad (3.1)$$

where resistances are

$$R_{k1} = \frac{\ell n(r_1/r_{1m})}{2\pi k_{e\ell}} \quad , \quad R_{k2} = \frac{\ell n(r_{2m}/r_2)}{2\pi k_{e\ell}} \qquad (3.2,3)$$

and the effective liquid conductivity is $k_{e\ell}$. Similarly

$$Q_{ks} = \frac{T_{1m} - T_{2m}}{R_{ks}} \quad , \quad R_{ks} = \frac{\ell n(r_{1m}/r_{2m})}{2\pi k_{es}} \qquad (3.4,5)$$

$$Q_{h2} = h_f A_2 (T_2 - T_f) \qquad (3.6)$$

Energy balances on surfaces 1 and 2 yield, respectively

$$Q_s = Q_{k1} + Q_{r1} \quad , \quad Q_{r1} = Q_{k2} + Q_{h2} \qquad (3.7,8)$$

where Q_{r1} is given by (2.15), and (2.16) or (2.17). At the phase boundaries the heat added results in the movement of the boundaries through $H_{s\ell}$, the latent heat:

$$Q_{k1} - Q_{ks} = - 2\pi \rho_\ell H_{s\ell} r_{1m} \frac{dr_{1m}}{dt} \qquad (3.9)$$

$$Q_{k2} + Q_{ks} = + 2\pi \rho_\ell H_{s\ell} r_{2m} \frac{dr_{2m}}{dt} \qquad (3.10)$$

3.2 Adiabatic Inner Wall (Case a)

For the adiabatic inner wall, with $R_{ks} = R_h = \infty$, the above energy balances and rate equations combine as follows:

$$(1 - \Lambda\delta_1)\frac{d\delta_1}{d\tau} = 1 - N(\theta_1 - \theta_2) \qquad (3.11)$$

$$(\Gamma + \Lambda\delta_2)\frac{d\delta_2}{d\tau} = 0 + N(\theta_1 - \theta_2) \qquad (3.12)$$

$$N(\theta_1 - \theta_2) + \frac{\theta_1}{v} = 1 \qquad (3.13)$$

$$N(\theta_2 - \theta_1) + \frac{\theta_2}{u} = 0 \qquad (3.14)$$

where δ_1 and δ_2 are the scaled liquid-gap thicknesses,

$$\delta_1 = \frac{r_1 - r_{1m}}{r_1 - r_2} = \frac{1 - r_{1m}/r_1}{\Lambda} \qquad (3.15)$$

$$\delta_2 = \frac{r_{2m} - r_2}{r_1 - r_2} = \frac{r_{2m}/r_1 - \Gamma}{\Lambda} \qquad (3.16)$$

the scaled excess temperatures ($i = 1,2$) are,

$$\theta_i = (T_i - T_m)/T_r \qquad (3.17)$$

the logarithmic terms are,

$$v = \ell n\{1/(1-\Lambda\delta_1)\}/\Lambda, \quad u = \ell n\{1+\Lambda\delta_2/\Gamma\}/\Lambda \qquad (3.18,19)$$

the radiation number is,

$$N = \sigma T_m^3 K_{r1}(r_1 - r_2)/k_{e\ell} = h_{r1}(r_1 - r_2)/k_{e\ell} \qquad (3.20)$$

where $\tau = t/t_r$, $\Gamma = r_2/r_1$, $\Lambda = 1 - \Gamma$, and where the reference temperature and time magnitudes, T_r and t_r, are determined as

$$T_r = \frac{q_r(r_1 - r_2)}{k_{e\ell}}, \quad t_r = \frac{(r_1 - r_2)\rho_\ell H_{s\ell}}{q_r} \qquad (3.21,22)$$

with $q_r = q_s$ for case *a*. Typical parameter values are shown in Table 3-1. It is noted that the time constant represents the ratio of the mass of PCM times the latent heat, divided by the source flux applied at the arithmetic average radius. The initial conditions for case *a* are that all $\theta_i(0) = \delta_i(0) = 0$.

3.3 Convective Inner Wall (Case b)

For the convective boundary condition on the inner wall, with $R_{k2} = 0$ ($T_{2m} = T_2$) and $T_r = T_m - T_f$, the energy balances and rate equations combine as follows:

$$(1 - \Lambda\delta_1)\frac{d\delta_1}{d\tau} = g_s - \beta\Gamma(1 + \theta_2) \tag{3.23}$$

$$N(\theta_1 - \theta_2) + \frac{\theta_1}{v} = g_s \equiv \frac{q_s}{q_r} \tag{3.24}$$

$$N(\theta_2 - \theta_1) + K\frac{\theta_2}{w} = -\beta\Gamma(1 + \theta_2) \tag{3.25}$$

where the additional logarithmic term is

$$w = \ell n\{(1-\Lambda\delta_1)/\Gamma\}/\Lambda \tag{3.26}$$

the effective conductivity ratio is $K = k_{es}/k_{e\ell}$, the Biot number is $\beta = h_f(r_1 - r_2)/k_{e\ell}$, and where q_r is obtained from (3.21).

4. RESULTS

4.1 Adiabatic Inner Wall (Case a)

From (3.11) and (3.12) it is seen that their sum is independent of the radiation number:

$$(1 - \Lambda\delta_1)\frac{d\delta_1}{d\tau} + (\Gamma + \Lambda\delta_2)\frac{d\delta_2}{d\tau} = 1 \qquad (4.1)$$

which has the exact integral

$$\delta_1 + \Gamma\delta_2 - \frac{\Lambda}{2}\left[\delta_1^2 - \delta_2^2\right] = \tau \qquad (4.2)$$

In particular for $\delta_1 + \delta_2 = 1$, when the solid is completely melted, (4.2) yields the maximum τ, or scaled melting time

$$\tau_m = \frac{1 + \Gamma}{2} = \frac{r_1 + r_2}{2r_1} \qquad (4.3)$$

or, with the definition of the time constant, the time for charging or melting the PCM in the annulus is obtained as

$$t_m = \frac{\pi(r_1^2 - r_2^2)\rho_\ell H_{s\ell}}{2\pi r_1 q_s} \qquad (4.4)$$

That is, the melting time is precisely the phase-change heat content divided by the total rate of heat input, independent of radiative and conductive properties. This, of course, is a consequence of the energy balance and the adiabatic boundary condition which restrict the phase-change process as the only sink for the source, $2\pi r_1 q_s$.

The above behavior can be seen analytically for the limiting condition $\Lambda \dashrightarrow 0$ ($\Gamma \dashrightarrow 1$) which is the parallel plate limit. In this limit, the system (3.11) to (3.14) can be combined as

$$\frac{d(N\delta_1)}{d(1+N\tau)} + \frac{N\delta_1}{1 + N\tau} = 1 \qquad (4.5)$$

which, with (4.2), has the solutions

$$N\delta_1 = \frac{N\tau}{2}\left[\frac{2 + N\tau}{1 + N\tau}\right], \quad N\delta_2 = \frac{N\tau}{2}\left[\frac{N\tau}{1 + N\tau}\right] \qquad (4.6,7)$$

$$N\theta_1 = N\tau\left[\frac{2 + N\tau}{4}\right]\frac{1 + (1+N\tau)^2}{(1 + N\tau)^3}, \quad N\theta_2 = \frac{2 + N\tau}{4}\left[\frac{N\tau}{1 + N\tau}\right]^3 \qquad (4.8,9)$$

These solutions are shown in figures 4-1 and 4-2, where the double surface phase-change phenomenon is clearly evident. It is seen in (4.6,7), and in figure 4-1, that δ_1 grows linearly with τ for small $N\tau$ (i.e., initially), whereas δ_2 grows quadratically; moreover, the growth of δ_2 depends on the radiation number, N, as seen by the ratio (4.10) of (4.7) to (4.6)

$$\frac{\delta_2}{\delta_1} = \frac{N\tau}{2 + N\tau}, \quad \frac{\theta_2}{\theta_1} = \frac{(N\tau)^2}{1 + (1+N\tau)^2} \qquad (4.10,11)$$

where $\delta_2 \dashrightarrow 0$ for $N \dashrightarrow 0$, and $\delta_2 \dashrightarrow \delta_1$ for $N \dashrightarrow \infty$. That is, for small radiation number the phase change will occur primarily from side 1, whereas for a large radiation number it will occur equally from both sides; for N = 1 and the end of the charging process where in the present case $\tau = 1$, the ratio of phase growths in (4.10) is 1:3. However, depending on the surface emissivities, N and the radiation effect can be quite small, as indicated in Table 3-1.

In the present formulation, wall temperatures are determined rather than specified, as in figure 4-2. The gradual increase in the wall temperatures (absence of thermal boundary layers) validates the quasi-steady approximation, and with T_r = 26.6 K, the small changes of T_1 and T_2 from T_m validates linearization of the radiation term. In (4.8,9,11), and in figure 4-2, it is seen that initially θ_1 increases linearly with τ, but that θ_2 increases cubically with τ.

In the case of an annulus with finite radii ($r_2/r_1 = \Gamma \neq 1$), equations (3.19) to (3.22) were solved by numerical integration, with results as shown in figure 4-3, to the same scale as previously, but for Γ = 0.5. Here the phase front movements were calculated for the series of radiation numbers shown, up to the maximum time $\tau_m = (1+\Gamma)/2 = 3/4$. There appears to be no dependence of $N\delta_2$ on N, and only slight dependence for $N\delta_1$;

however, the curves are shifted somewhat, relative to the "planar annulus" result in figure 4-1. Without the N-scaling, the phase fronts appear as in figure 4-4 for the radius ratio, 0.5.

4.2 Convective Inner Wall (Case b)

With the convection heat sink at the inner wall, the possibility exists that q_s may not be sufficient to cause any melting at all. This is seen in (3.23) where the initial slope must be positive for δ_1 to grow; thus, g_s must be greater than the minimum

$$g_{s0} = \beta\Gamma(1 + \theta_{20}) = \beta\Gamma \frac{N + K/w_0}{N + K/w_0 + \beta\Gamma} \qquad (4.12)$$

where θ_{20} is obtained from (3.25) with $\theta_{10} = 0$:

$$\theta_{20} = \theta_2(0) = \frac{-\beta\Gamma}{N + K/w_0 + \beta\Gamma} \qquad (4.13)$$

where $w_0 = \lim(w)$ as $\delta_1 \dashrightarrow 0$. In dimensional variables with $h_{r1} = \sigma T_m{}^3 K_{r1}$, the limiting minimum heat flux for phase change to occur is

$$q_{s0} = \frac{T_m - T_f}{\frac{r_1}{h_f r_2} + \frac{r_1}{h_{r1} r_1 + k_s/\ell n(r_1/r_2)}} \qquad (4.15)$$

which is the initial overall temperature difference over the total thermal resistance.

Similarly, there is a critical heat flux for which the PCM just becomes 100% melted and at steady state with zero slope at $\delta_1 = 1$. This is given by (3.23) as:

$$g_{s1} = \beta\Gamma \qquad (4.16)$$

which, in dimensional terms, simply is

$$q_{s1} = h_f(T_m - T_f)r_2/r_1 \qquad (4.17)$$

Finally, it may be asked if there is a q_s above which melting also occurs at the inner wall. This limit is given by (3.24) and (3.25) with $\theta_2 = 0$:

$$g_{s2} = \beta\Gamma\left[1 + \frac{1}{Nw_0}\right] \qquad (4.18)$$

However, for small N as in Table 3-1, this flux limit is quite high so that (unlike case *a*) two-surface melting does not usually occur with the convective boundary condition and practical flux levels.

To summarize these conditions we have case *b0* ($g_s \leq g_{s0}$) which results in no phase change, *b1* ($g_{s0} < g_s < g_{s1}$) which results in a steady state with only partial melting, *b2* ($g_{s1} \leq g_s \leq g_{s2}$) which results in 100% melting in finite time from the outer surface only, and *b3* ($g_s > g_{s2}$) which results in melting from both surfaces.

The numerical integration of (3.23) to (3.25) for case *b1* is shown in figure 4-5, where the scaled heat flux was taken as

$$g_s = \phi g_{s1} + (1 - \phi)g_{s0}\ , \quad 0 \leq \phi \leq 1 \qquad (4.19)$$

The partially melted, steady state condition is evident, as well as the effect of the surface emissivity. For comparison, computations were also made with the full nonlinear radiation term (2.16), but the results differed less than 3% from those in figure 4-5. Partially melted, and unmelted, conditions have also been found experimentally [Strumpf and Coombs 1990].

This steady state condition may also be seen analytically for the parallel plate limit, $\Lambda \dashrightarrow 0$, where the system equations combine as follows

$$\frac{dx}{Nd\tau} + \frac{\beta}{N}\frac{(N-x)(g_s x+N) + KN(1+x)}{(N-x)[1 + \beta(1+x)/N] + K(1+x)} = g_s \qquad (4.20)$$

where $x = N\delta_1$; this is a quadratic form which, with (4.19), has the steady state solution

$$\delta_{1,ss} = \frac{\phi(N + K + \beta)}{\phi\beta + N + K + (1-\phi)(K-1)N} \qquad (4.21)$$

For case *b2* the phase-change front grows rapidly to complete

melting, as shown figure 4-6, where the applied flux was taken as $g_s = \phi g_{s1}$. Also shown is the effect of radiation, which may be compared to other models where the effect of radiation was not included [Kerslake and Ibrahim 1990].

The discharge mode, in the present context, utilizes the same system equations, (3.23) to (3.25), but with $g_s = 0$. The result is the decay of δ_1 to 0, from the melt condition when the applied flux is turned off, as shown in figure 4-7 for several case *b2* conditions.

CONCLUSION

The phase-change behavior of a high-temperature salt enclosed in an annulus with specified outer-wall heat flux has been analyzed, including the effects of radiation within the enclosure and two inner-wall boundary conditions.

For the adiabatic inner wall condition, radiation resulted in the melting of solid PCM from two surfaces, and the time to complete melting is a fixed quantity.

For the convective inner wall condition, melting was found to occur from the outer wall, only (or not at all), for practical heat fluxes; partially melted or fully melted conditions were found depending on the flux level; the effect of radiation is to "by pass" the melting process and, thus, increase the time for complete melting.

For both boundary conditions, the imposed flux condition resulted in gradual changes in the wall temperatures, thus validating the quasi-steady models. This contrasts with the traditional Stefan problem with imposed rapid changes of the wall temperatures.

Radiative exchange between the two walls was found to be about twice as high for the LiF medium as for vacuum; however, wall temperatures differed only slightly from the melting temperature during the phase-change processes, and the overall effect of radiation was about ten percent of the total heat transfer rate for practical heat fluxes and annuli dimensions. This results from the assumption of continuous contact of the liquid PCM with the canister walls; further analysis is required to evaluate the effect of voids within the canister, where radiation would be more important.

REFERENCES

American Institute of Physics Handbook, McGraw-Hill, 1957.

Arnold, W., Gaug, J. R., and Chait, A., 1990, "Convection Phenomena in Low-Gravity Processing: The GTE GaAs Space Experiment," Paper No. AIAA 90-0409, Aerospace Sciences Meeting, Reno, Nevada, Jan. 8-11.

Arpaci, V. S. and Larsen, P. S., 1984, *Convection Heat Transfer*, Prentice-Hall.

Bayazitoglu, Y. and Lam T. T., 1987, "Marangoni Convection in Radiating Fluids," J. Heat Transfer, Vol. 109, pp. 717-721.

Burmeister, L. C., 1983, *Convective Heat Transfer*, Wiley & Sons, p 169.

Edwards, D. K., 1981, *Radiation Heat Transfer Notes*, Hemisphere Publishing.

Incropera, F. P., and DeWitt, D. P., 1985, *Introduction to Heat Transfer*, Wiley & Sons.

Kerslake, T. W. and Ibrahim, M. B., 1990, "Analysis of Thermal Energy Storage Material with Change-of-Phase Volumetric Effects", Proc. ASME Int'l Solar Energy Conf., Miami, FL, April 1-4, pp. 315-325.

Labus, T.L., Secunde, R.R., and Lovely, R.G., 1989, "Solar Dynamic Power for Space Station *Freedom*," Space Power, Vol. 8, Nos.1/2, pp. 97-114.

Lund, K.O., 1991, "Heat Rejection in Thermal Energy Storage Experiments for Solar Dynamic Power Development," Trans. ASME-JSME-JSES Solar Energy Conf., Reno, NV, March 17-20.

Namkoong, D., 1989a, "Thermal Energy Storage Flight Experiments", Proc. ASME Solar Energy Conference, San Diego, CA., April 2-5, pp. 19-24.

Namkoong, D., 1989b, "Flight Experiment of Thermal Energy Storage", Proc. 24th Intersociety Energy Conversion Engineering Conf., Washington, D.C., August 6-11.

NORVEX, NASA Oak Ridge Void Experiment Computer Program, ORNL, Oak Ridge, TN, (VAX version, June 1989).

Palik, E. D., and Hunter, W. R., 1985, "Lithium Fluoride (LiF)," *Handbook of Optical Constasnts of Solids*, Academic Press, pp. 675-693.

Siegel, R., and Howell, J. R., 1981, *Thermal Radiation Heat Transfer*, 2nd Ed, Hemisphere Publishing.

Solomon, A., 1981, "A Note on the Stefan Number in Slab Melting and Solidification," Letters Heat Mass Transfer, Vol 8, pp. 229-235.

Song, B., and Viskanta, R., 1990, "Deicing of Solids Using Radiant Heating," J. Thermophysics and Heat Trans., Vol. 4, No. 3, pp 311-317.

Sparrow, E. M., and Cess, R. D., 1978, *Radiation Heat Transfer - Augmented Edition*, McGraw-Hill.

Strumpf, H. J., and Coombs, M. G., 1990, "Solar Receiver Experiment for the Space Station Freedom Brayton Cycle," J. Solar Energy Eng., Vol 112, pp. 12-18.

Tsai, J.R., and Ozisik, M.N., 1990, "Radiation in Cylindrical Symmetry with Anisotropic Scattering and Variable Properties," Int. J. Heat Mass Transfer, Vol. 33, No. 12, pp. 2651-2658.

Wichner, R.P., et al., 1988, "Thermal Analysis of Heat Storage Canisters for a Solar Dynamic, Space Power System", Proc. ASME Solar Energy Conference, Denver, CO., April 10-14, pp. 319-328.

Williams, P. T., 1988, "Thermal Radiative Transport through Lithium Fluoride for Temperatures near the Melting Point," Report K/CSD/TM-77, Oak Ridge Gaseous Diffusion Plant, Oak Ridge, Tennessee,

Yao, L. S., and Prusa, J., 1989, "Melting and Freezing," *Advances in Heat Transfer*, Vol. 19, Academic Press, pp. 1-95.

Yuen, W.W., and Khatami, M., 1990, "Transient Radiative Heating of an Absorbing, Emitting, and Scattering Material," J. Thermophysics, Vol. 4, No. 2, pp. 193-198.

Yucel, A., Acharya, S. and Williams, M. L., 1989, "Natural Convection and Radiation in a Square Enclosure," Numerical Heat Transfer, Part A, Vol. 15, pp. 261-278.

Zhang, Z., and Bejan, A., 1989, "Melting in an Enclosure Heated at a Constant Rate," Int. J. Heat Mass Transfer, Vol. 32, No. 6, pp. 1063-1076.

Acknowledgement

This work was carried out under NASA contract NAG3-1106, Lewis Research Center, Cleveland, OH 44135.

Table 3-1. Typical Parameter Magnitudes

Parameter	Flight Exp.*	Space Station#	
Outer Radius, r_1 [cm]	3.51	2.11	
Inner Radius, r_2 [cm]	1.95	1.19	
PCM, Melting Temp., T_m [K]	LiF, 1120	$LiF-CaF_2$, 1040	
Latent Heat, $H_{s\ell}$ [J/g]	1037	816	
Liquid Density, ρ_ℓ [g/cm^3]	1.79	2.19	
Solid Density, ρ_s [g/cm^3]	2.33	2.59	
Liquid Conductivity, k_ℓ [W/cmK]	0.037	0.017	
Solid Conductivity, k_s [W/cmK]	0.060	0.038	
Radiation Cond., k_r [W/cmK]	0.020	0.018	
Radiation Nr., N ($\varepsilon_{m,v}$=0.1/0.3)	0.102/0.365	0.069/0.242	
Heat Source, q_s [W/cm^2] (avg./peak)	0.921/---	0.650/1.05	
Fluid Film Coeff., h_2 [W/cm^{2}K]	0	0.028	
Biot Number, β	0	0.81	
Fluid Temp., T_f [K] (min max)	---	800	1000
Temperature Scale, T_r [K]	26.6	240	40
Time Scale, t_r [minutes]	52.4	3.0	18
Heat Flux Limits [W/cm^2]			
q_{s0} ($\varepsilon_{m,v}$=0.1/0.3)		1.75/2.95	.29/.49
q_{s1}		3.79	.63
q_{s2} ($\varepsilon_{m,v}$=0.1/0.3)		45.5/15.7	7.6/2.6

* Namkoong 1989; Williams 1988.
\# Strumpf and Coombs 1990; Kerslake and Ibrahim 1990.

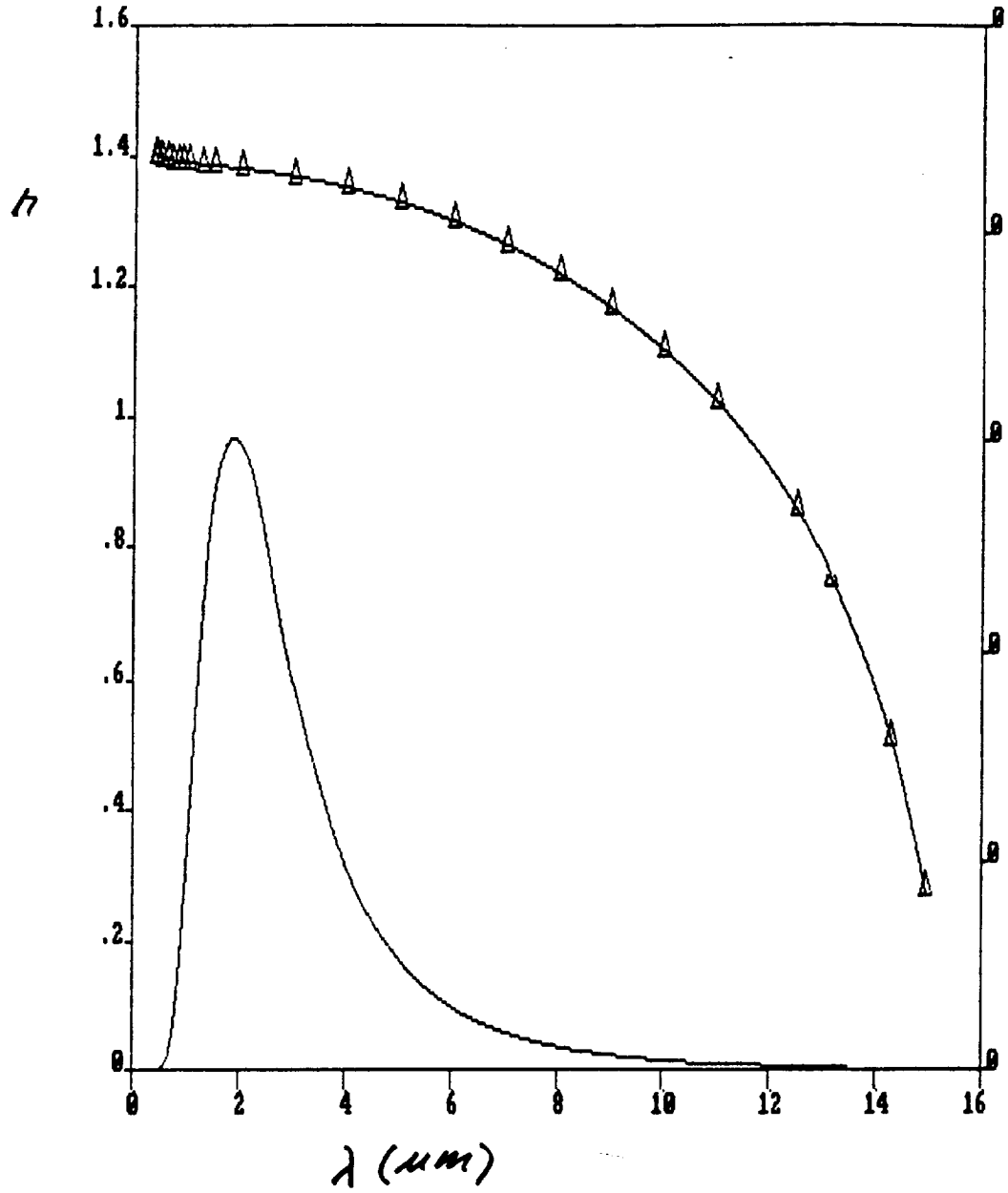

Fig. 2-1. Spectral Refractive Index for Lithium Flouride, and Blackbody Emissive Power at 1120 K.

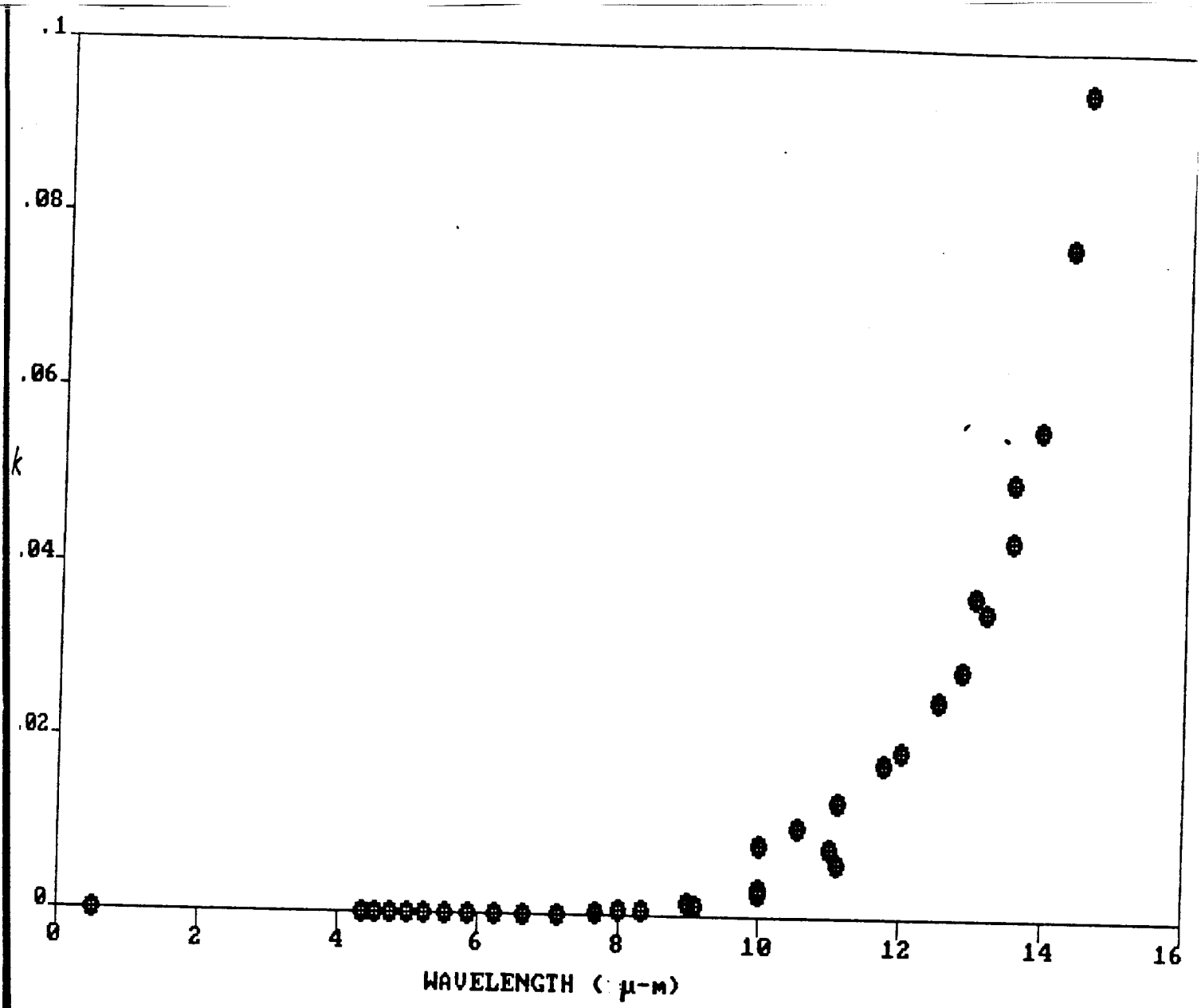

Fig. 2-2. Extinction Coefficient for Lithium Flouride.

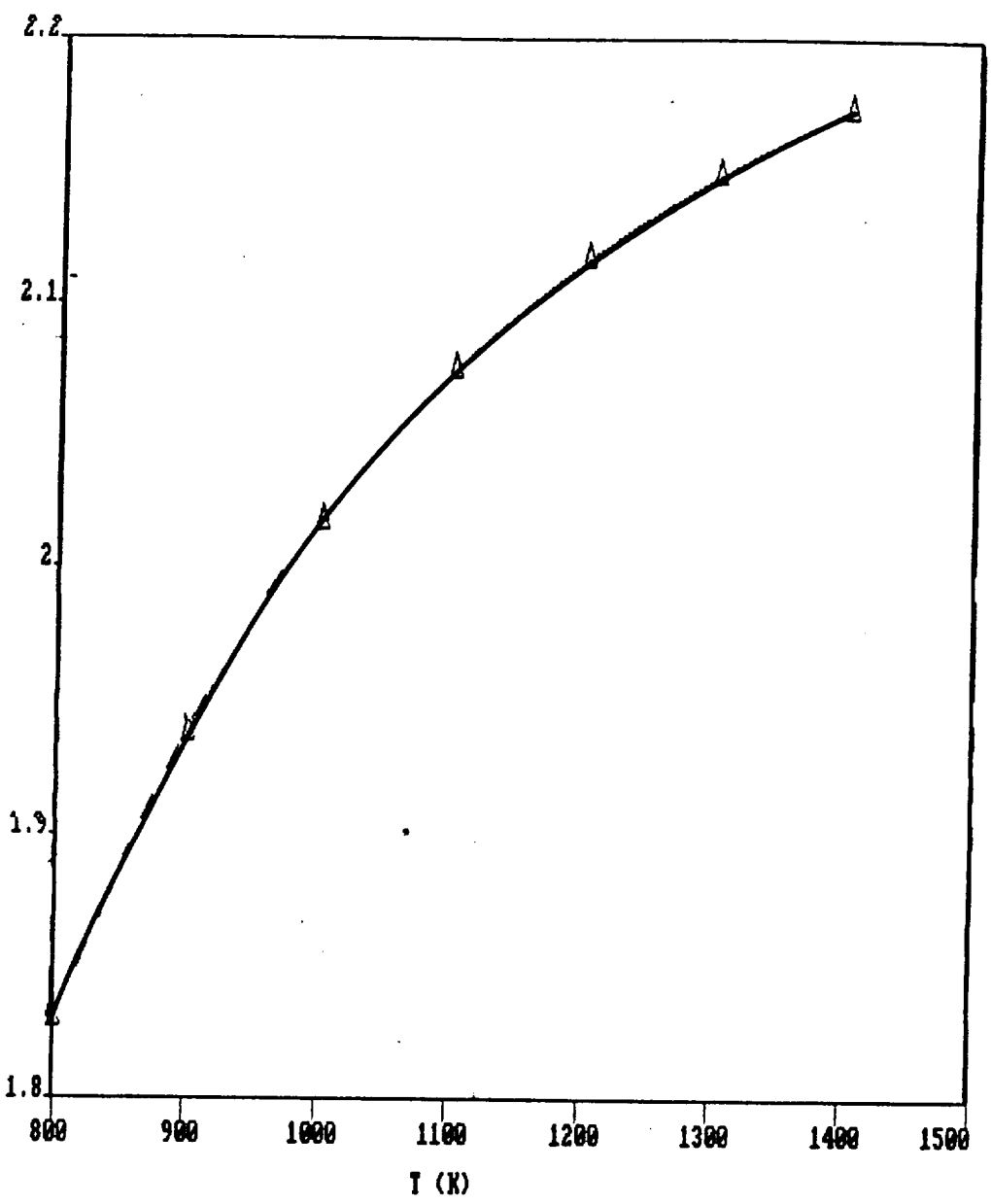

$f_{\epsilon a}$

Fig. 2-3. Lithium Flouride Emissivity Fractional Function.

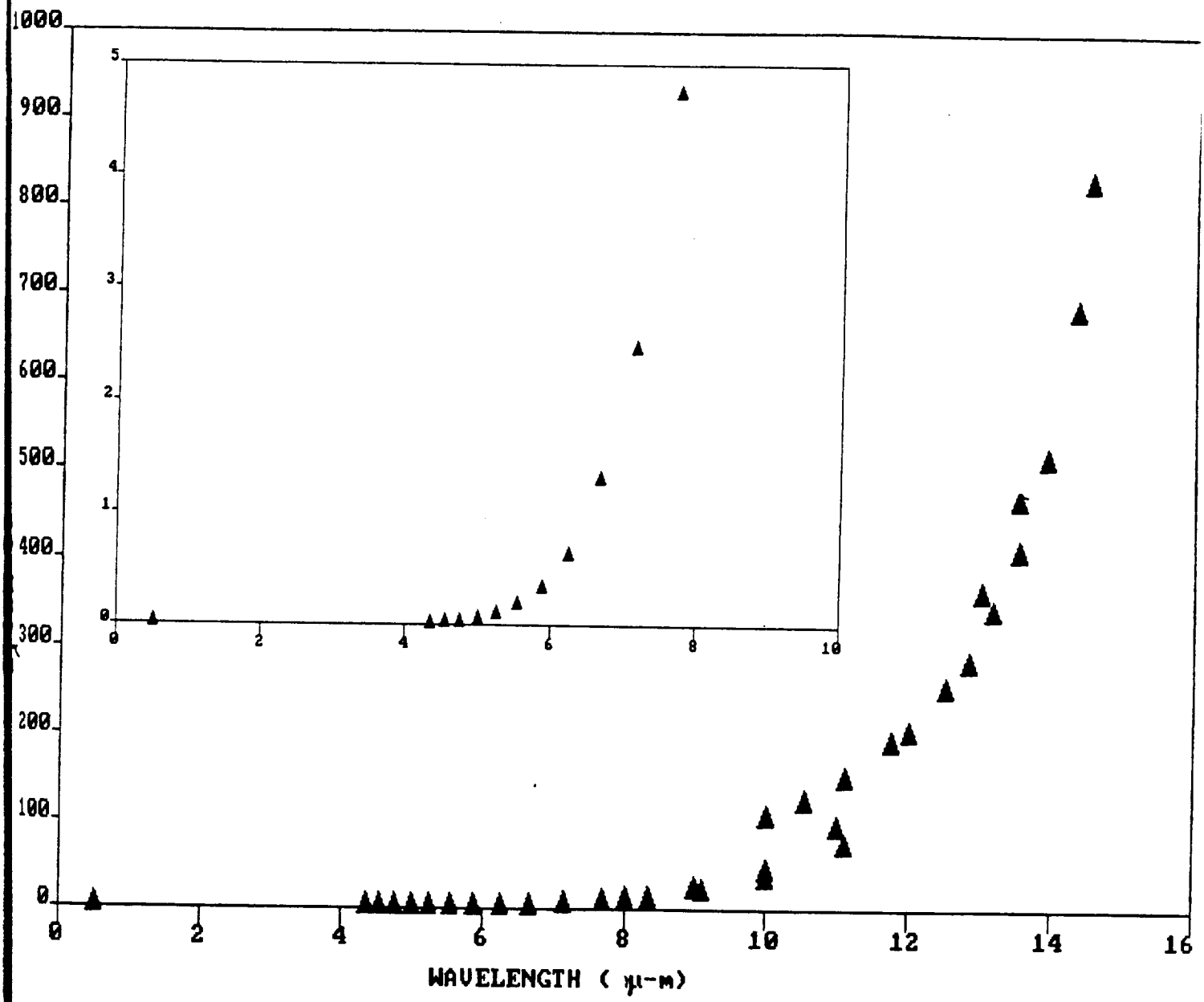

Fig. 2-4. Spectral Absorption Coefficient for Lithium Flouride.

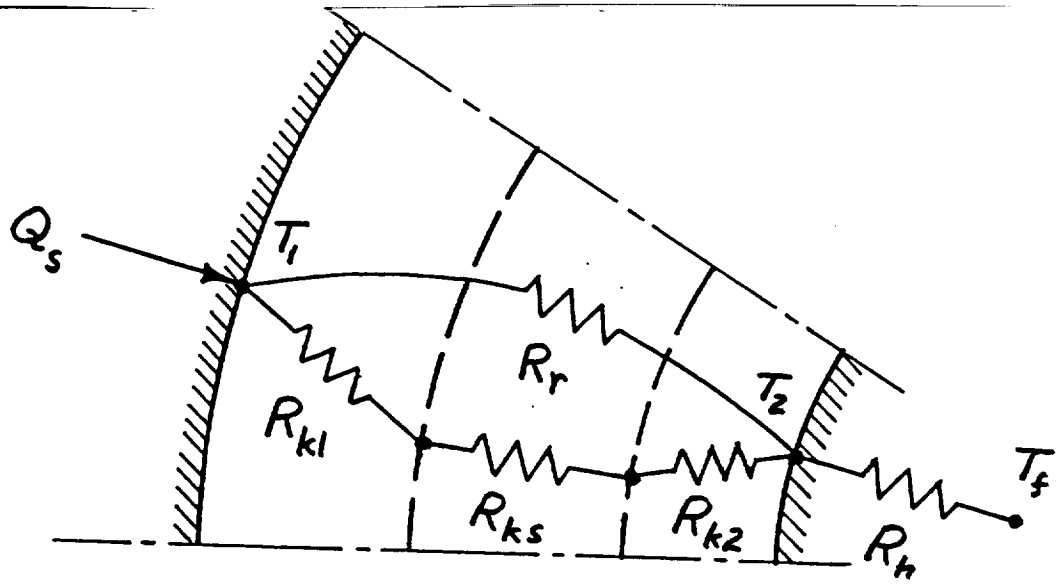

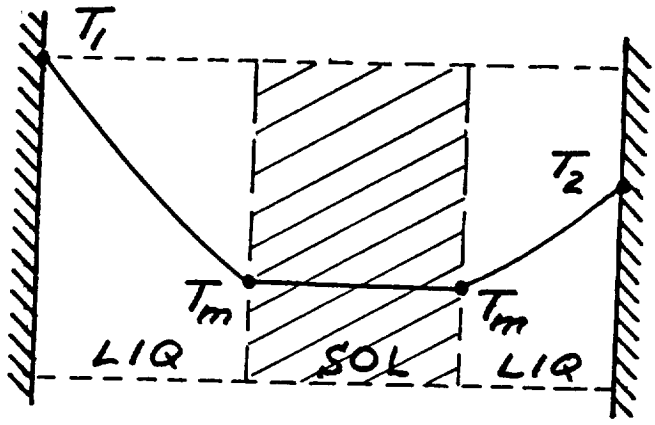

$R_{ks} = \infty$

$R_h = \infty$

(a)

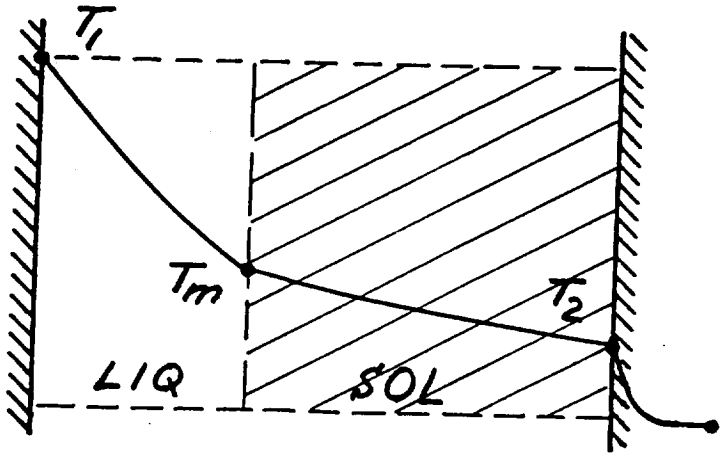

$R_{k2} = 0$

(b)

Fig. 3-1. Thermal Model for Radiation and Phase-Change in Annulus.

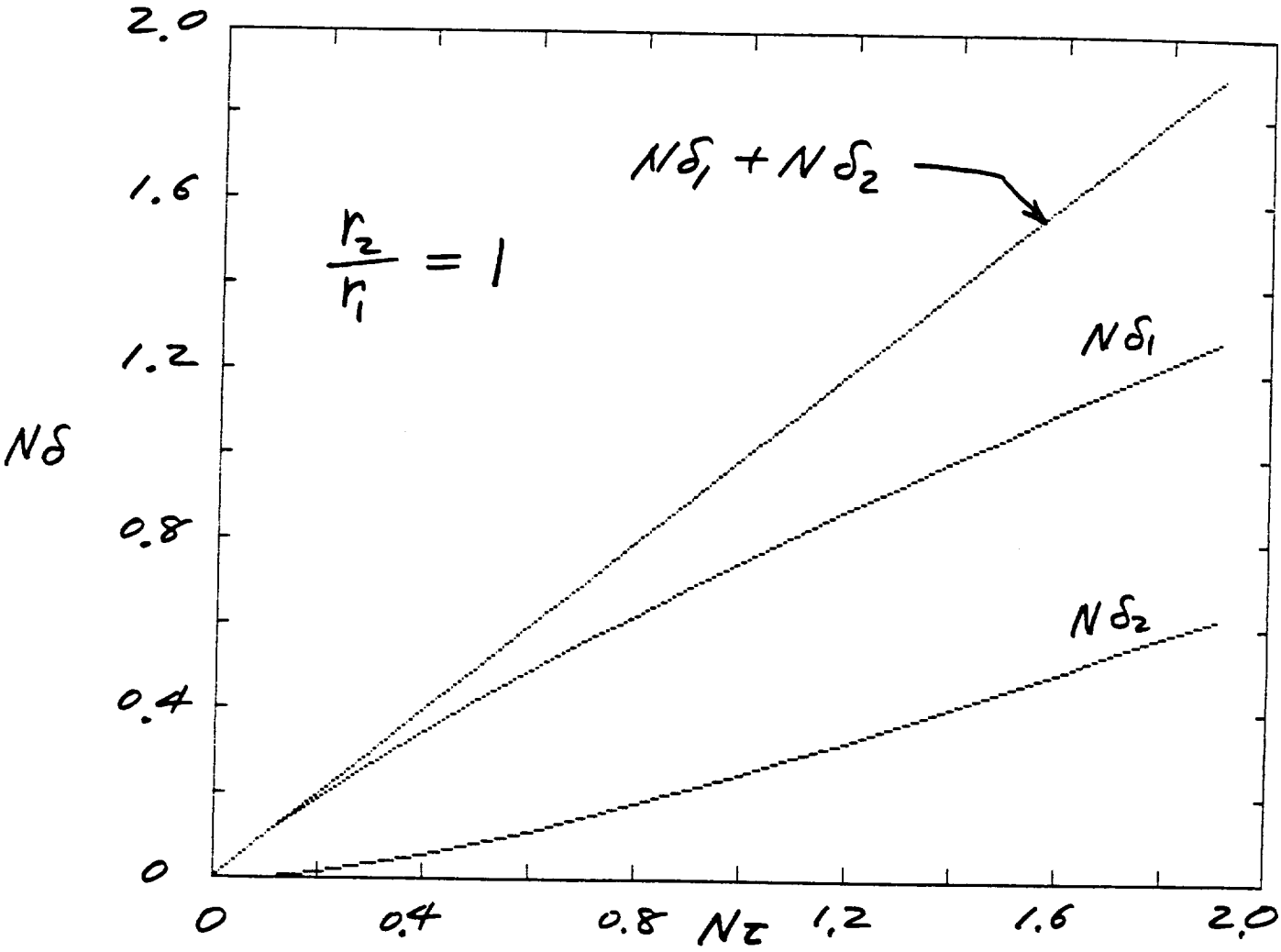

Fig. 4-1. Growth of Phase-Change Fronts for Plane Slab, Adiabatic Inner Wall.

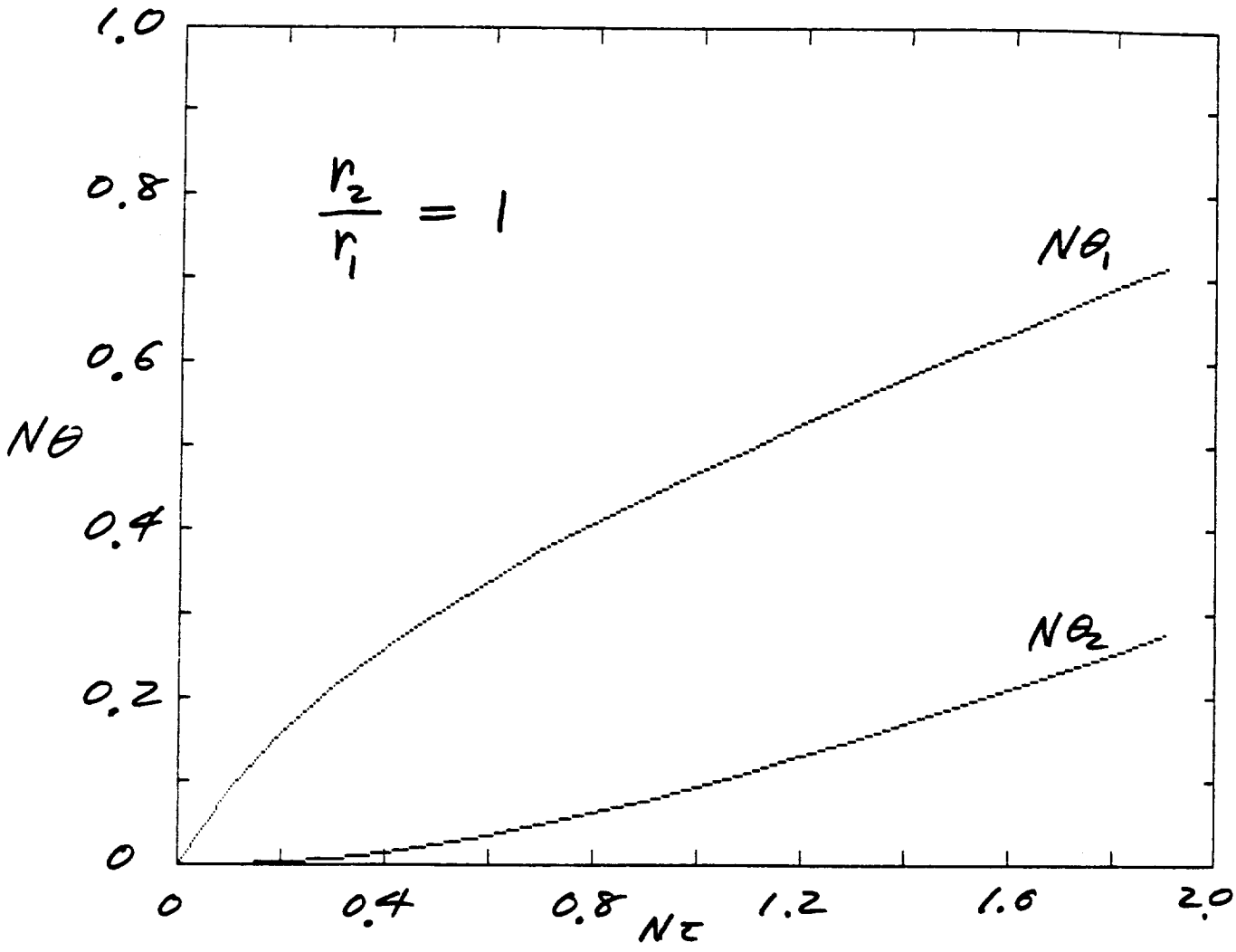

Fig. 4-2. Wall Temperature Variations for Plane Slab, Adiabatic Inner Wall.

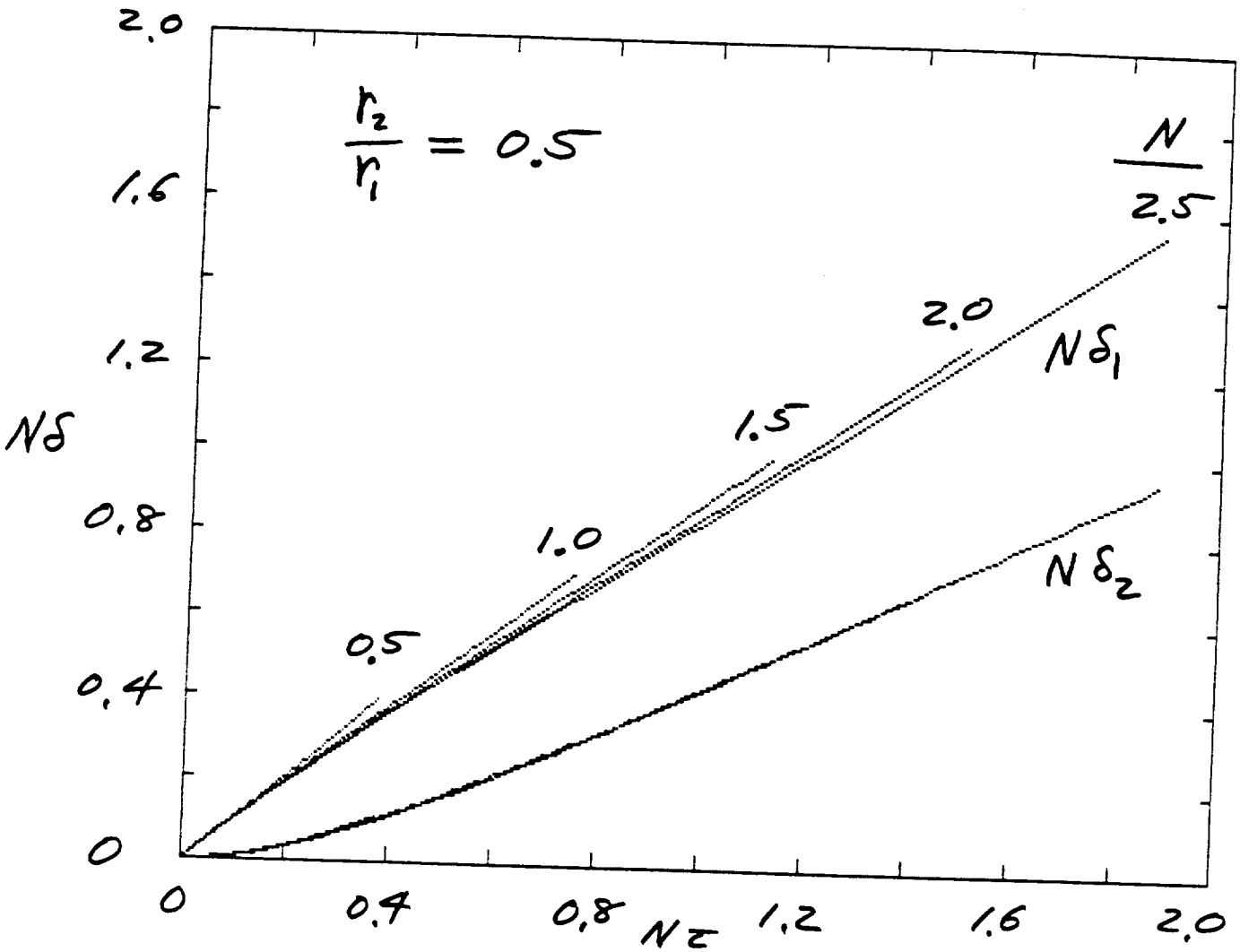

Fig. 4-3. Growth of Phase-Change Fronts for Annulus, Adiabatic Inner Wall.

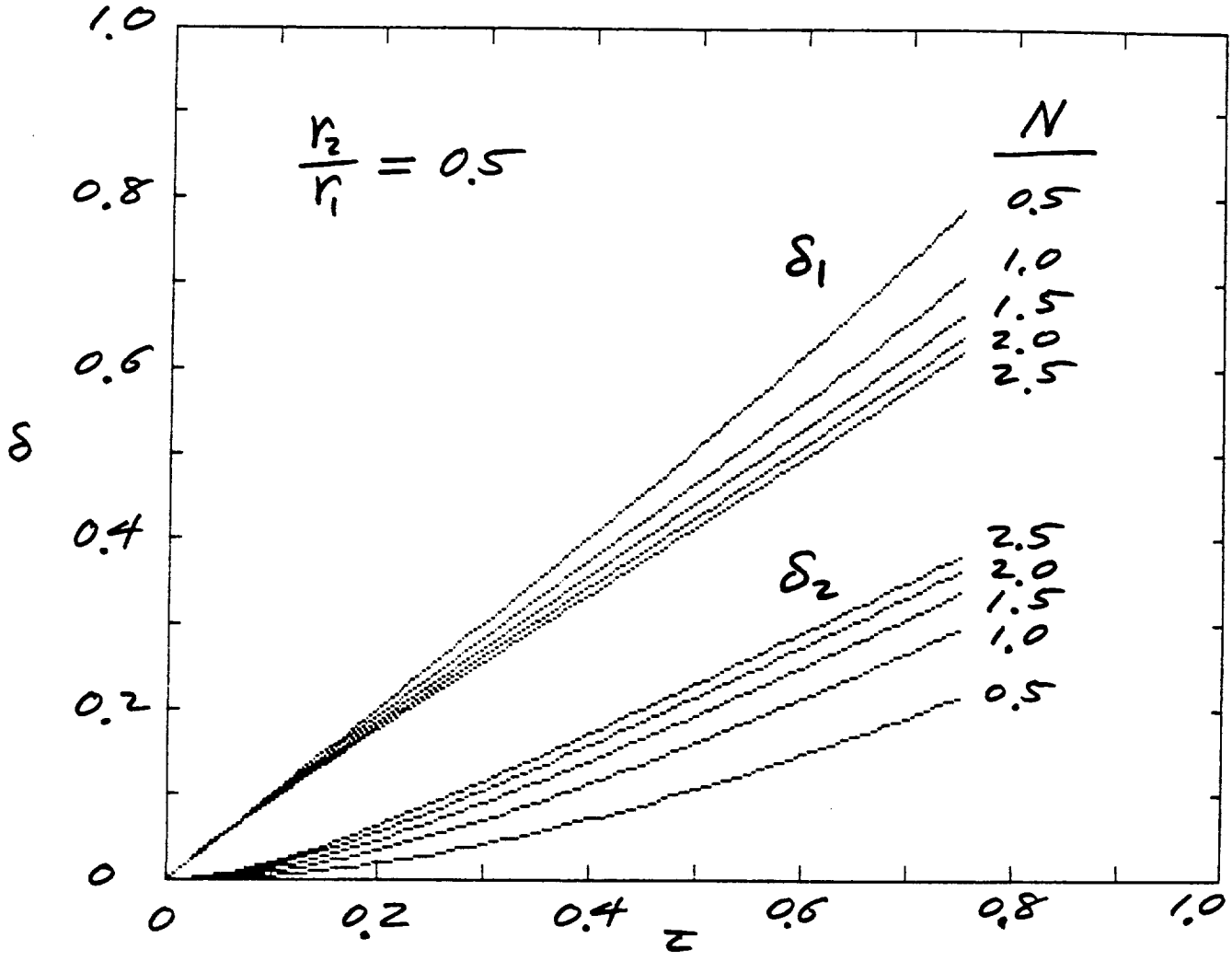

Fig. 4-4. Growth of Phase-Change Fronts for Annulus, Adiabatic Inner Wall.

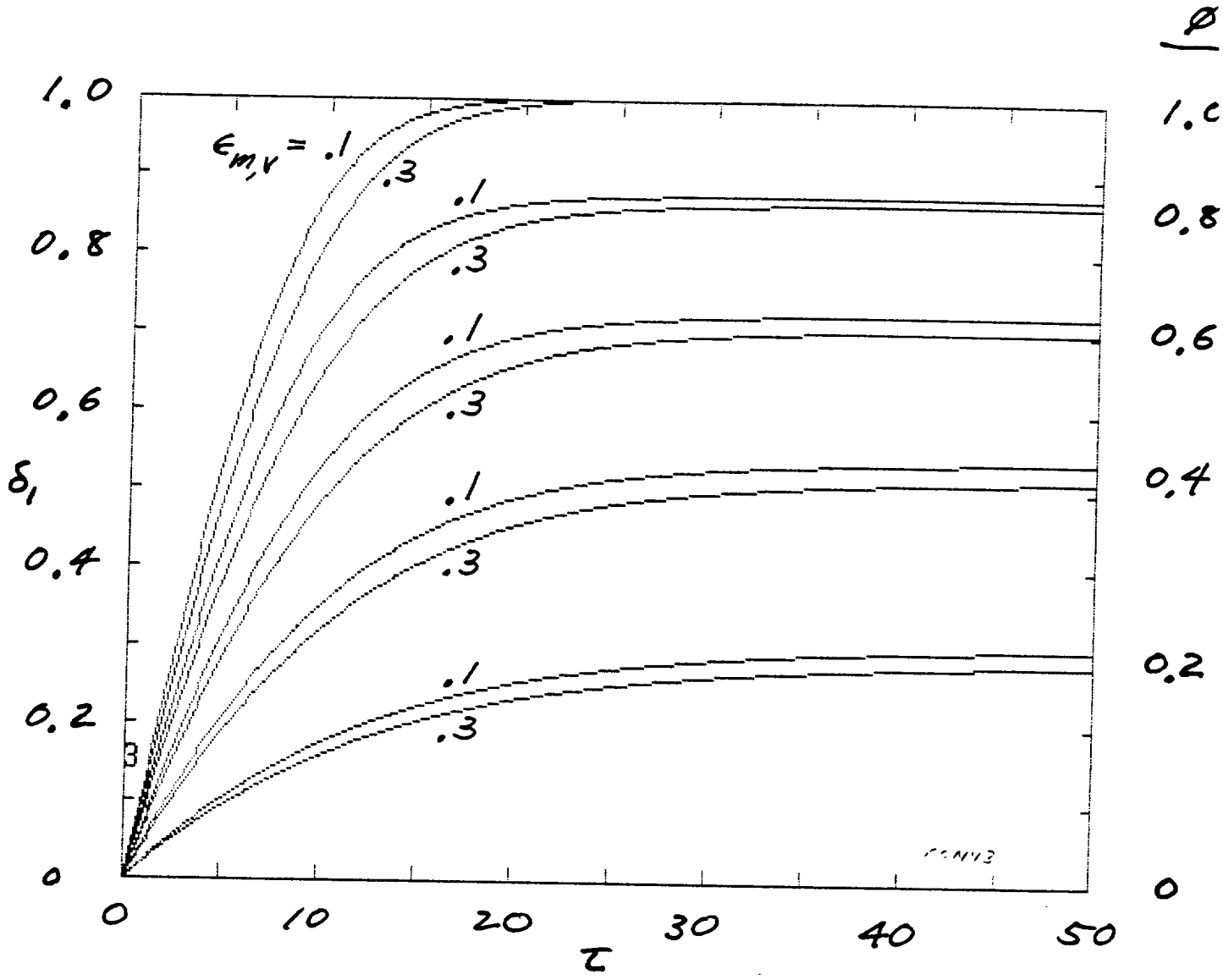

Fig. 4-5. Growth of Phase-Change Front for Partially Melted Condition, Convective Inner Wall. (Annulus parameters per Space Station, Table 3-1.)

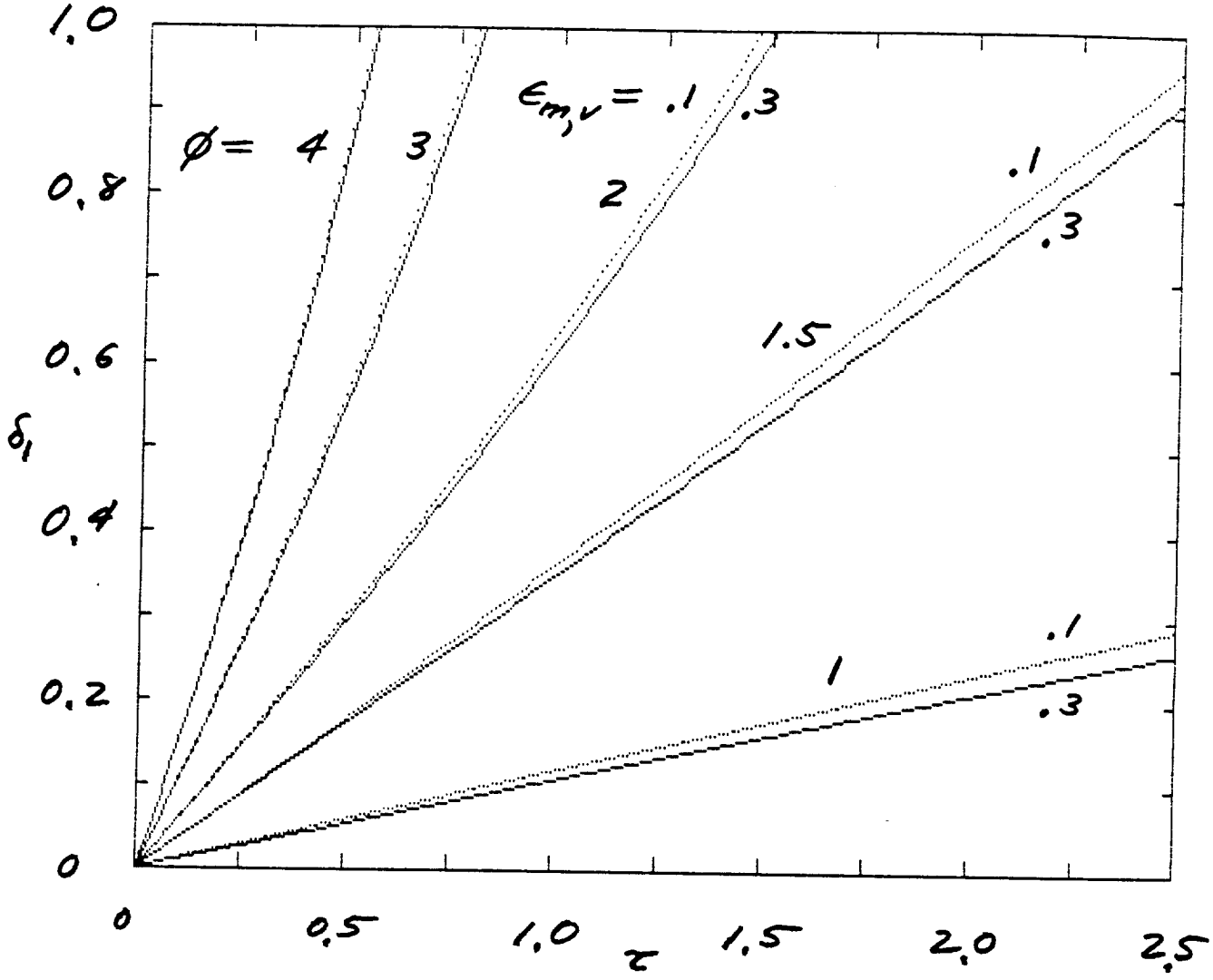

Fig. 4-6. Growth of Phase-Change Front for 100% Melted Condition, Convective Inner Wall. (Annulus parameters per Space Station, Table 3-1.)

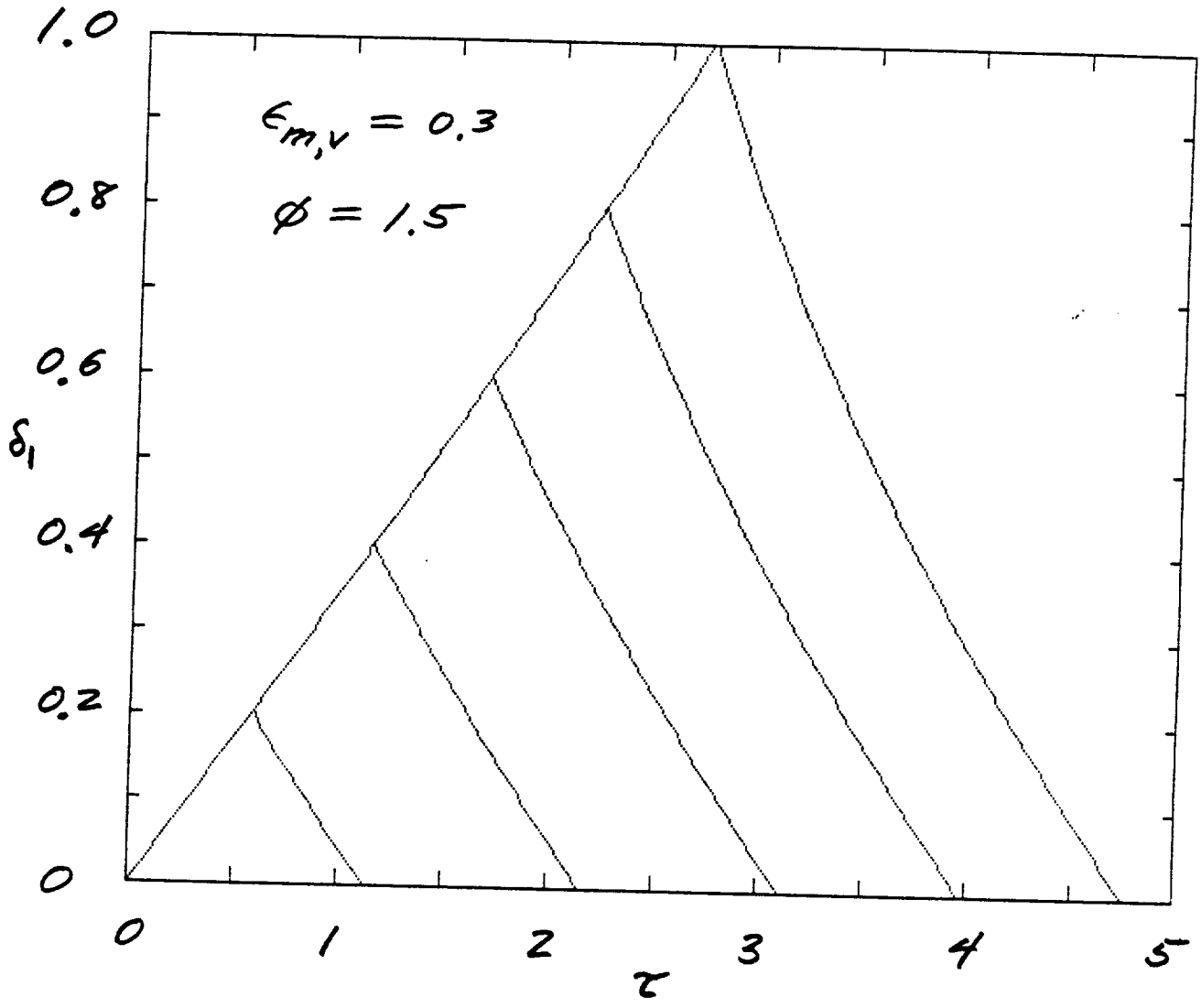

Fig. 4-7. Resolidification of Phase-Change Front from Melted Conditions, Convective Inner Wall. (Annulus parameters per Space Station, Table 3-1.)

PART III

ANALYSIS OF RADIATIVE AND PHASE CHANGE PHENOMENA WITH APPLICATION TO SPACE-BASED THERMAL ENERGY STORAGE

Kurt O'Ferrall Lund

135 Sixth Street
Del Mar, CA 92014

INTERIM REPORT

Prepared for

NASA Lewis Research Center

November 30, 1990

1. INTRODUCTION

The behavior of phase transition is central to the understanding of phase-change thermal energy storage for development of Solar Dynamic Space Power. Therefore, Space Shuttle flight experiments have been planned [Namkoong 1989a, 1989b], and numerical analyses have been performed to determine two and three dimensional effects of the phase transition process [Kerslake 1990, Wichner 1988]. These analyses and experiments utilize an annular canister containing the phase change material (PCM), where a solar heat flux is impressed on the outer wall of the canister (here radius r_1) to melt the PCM, and convection at the inner wall (here radius r_2) to freeze or solidify the PCM (in the experiments the solar flux is electrically simulated, and the convection is simulated by conduction and radiation). This annular canister geometry is also the current design for the Solar Dynamic Heat Receiver of the proposed Space Station [Strumpf and Coombs 1990].

In application to heat receivers the PCM's are high-temperature salts, such as lithium-fluoride (LiF) with a melting temperature of 1121 K (1558 F). At these temperatures radiative transport is a significant part of the overall heat transfer processes within the canisters. In the previous two-dimensional model [Kerslake and Ibrahim 1990] radiation was not included, and in the three-dimensional model [Wichner et al. 1988] the effect of radiation is obscured by the complexity of the numerical computations; in the flight experiments [Namkoong 1989] radiation will occur naturally, but the radiative effect cannot be determined directly as only canister surface temperatures will be measured; although convection and radiation in vacuum was investigated recently [Yucel et al. 1989] the combined radiation and phase change effect is not generally treated in the technical literature. Thus, there is a need for basic models and solutions which illustrate this effect. To this end a one-dimensional analysis is here presented.

Although the canisters invariably are finite in length, and actual heat fluxes may be circumferentially and axially non-uniform, there are a number of reasons why a one-dimensional approximation is useful:

a) closed-form or simplified solutions are possible which illustrate the basic phenomenological interactions;
b) solutions provide bases against which complex numerical models bay be compared for identical boundary conditions;
c) solutions provide ready estimation of experimental behaviors, such as surface temperature-time variations;

d) the phase-change process is predominantly one-dimensional in the radial direction for canisters with larger length-to-thickness aspect ratios.

Radiation within the canister enclosure follows conventional exchange between diffuse surfaces, except that the intervening medium, LiF, has spectral properties which differ from those of vacuum. Therefore, accurate application requires spectral integration. Following Williams [1988] a two-band approximation is made utilizing recent measurements of LiF optical properties [Palik and Hunter 1985]. It is shown in Section 2 that at the melting temperature, Tm = 1121 K, the majority of radiation emissive power occurs in the transparent part of spectrum for LiF. For the smaller part at longer wavelengths, a "thick-gas" approximation is used which adds a factor to the apparent thermal conductivity [Williams 1988].

The emissive properties of the metal canister surfaces is assumed to follow the Hagen-Rubens relation [Siegel and Howell 1981, p. 112]. With the spectral properties of LiF this leads to a spectrally integrated emissivity fractional function which is the ratio of the average emissivity of the surface contacting LiF to the emissivity of the surface in vacuum at the same temperature. A two-surface radiant energy exchange model is then developed which, when linearized, results in a factor of 5.47 in the equivalent radiation heat transfer coefficient, as compared to the usual factor of 4, a 37% increase over radiation exchange in vacuum.

The PCM "Basic Charging Mode" is considered in Section 3, where the PCM is initially at temperature, T_m, and a heat flux is suddenly applied at the canister outer surface, while the inner surface remains adiabatic. The usual Stefan problem is one in which the temperature at a boundary is suddenly changed [e.g., Yao and Prusa 1989, Burmeister 1983, or Solomon 1981], resulting in a boundary layer growing in time as the error function [e.g., Arpaci and Larsen 1984]; however, with the presently imposed heat flux boundary condition, this layer does not develop, with the result that the surface temperature changes only slowly in a quasi-steady fashion.

Besides the quasi-steady approximation in the liquid, it is further assumed that the conduction limit applies, such that natural convection boundary layers do not develop significantly and such that the phase-change boundary remains axially uniform. This is valid for Rayleigh numbers below 1700, for rectangular enclosures [Incropera and DeWitt 1985, p. 401], but has also been demonstrated experimentally for much larger Rayleigh numbers with a heat flux boundary and an aspect ratio of 4.5 [Zhang and Bejan 1989]; since in the flight experiments the Rayleigh number remains small

over the melting process for an applied heat flux of 0.921 W/cm^2, the conduction limit in the liquid is considered an excellent approximation under 1-g axial gravitational acceleration. Under microgravity conditions the magnitude of natural convection is suppressed, although some convection effects may be present [Bayazitoglu and Lam 1987, Arnold et al. 1990].

Assumptions regarding the second boundary condition (at r_2) are tied in with the radiation model (i.e., without radiative energy exchange between the two walls, the PCM would simply melt from the outer surface and the effect would not appear at the inner surface until the phase-change front "arrives" there). Here, an adiabatic condition is chosen as representing the best that can be done (as far as melting the PCM), and also yielding the simplest analytical results; other conditions, such as convective or thermal-mass sink would change the present results somewhat, but not to a large extent.

The results of the analysis are that, with an adiabatic inner wall, the rate of melting of the PCM is independent of radiative and conductive effects within the annulus, but depends only on the heat flux at the outer wall, and the volume and heat of fusion of the PCM. The effect of radiation and liquid conduction is to redistribute energy and cause melting of the solid PCM at both its outer and inner surfaces; solid conductivity did not enter into this process. It was also found that the wall temperatures increased smoothly and slowly during the melting, thus validating initial assumptions.

2. TWO-BAND RADIATION MODEL

To determine the effect of radiation within the LiF enclosure, it is necessary to know the optical properties of LiF, which differ considerably from vacuum. In particular, if the specular optical constants are known (refractive index, n, and absorptive index, or extinction coefficient, k), other radiative properties can be obtained. A summary of recent measurements [Palik and Hunter 1985] is shown in Fig. 2-1. It is seen that there is a transparent region of the spectrum near 1 μm (where k --> 0), which is the region of interest for emission near the melting temperature of 1121 K. The refraction index appears relatively constant in this region, but decreases somewhat with increasing wave length. This is shown in Fig. 2-2 where the data of Palik and Hunter are replotted on a linear scale. Also plotted is the Planck spectral emissive power for 1121 K, which shows that emissions whithin the canister lie primarily between 1 μm and 6 μm. The corresponding extinction coefficient data are shown in Fig. 2-3. Thus for most of the relevant spectrum, the single crystal LiF is transparent to radiation. This is also shown by previous data [Amr. Inst. Physics Handbook 1957], as reported by Williams [1988].

2.1 Blackbody Emission

For the transparent part of the spectrum, $\lambda \leq \lambda_a$, the blackbody emissive power is given by

$$e_{b,a} = \int_0^{\lambda_a} \frac{c_1 \, d\lambda}{n^2 \lambda^5 \left[e^{c_2/n\lambda T} - 1 \right]} \qquad (2.1)$$

where c_1 and c_2 are the radiation constants (based on c_0, the speed of light in vacuum):

$$c_1 = 2\pi h c_0^2 = 3.7415 \times 10^{-16} \ \mathrm{Jm^2/s}$$

$$c_2 = hc_0/k = 14{,}388\ \mu mK$$

The index of refraction for LiF is the spectral quantity shown in Fig. 2-2, which is here approximated as

$$n = 1.39 - 0.00271\lambda^2 = a - b\lambda^2 \qquad (2.2)$$

To evaluate (2.1) the change of variable is made,

$$\xi = c_2/n\lambda T \qquad (2.3)$$

so that

$$d\xi = -\xi\left[\frac{n + \lambda n'}{n\lambda}\right]d\lambda \qquad (2.4)$$

where $n' = dn/d\lambda = -2b\lambda$. Substitution of (2.3) and (2.4) into (2.1) then yields the expression

$$e_{b,a} = \sigma T^4 \frac{15}{\pi^4}\int_{\xi_a}^{\infty} \frac{n^3}{n + \lambda n'}\frac{\xi^3 d\xi}{e^{\xi} - 1} \qquad (2.5)$$

where $\xi_a = c_2/n_a\lambda_a T = c_3/T = 1995/T(K)$.

An example of the numerical evaluation (2.5) is shown in Fig. 2-4 for $\lambda_a = 5.5\ \mu m$, where the upper limit of $\xi = 16$ is well whithin the validity of (2.2). This may also be written in terms of an effective index

$$e_{b,a} = n_a^2\,\sigma\,T^4 \qquad (2.6)$$

The effective index, n_a^2, obtained from the integral in (2.5) with $\lambda_a = 5.5\ \mu m$, has a temperature dependence because of the spectral dependence of $n(\lambda)$, as shown in Fig. 2-5. This result is similar to that previously obtained [Williams 1988], except that previously the effect of n' (a 10% effect) was not accounted for and the blackbody fractional function was included in the effective index.

2.2 Emissivity and Absorptivity

The assumption is made in this analysis that the metal

surfaces bounding the LiF are diffuse. For spectral emissivity, ε_λ, the emissive power of the surface is given by

$$e_a = \int_0^{\lambda_a} \varepsilon_\lambda e_{b\lambda} d\lambda$$

so that with the above change of variables

$$e_a = \sigma T_s^4 \frac{15}{\pi^4} \int_{\xi_a}^{\infty} \frac{n^3}{n + \lambda n'} \varepsilon_\lambda \frac{\xi^3 d\xi}{e^\xi - 1} \qquad (2.7)$$

For metals, a recommended formula for the normal spectral emissivity is [Sparrow and Cess 1978]

$$\varepsilon_{\lambda n} = 36.5\sqrt{r/\lambda} - 464\, r/\lambda \qquad (2.8)$$

where r is the electrical resistivity in Ohm-cm, and λ is the wavelength in μm. At $\lambda = 2.5$ μm (maximum radiation at 1121K) and the rather large value $r = 10^{-5}$ Ω cm, the second term is only 2.5% of the first term and therefore neglected. The result in vacuum of spectrally integrating (2.8) is total normal emissivity

$$\varepsilon_{n,v} = 0.576\sqrt{rT_s} \qquad (2.9)$$

where T_s is the surface temperature in degrees Kelvin. Let r be proportional to the absolute temperature, then $r = r_0 T_s/T_0$, where r_0 is the resistivity at temperature T_0, and where from (2.9) the total normal vacuum emissivity at this temperature is $\varepsilon_{0,v}$. Substitution of these variables into (2.8) results in the normal (or hemispherical) emissivity ratio

$$\frac{\varepsilon_\lambda}{\varepsilon_{0,v}} = \frac{36.5}{0.576 T_0}\sqrt{T_s/\lambda} = \frac{T_s}{T_0} c_4 \sqrt{n\xi} \qquad (2.10)$$

where c_4 is the nondimensional number

$$c_4 = 36.5/0.576\sqrt{c_2} = 0.529$$

Now, substitution of (2.10) into (2.7) results in

$$e_a = \sigma T_s^4 \left[T_s/T_0\right] \varepsilon_{0,v} f_{\varepsilon a}(T_s) \qquad (2.11)$$

where the emissivity fractional function is defined by

$$f_{\varepsilon a}(T) = c_4 \frac{15}{\pi^4} \int_{\xi_a}^{\infty} \frac{n^3}{n + \lambda n'} \sqrt{n\xi} \, \frac{\xi^3 d\xi}{e^{\xi} - 1} \qquad (2.12)$$

This function is shown in Fig. 2-6 for $\lambda_a = 5.5$ μm, where it is seen that the effective total emissivity is roughly twice that of the value in vacuum:

$$\varepsilon_a(T_s) = \varepsilon_{0,v} \, (T_s/T_0) \, f_{\varepsilon a}(T_s) \qquad (2.13)$$

A completely similar procedure yields the effective absorptivity

$$\alpha_a(T_s,T_e) = \varepsilon_{0,v} \frac{\sqrt{T_s T_e}}{T_0} f_{\varepsilon a}(T_e) \qquad (2.14)$$

where T_e is the environment (other surface) temperature.

2.3 Thick Gas Approximation

It would appear from Figs. 2-1 or 2-3 that k is sufficiently small for the wavelengths of interest that the medium can be considered perfectly transparent. there is, however, a region at the longer wavelengths where absorption occurs in the medium, as can be shown by evaluating the absorption coefficient [Siegel and Howell 1981, p 427] from the data of Palik and Hunter [1985]:

$$a_\lambda = \frac{4\pi k}{\lambda} ,$$

as shown in Fig. 2-7. These values may also be read as the optical thickness for a 1 cm layer of LiF (or as half the optical thickness for a 2 cm layer). The results are in general agreement with previous measurements [Amr. Inst. Phys. Handbook 1957]; thus, the assumption of an optically thick gas above λ = 6 or 7 μm is supported by the more recent measurements. Therefore, following Williams [1988], the two-band approximation can be made that the LiF is transparent to radiation below wavelengths of

approximately 5.5 μm, and acts as a thick gas above this wavelength. Since, as seen in Fig. 2-2, there is but little radiant energy at the higher wavelengths, this two-band radiation model is considered an adequate approximation, especially in view of uncertainties associated with the canister surface properties.

2.4 Radiant Energy Exchange

For each surface, i, in an enclosure we have the net radiative flux,

$$q_i = q_i^+ - q_i^- \tag{2.15}$$

and the radiosity definition for diffuse, opaque surfaces,

$$q_i^+ = \varepsilon_i B_i + \rho_i q_i^- \tag{2.16}$$

where $B_i = \sigma T_i^4$ is the blackbody radiosity [Edwards 1981]. Eliminating the irradiance, q_i^-, between (2.15) and (2.16) we have

$$q_i = [\varepsilon_i B_i - \alpha_i q_i^+]/\rho_i$$

or

$$Q_i = \frac{C_i - q_i^+}{R_i} \tag{2.17}$$

where the total heat transfer rate is $Q_i = q_i A_i$, the modified blackbody radiosity is $C_i = \varepsilon_i B_i/\alpha_i$, and where the surface resistance is

$$R_i = \frac{1 - \alpha_i}{\alpha_i A_i} \tag{2.18}$$

Additionally, the following relation applies in the transparent medium,

$$Q_i = \sum_{j=1}^{N} A_i F_{ij} (q_i^+ - q_j^+) = \sum_{j=1}^{N} \frac{q_i^+ - q_j^+}{R_{ij}} \qquad (2.19)$$

so that conventional radiation network solutions may be used with the modified blackbody surface radiation, and with the surface resistance given by (2.18). A closed-form analytical solution is, of course, not possible as α_i depends on the "other-surface" temperatures, as shown in (2.14); however, an adequate iterative solution can be obtained with a weighted average for T_e.

For a two-surface enclosure, (2.17) to (2.19) yield

$$Q_1 = -Q_2 = \frac{C_1 - C_2}{\frac{1-\alpha_1}{A_1\alpha_1} + \frac{1}{A_1 F_{12}} + \frac{1-\alpha_2}{A_2\alpha_2}} \qquad (2.20)$$

where, with (2.13) and (2.14),

$$C_1 = \frac{g(T_1)}{g(T_2)} \sigma T_1^4 , \qquad C_2 = \frac{g(T_2)}{g(T_1)} \sigma T_2^4 \qquad (2.21,22)$$

$$g(T) = f_{\epsilon a}(T)\sqrt{T} \qquad (2.23)$$

For a linearization of (2.20), C_1 and C_2 may be expanded in a Taylor Series about the melting temperature, T_m:

$$C_i \approx C_m + (T_1 - T_m)C_{i,1m} + (T_2 - T_m)C_{i,2m}$$

with the result that

$$C_1 - C_2 \approx (4 + 2T_m g_m'/g_m)\, \sigma T_m^3 (T_1 - T_2) \qquad (2.24)$$

or, with $(Tg'/g)_m = 0.237$ from Fig. 2.~~4~~ 6,

$$C_1 - C_2 = 5.47\ \sigma T_m^3\ (T_1 - T_2) \tag{2.25}$$

Thus, the radiant heat transfer rate between two surfaces may be approximated as

$$Q_1 = -Q_2 = h_{r1} A_1 (T_1 - T_2) \tag{2.26}$$

where the effective radiation heat transfer coefficient is

$$h_{r1} = \frac{5.47\ \sigma\ T_m^3}{\frac{1 - \alpha_1}{\alpha_1} + \frac{1}{F_{12}} + \frac{A_1}{A_2}\frac{1 - \alpha_2}{\alpha_2}} \tag{2.27}$$

Since the denominator of (2.27) does not involve differences in absorptivities it is considered adequate to evaluate α_1 and α_2 at T_m. The linearized model (2.26) is utilized subsequently in obtaining an analytical solution to the two-surface phase change problem. That is, for $\alpha_1 = \alpha_2 = \alpha_m$, and $T_m = 1121$ K,

$$h_{r1} = \frac{5.47\ \sigma\ T_m^3}{\frac{1}{\alpha_m}\left[1 + r_1/r_2\right] - 1} = \frac{43.7\ W/m^2K}{\frac{1}{\alpha_m}\left[1 + r_1/r_2\right] - 1} \tag{2.28}$$

3. BASIC PCM CHARGING MODE

The LiF PCM contained by the annular canister in the flight experiment, as well as in applications with annular geometry, is to cycle between the charging (heat addition) and discharging (heat removal) modes. In the first mode heat is added to (impressed upon) the large diameter, external wall to melt the PCM while some heat may or may not be removed from the small-diameter, internal wall; in the second mode, heat is removed from the interior wall to solidify the PCM while the outside wall is, more or less, insulated.

Here is considered the basic charging mode where at time zero the external heat source is Q_s(W/m) and the PCM is 100% solid and at uniform temperature, T_m, and where the inside wall remains adiabatic throughout the charging process. Furthermore, to obtain a basic (or fundamental) solution to the charging problem, an infinitely long cylinder is assumed together with axissymetric heat input.

The above assumptions result in a radially one-dimensional time-dependent system, as illustrated in Fig. 3-1. because of the transparent part of the LiF spectrum there is radiation from the outer wall (surface 1) to the inner wall (surface 2), where the latter acts as a refractory or reradiation surface, such that the energy source, Q_s, causes phase change at both melt-surfaces, 1m and 2m, as shown. Additionally, axial gravitational acceleration is assumed such that any void is removed to the end region, and such that liquid remains continuously in contact with the two walls and the phase-change boundaries.

Although the above stated problem is quite restrictive from a practical view, it nevertheless results in closed-form solutions to which more general numerical solutions may be compared. Additionally it enhances our basic understanding of the PCM charging process when radiation is included.

3.1 Model Equations

The model considered is for a solid region surrounded by liquid at both radii r_{1m} and r_{2m}, as indicated in Fig. 3-1. In these annular liquid gaps convection is described by the general energy transport equation

$$\frac{\partial T}{\partial t} + u\frac{\partial T}{\partial x} + v\frac{\partial T}{\partial r} = a\nabla^2 T \qquad (3.1)$$

where u,x are in the axial direction and v,r are in the radial direction. However, under the parallel flow assumption for long cylinders, u = u(t,r), v = 0, and T = T(t,r). This means that the fluid transport terms on the left hand side of (3.1) are zero and the temperature field is determined entirely by conduction (including the conductive effect of the thick-gas radiation absorption), even though there will be convective flow driven by the Boussinesque temperature term [Arpaci and Larsen 1984]:

$$\frac{\nu}{r}\frac{\partial(ru)}{\partial r} - \frac{\partial u}{\partial t} = g\beta(T - T_0) \qquad (3.2)$$

Thus, the long-cylinder, parallel flow assumption essentially uncouples the momentum and energy equations such that the temperature field is determined by conduction, independent of the velocity field, and then can be used to determine the velocity field as in (3.2).

Because the movement of the phase fronts is much slower than the liquid response the problem may be regarded as quasi-steady with known solutions utilized for the temperature distributions. Thus, the conduction heat transfer from surface i to im for (i = 1 or 2) is given by:

$$Q_{ki} = \frac{T_i - T_{im}}{R_{ki}} \qquad (3.3)$$

where resistances are

$$R_{k1} = \frac{\ell n(r_1/r_{1m})}{2\pi k_{e\ell}}, \quad R_{k2} = \frac{\ell n(r_{2m}/r_2)}{2\pi k_{e\ell}} \qquad (3.4,5)$$

and the effective liquid conductivity is $k_{e\ell}$. An energy balance on surface 1 yields

$$Q_s = Q_{k1} + Q_{r1} \qquad (3.6)$$

where Q_{r1} is given by (2.26), and for the adiabatic surface 2,

$$Q_{r1} = Q_{k2} \tag{3.7}$$

On a flux basis (2.26), (3.3), and (3.4) and (3.6) combine as

$$h_{r1}(T_1 - T_2) + \frac{k_{e\ell}(T_1 - T_m)}{r_1 \ell n(r_1/r_{1m})} = q_s \tag{3.8}$$

and (2.26), (3.3), (3.5) and (3.7) combine as

$$h_{r1}(T_2 - T_1) + \frac{k_{e\ell}(T_2 - T_m)}{r_1 \ell n(r_{2m}/r_2)} = 0 \tag{3.9}$$

At the phase boundaries the heat added results in the movement of the boundaries through $H_{s\ell}$, the latent heat:

$$Q_{ki} = 2\pi r_{im} G_i H_{s\ell} \tag{3.10}$$

where G_i is the mass velocity of surfaces 1m and 2m,

$$G_1 = -\rho_\ell \frac{dr_{1m}}{dt}, \quad G_2 = +\rho_\ell \frac{dr_{2m}}{dt} \tag{3.11,12}$$

Now, combining (3.10), (3.11) and (3.12) with the previous relations we obtain the differential equations for the phase boundaries:

$$\ell n\left[\frac{r_1}{r_{1m}}\right] r_{1m} \frac{dr_{1m}}{dt} = -\frac{k_{e\ell}}{\rho_\ell H_{s\ell}}(T_1 - T_m) \tag{3.13}$$

$$\ell n\left[\frac{r_{2m}}{r_2}\right] r_{2m} \frac{dr_{2m}}{dt} = -\frac{k_{e\ell}}{\rho_\ell H_{s\ell}}(T_2 - T_m) \tag{3.14}$$

These equations, together with (3.8) and (3.9), are the nonlinear system equations to be solved for the four unknown functions, $r_{1m}(t)$, $r_{2m}(t)$, $T_1(t)$ and $T_2(t)$.

It should be noted in this derivation that there is no effect of conduction in the solid. This occurs because there is phase-change at both surfaces 1m and 2m, which are therefore both at the melting temperature, and because the initial condition is

taken as a uniform solid at T_m. Thus, for basic charging the process is independent of the solid properties (under the assumed two-band, transparent/thick-gas radiation model), and the solid PCM remains at the uniform temperature, T_m, as indicated in Fig. 3-1.

3.2 Scaling of Equations

For the solution of the above system it is convenient to introduce the following scaling of variables:

$$\delta_1 = \frac{r_1 - r_{1m}}{r_1 - r_2} = \frac{1 - r_{1m}/r_1}{\varepsilon} \tag{3.15}$$

$$\delta_2 = \frac{r_{2m} - r_2}{r_1 - r_2} = \frac{r_{2m}/r_1 - \Gamma}{\varepsilon} \tag{3.16}$$

where δ_1 and δ_2 are the scaled liquid-gap thicknesses, $\Gamma = r_{2/}r_1$, $\varepsilon = 1 - \Gamma$,

$$\theta_i = (T_i - T_m)/T_r \ , \qquad \tau = t/t_r \tag{3.17,18}$$

and where the reference magnitudes, T_r and t_r, are to be determined. Substitution of (3.5) to (3.18) into (3.8), (3.9), (3.13) and (3.14) then yields the scaled system equations,

$$(1 - \varepsilon\delta_1)\ln\left[\frac{1}{1 - \varepsilon\delta_1}\right]\frac{d\delta_1}{d\tau} = \varepsilon\theta_1 \tag{3.19}$$

$$(\Gamma + \varepsilon\delta_2)\ln\left[1 + \frac{\varepsilon}{\Gamma}\delta_2\right]\frac{d\delta_2}{d\tau} = \varepsilon\theta_2 \tag{3.20}$$

$$N(\theta_1 - \theta_2) + \frac{\varepsilon\theta_1}{\ln\{1/(1-\varepsilon\delta_1)\}} = 1 \tag{3.21}$$

$$N(\theta_2 - \theta_1) + \frac{\varepsilon\theta_2}{\ln\{1+\varepsilon\delta_2/\Gamma\}} = 0 \tag{3.22}$$

where the radiation Biot number is $N = h_{r1}(r_1 - r_2)/k_{e\ell}$, and where the

reference temperature and time magnitudes are

$$T_r = \frac{q_s(r_1 - r_2)}{k_{e\ell}}, \quad t_r = \frac{(r_1 - r_2)\rho_\ell H_{s\ell}}{q_s}$$

It is noted that the time constant represents the ratio of the mass of PCM times the latent heat, divided by the input flux applied at the arithmetic average radius. The initial conditions are that all $\theta_i(0) = \delta_i(0) = 0$.

3.3 Solutions

The system, (3.19) to (3.22) does not possess a closed-form general analytical solution (primarily, because of the curvature effect represented by the logarithmic terms). However, by combining (3.19) with (3.21), and (3.20) with (3.22) we obtain the equations

$$(1 - \varepsilon\delta_1)\frac{d\delta_1}{d\tau} = 1 - N(\theta_1 - \theta_2) \tag{3.23}$$

$$(\Gamma + \varepsilon\delta_2)\frac{d\delta_2}{d\tau} = 0 + N(\theta_1 - \theta_2) \tag{3.24}$$

such that the sum of (3.23) and (3.24) results in an equation which is independent of the radiation Biot number and the wall temperatures:

$$(1 - \varepsilon\delta_1)\frac{d\delta_1}{d\tau} + (\Gamma + \varepsilon\delta_2)\frac{d\delta_2}{d\tau} = 1 \tag{3.25}$$

which has the exact integral

$$\delta_1 + \Gamma\delta_2 - \frac{\varepsilon}{2}\left[\delta_1^2 - \delta_2^2\right] = \tau \tag{3.26}$$

Although (3.26) does not provide $\delta_1(\tau)$ or $\delta_2(\tau)$ individually, it has the interesting interpretation: the maximum time, t_m, for the basic charging process occurs when all the solid has melted, or when $\delta_1 + \delta_2 = 1$. Substitution of this condition into (3.26) results in

$$\tau_m = \frac{1 + \Gamma}{2} = \frac{r_1 + r_2}{2r_1} \qquad (3.27)$$

Hence, with the definition of the time constant, the time for charging or melting the PCM in the annulus is obtained as

$$t_m = \frac{\pi(r_1^2 - r_2^2)\rho_\ell H_{s\ell}}{2\pi r_1 q_s} \qquad (3.28)$$

that is, the melting time is precisely the phase-change heat content divided by the total rate of heat input, independent of radiative and conductive properties! This is perhaps a surprising result, but quite reasonable: since in the basic charging model the phase-change boundaries are the only sinks for the energy source, $2\pi r_1 q_s$, the net result must be the melting of the PCM, with conductive and radiative effects redistributing the energy input and determining the relative locations of phase boundaries.

The above behavior can be seen analytically for the limiting condition $\epsilon \dashrightarrow 0$ ($\Gamma \dashrightarrow 1$) which is the parallel plate limit. In this limit, the system (3.19) to (3.22) becomes

$$\delta_1 \frac{d\delta_1}{d\tau} = \theta_1 \ , \quad \delta_2 \frac{d\delta_2}{d\tau} = \theta_2 \qquad (3.29,30)$$

$$N(\theta_1 - \theta_2) + \theta_1/\delta_1 = 1 \qquad (3.31)$$

$$N(\theta_2 - \theta_1) + \theta_2/\delta_2 = 0 \qquad (3.32)$$

Equations (3.31) and (3.32) may be solved for the temperatures in terms of the phase fronts,

$$\theta_1 = \delta_1 \frac{N\delta_2 + 1}{1 + N\delta_1 + N\delta_2} \qquad (3.33)$$

$$\theta_2 = \delta_2 \frac{N\delta_1}{1 + N\delta_1 + N\delta_2} \qquad (3.34)$$

such that substitution of (3.33) and (3.34) into (3.29) and (3.30) yields equations for the phase fronts, only:

$$\frac{d\delta_1}{d\tau} = \frac{1 + N\delta_2}{1 + N\delta_1 + N\delta_2} \tag{3.35}$$

$$\frac{d\delta_2}{d\tau} = \frac{N\delta_1}{1 + N\delta_1 + N\delta_2} \tag{3.36}$$

One solution is obtained from the sum of (3.35) and (3.36), or from (3.26) with $\epsilon = 0$:

$$\delta_1 + \delta_2 = \tau \tag{3.37}$$

Eliminating δ_2 between (3.37) and (3.35) yields the Euler equation in $1 + N\tau$,

$$\frac{d(N\delta_1)}{d(1+N\tau)} + \frac{N\delta_1}{1 + N\tau} = 1 \tag{3.38}$$

Thus, the solution to (3.37) and (3.38) is

$$N\delta_1 = \frac{N\tau}{2}\left[\frac{2 + N\tau}{1 + N\tau}\right], \quad N\delta_2 = \frac{N\tau}{2}\left[\frac{N\tau}{1 + N\tau}\right] \tag{3.39,40}$$

It is seen in these equations, and in Fig. 3-2 that δ_1 grows linearly with τ for small $N\tau$ (i.e., initially), whereas δ_2 grows quadratically; moreover, the growth of δ_2 depends on the radiation Biot number, N, as seen by the ratio of (3.40) to (3.39)

$$\frac{\delta_2}{\delta_1} = \frac{N\tau}{2 + N\tau} \tag{3.41}$$

where δ_2 ---> 0 for N ---> 0, and δ_2 ---> δ_1 for N ---> ω . That is, for small radiation Biot number the phase change will occur primarily from side 1, whereas for a large radiation number it will occur equally from both sides; for N = 1 and the end of the charging process where in the present case $\tau = 1$, the ratio of phase growths in (3.41) is 1:3, or, 75% melted from the outside surface and 25% from the inside surface. This result contrasts with other recent models where the effect of radiation was not included [Kerslake and Ibrahim 1990]. However, regardless of the value of N, the PCM is 100% melted when $\tau = 1$ (for this parallel plate limit of the annulus); this is a consequence of the imposed

heat flux boundary condition arising from actual or electrically simulated solar irradiation, which differs from the Stephan-type problem where the bounding temperatures are specified, and from the assumed adiabatic inner radius.

In the present formulation, wall temperatures are determined rather than specified. Thus, substitution of (3.39) and (3.40) into (3.33) and (3.34) yields the temperature functions

$$N\theta_1 = N\tau \left[\frac{2 + N\tau}{4}\right] \frac{1 + (1+N\tau)^2}{(1 + N\tau)^3} \tag{3.42}$$

$$N\theta_2 = \frac{2 + N\tau}{4} \left[\frac{N\tau}{1 + N\tau}\right]^3 \tag{3.43}$$

and the ratio

$$\frac{\theta_2}{\theta_1} = \frac{(N\tau)^2}{1 + (1+N\tau)^2} \tag{3.44}$$

Here, and in Fig. 3-3, it is seen that initially θ_1 increases linearly with τ, but that θ_2 increases cubically with τ.

In the case of an annulus with finite radius ratio, $r_2/r_1 = \Gamma$, equations (3.19) to (3.22) were solved by numerical integration, with results as shown in Fig. 3-4 with the same scale as previously, but for $\Gamma = 0.5$. Here the phase front movements were calculated for the series of radiation numbers shown, up to the maximum time $\tau_m = (1+\Gamma)/2 = 3/4$. There appears to be no dependence of $N\delta_2$ on N, and only slight dependence for $N\delta_1$; however, the curves are shifted somewhat, relative to the "planar annulus" result in Fig. 3-2. Without the N-scaling, the phase fronts appear as in Fig. 3-5 for the radius ratio, 0.5.

The results of the present analytical one-dimensional model may be compared with those of the numerical three-dimensional model, NORVEX. Such a comparison is shown in Fig. 3-6 using the following data:

$r_1 = 3.51$ cm, $r_2 = 1.95$ cm, $T_m = 1121$ K, $H_{sl} = 1037$ J/g,

ρ_ℓ = 1.79 g/cm^3, ρ_s = 2.33 g/cm^3,

k_ℓ = 0.037 W/cmK, k_s = 0.06 W/cmK, (k_e=0.037+0.017=0.054)

c_ℓ = 2.45 J/gK, c_s = 2.45 J/gK

α_m = 0.3, N = 0.15, h_{r1} = 0.00524 W/cm^{2}K, q_s = 0.921 W/cm^2

where the canister length was 6.6 cm, and where the solid unmarked curves are from the analytical model and the marked curves are from the NORVEX calculations. It is seen that analytically a smooth increase in outer wall temperature is predicted, whereas the numerical results show no increase above the initial melting temperature in the first 40 minutes of heating. Also, the analytical melting rate is somewhat higher than the numerically predicted rate.

These differences are not easily ascribed to three-dimensional versus one-dimensional effects as only weak axial gradients occured in the numerical calculations, where the canister aspect ratio was 4.2. Nor do the differences appear to result from the adiabatic inner wall of the analytical model versus the solid conductor-rod of the numerical model, as the rod also showed no change in temperature over 40 minutes. A more direct comparison would result for an aspect ratio of, say, 10 in the numerical model, together with a program modification allowing an adiabatic inner wall or a thermal mass in the analytical model.

Finally it is noted that, for comparison with the flight experiments, the analytical results are only as accurate as are the knowledge of the material properties. This is illustrated in Fig. 3-7 where the annulus surface temperature variations are shown parametrically with the canister surface absorptivity. It is seen that there can be substantial changes in the outer wall temperatures, resulting from changes in the canister surface properties. Therefore, for best comparison, it is highly desirable that these properties be known in the experiments.

NOMENCLATURE

a	diffusivity (cm^2/s)
a,b	fitted constants
B	blackbody radiosity (W/cm^2)
C	modified blackbody radiosity (W/cm^2)
c	radiation constant, specific heat (J/gK)
c_o	speed of light in vacuum (m/s)
e	emmissive power (W/cm^2)
f	emissivity fractional function
G	mass velocity ($g/s\text{-}cm^2$)
g	gravitational acceleration (m/s^2)
H	latent heat of fusion (J/g)
h	Planck's constant, heat transfer coefficient (W/cm^2K)
k	extinction coefficient, thermal conductivity (W/cmK)
N	radiation Biot number
n	refractive index
Q	heat transfer rate per unit length (W/cm)
q	heat flux (W/cm^2)
q-	irradiance (W/cm^2)
q+	radiosity (W/cm^2)
R	radiation network resistance (cm^{-2})
r	electrical resistivity ($Ohm\text{-}cm$), radius (cm)
T	absolute temperature (K)
t	time (s)
u,v	velocities (cm/s)

Greek

α	absorptivity
ρ	density (g/cm^3), reflectivity
ε	emissivity
ξ	integration variable
λ	wave length
θ	nondimensional surface temperature
τ	nondimensional time
Γ	radius ratio
σ	Stefan-Boltzmann constant (W/cm^2K^4)
β	volumetric expansion coefficient (K^{-1})

Subscripts

0	pertaining to T_0
a	pertaining to transparent upper limit,
b	blackbody
e	effective

i	surface i
ij	surface i to surface j
k	conduction
ℓ	liquid
m	melting or phase-change temperature
n	normal direction
r	radiation, reference
s	solid, source
v	vacuum
λ	spectral quantity

REFERENCES

American Institute of Physics Handbook, McGraw-Hill, 1957.

Arnold, W., Gaug, J. R., and Chait, A., 1990, "Convection Phenomena in Low-Gravity Processing: The GTE GaAs Space Experiment," Paper No. AIAA 90-0409, Aerospace Sciences Meeting, Reno, Nevada, Jan. 8-11.

Arpaci, V. S. and Larsen, P. S., 1984, *Convection Heat Transfer*, Prentice-Hall.

Bayazitoglu, Y. and Lam T. T., 1987, "Marangoni Convection in Radiating Fluids," J. Heat Transfer, Vol. 109, pp. 717-721.

Burmeister, L. C., 1983, *Convective Heat Transfer*, Wiley & Sons, p 169.

Edwards, D. K., 1981, *Radiation Heat Transfer Notes*, Hemisphere Publishing.

Incropera, F. P., and DeWitt, D. P., 1985, *Introduction to Heat Transfer*, Wiley & Sons.

Kerslake, T. W. and Ibrahim, M. B., 1990, "Analysis of Thermal Energy Storage Material with Change-of-Phase Volumetric Effects", Proc. ASME Int'l Solar Energy Conf., Miami, FL, April 1-4, pp. 315-325.

Namkoong, D., 1989a, "Thermal Energy Storage Flight Experiments", Proc. ASME Solar Energy Conference, San Diego, CA., April 2-5, pp. 19-24.

Namkoong, D., 1989b, "Flight Experiment of Thermal Energy Storage", Proc. 24th Intersociety Energy Conversion Engineering Conf., Washington, D.C., August 6-11.

NORVEX, NASA Oak Ridge Void Experiment Computer Program, ORNL, Oak Ridge, TN, (VAX version, June 1989).

Palik, E. D., and Hunter, W. R., 1985, "Lithium Fluoride (LiF)," *Handbook of Optical Constasnts of Solids*, Academic Press, pp. 675-693.

Siegel, R., and Howell, J. R., 1981, *Thermal Radiation Heat Transfer*, 2nd Ed, Hemisphere Publishing.

Solomon, A., 1981, "A Note on the Stefan Number in Slab Melting and Solidification," Letters Heat Mass Transfer, Vol 8, pp. 229-235.

Sparrow, E. M., and Cess, R. D., 1978, *Radiation Heat Transfer - Augmented Edition*, McGraw-Hill.

Strumpf, H. J., and Coombs, M. G., 1990, "Solar Receiver Experiment for the Space Station Freedom Brayton Cycle," J. Solar Energy Eng., Vol 112, pp. 12-18.

Wichner, R.P., et al., 1988, "Thermal Analysis of Heat Storage Canisters for a Solar Dynamic, Space Power System", Proc. ASME Solar Energy Conference, Denver, CO., April 10-14, pp. 319-328.

Williams, P. T., 1988, "Thermal Radiative Transport through Lithium Fluoride for Temperatures near the Melting Point," Report K/CSD/TM-77, Oak Ridge Gaseous Diffusion Plant, Oak Ridge, Tennessee,

Yao, L. S., and Prusa, J., 1989, "Melting and Freezing," *Advances in Heat Transfer*, Vol. 19, Academic Press, pp. 1-95.

Yucel, A., Acharya, S. and Williams, M. L., 1989, "Natural Convection and Radiation in a Square Enclosure," Numerical Heat Transfer, Part A, Vol. 15, pp. 261-278.

Zhang, Z., and Bejan, A., 1989, "Melting in an Enclosure Heated at a Constant Rate," Int. J. Heat Mass Transfer, Vol. 32, No. 6, pp. 1063-1076.

Acknowledgement

This work was carried out under NASA contract NAG3-1106, Lewis Research Center, Cleveland, OH 44135.

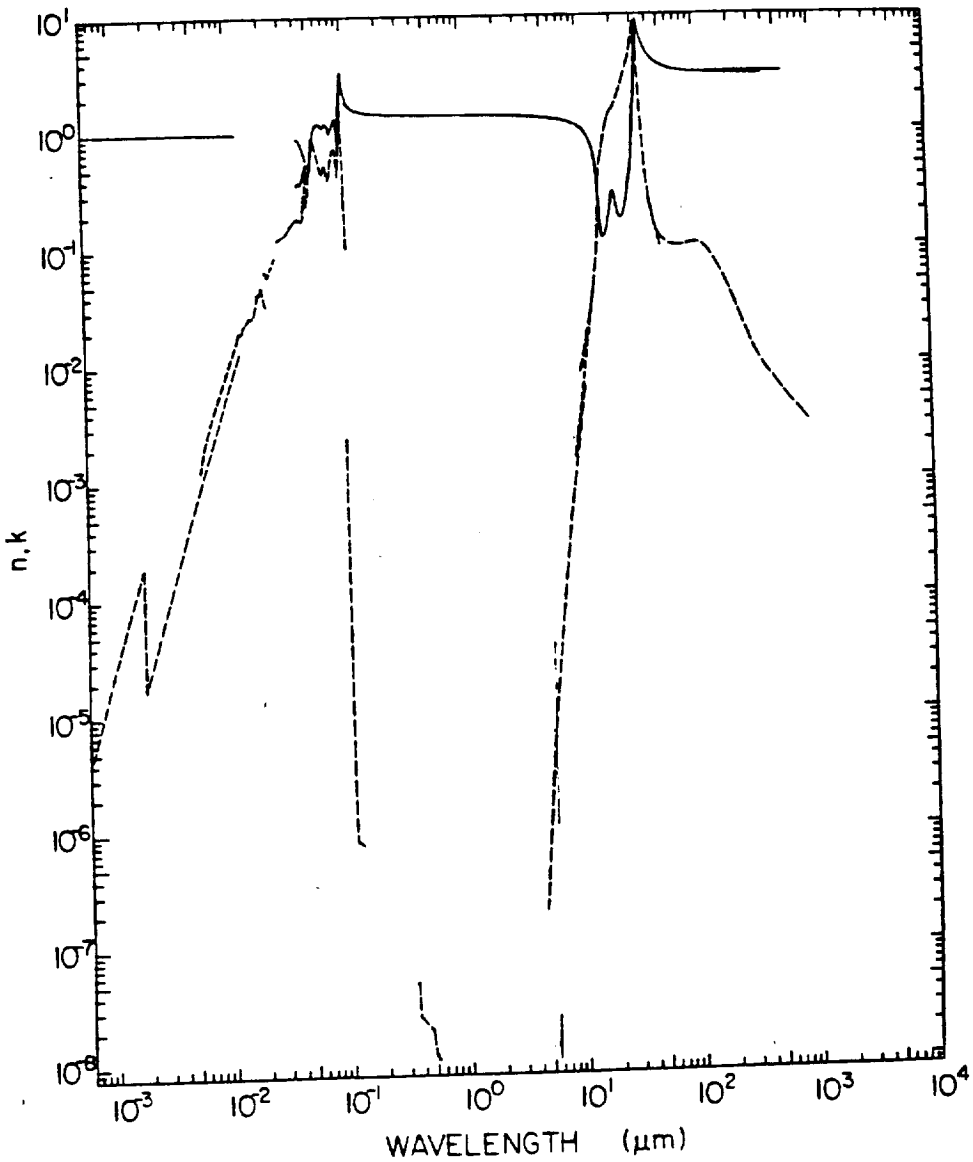

Fig. 2-1. Log-Log Plot of Refractive Index, n _____ , and Extinction coefficient, k - - - - , for Lithium Flouride [from Palik and Hunter 1985].

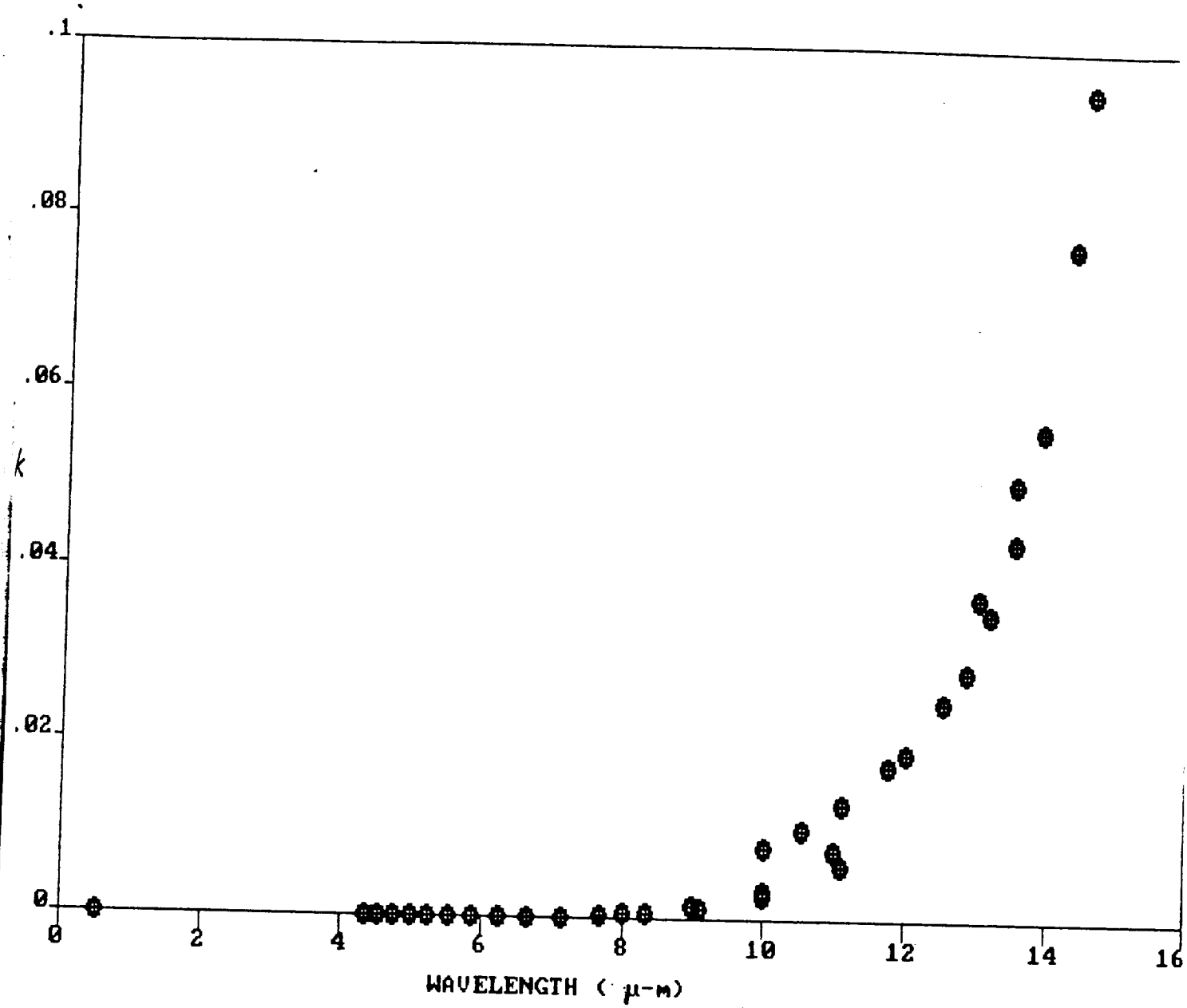

Fig. 2-3. Extinction Coefficient for Lithium Flouride.

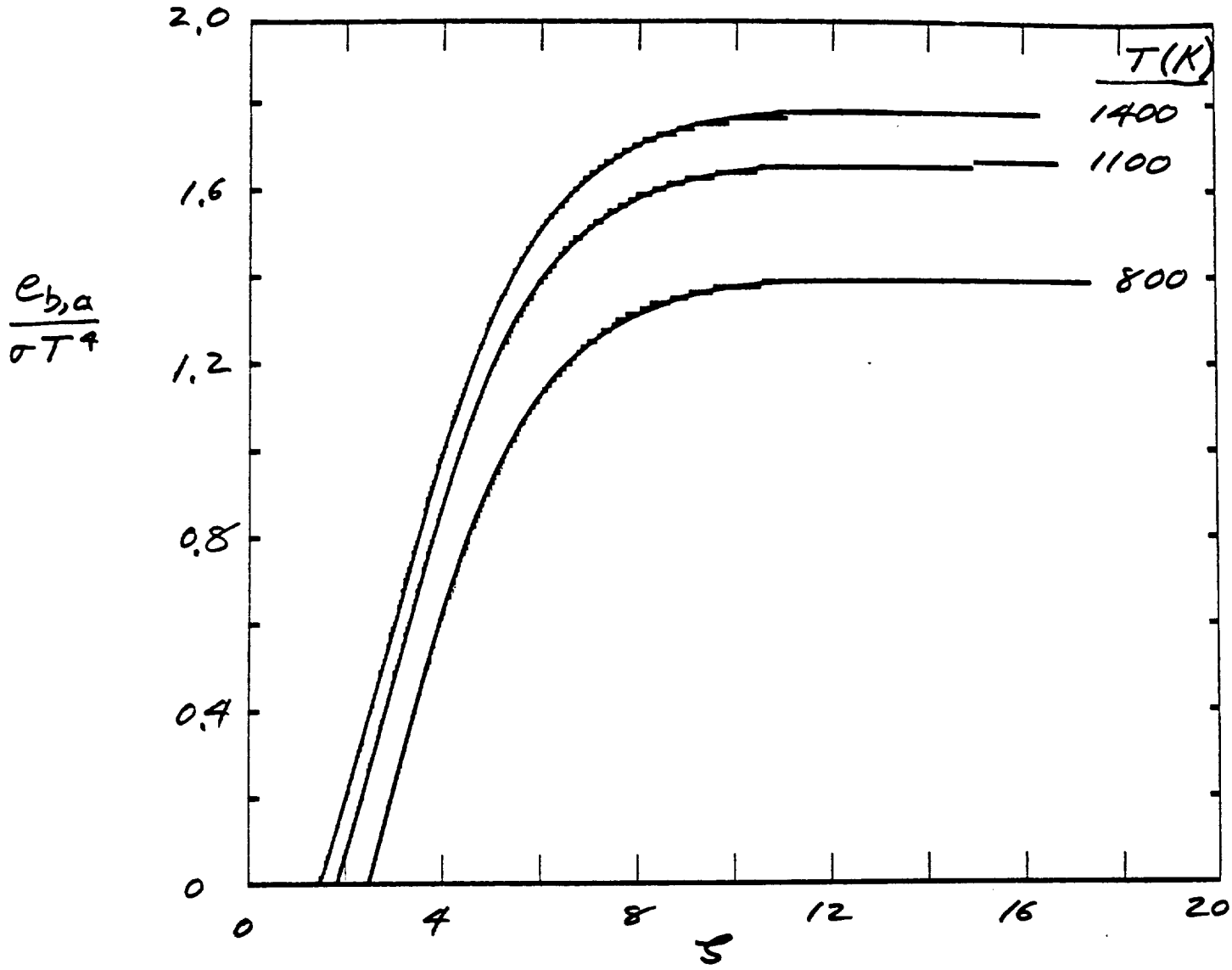

Fig. 2-4. Numerical Integration of Blackbody Total Emissive power in Lithium Flouride.

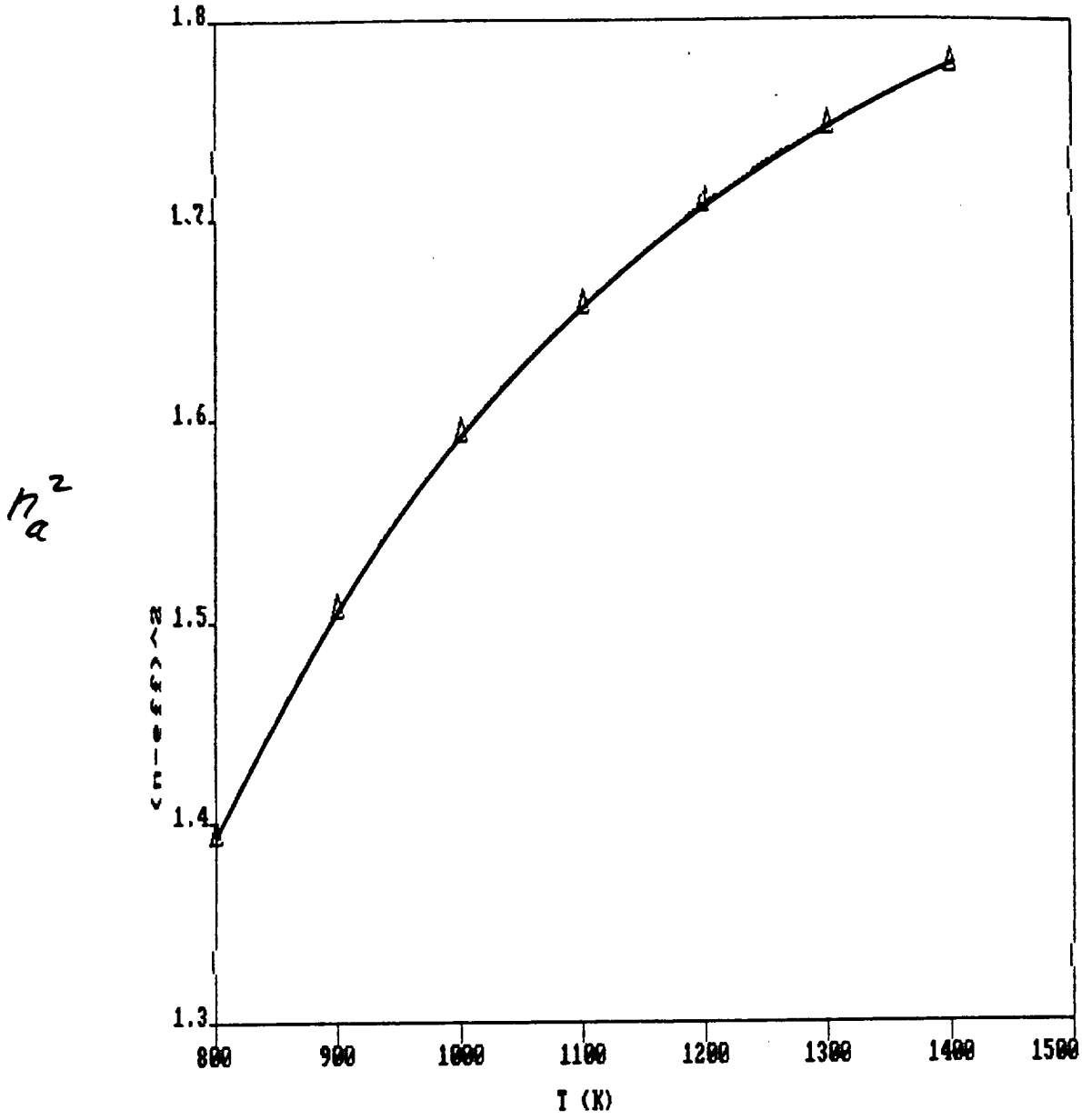

n_a^2

Fig. 2-5. Square of Effective Refractive Index for Lithium Flouride versus Temperature.